Dissertation

submitted to the

Combined Faculty of Natural Sciences and Mathematics

of the Ruperto Carola University Heidelberg, Germany

for the degree of

Doctor of Natural Sciences

Presented by

Ronja Isabelle Mülfarth, M.Sc.

born in: Cologne, Germany

Oral Examination: 28.10.2021

Role of endothelial Notch signaling on the recruitment and education of monocyte-derived macrophages in cancer

Referees: apl. Prof. Dr. Viktor Umansky

apl. Prof. Dr. Andreas Fischer

Summary

Malignant tumor diseases are still one of the leading causes of death worldwide and epithelial ovarian cancer (EOC) is one of the deadliest gynecologic cancers for women. Nowadays, in cancer research, stromal cells within tumor microenvironment (TME) are considered to play an important role in tumor growth. Tumor-associated macrophages (TAM) are the most prominent immune cell population within the TME of EOC and play a crucial role in tumor progression and metastasis.

Our group has previously described that there is frequent hyperactivation of the Notch1 signaling in endothelial cells (EC) within cancer patient samples, promoting immune cell infiltration, tumor cell (TC) transmigration, and metastasis. Ovarian cancer tissue samples showed increased infiltration of myeloid cells in the primary tumor associated with increased endothelial Notch1 activation. Therefore, the aim of this thesis was to better understand the mechanism behind the recruitment and activation of myeloid cells mediated by the Notch1 signaling in EC.

To evaluate the role of the endothelial Notch signaling cascade in a mouse model, an EC-specific inducible gain-of-function model (ecNICD mice) overexpressing the intracellular Notch1 domain (N1ICD) was used. In the corresponding loss-of-function model, an EC-specific inducible deletion of the transcription factor RBPJ (*Rbpj*$^{i\Delta EC}$ mice) was performed. In addition, two different tumor models were used.

The experiments showed that loss of Notch signaling in EC leads to a significant reduction of monocyte-derived macrophages in a subcutaneous tumor model with increased vessel density. To validate the reduced myeloid cell infiltration in an angiogenesis-independent cancer model, tumor progression and myeloid cell infiltration were examined in a metastatic EOC model. Here, increased infiltration of monocyte-derived macrophages into the peritoneum of ecNICD mice was observed, whereas significantly decreased recruitment of these cells occurred in the *Rbpj*$^{i\Delta EC}$ model. Mechanistically, secretion of angiocrine factors regulated by endothelial Notch signaling were examined. This revealed CXCL2 as a novel canonical Notch target gene. Interestingly, CXCL2 levels in ovarian cancer patients correlate with poor prognosis as well as infiltration of myeloid cells into the TME. Moreover, TCs are able to activate infiltrating macrophages in their favor to support tumor growth and a gene expression profile of these TAMs during metastatic EOC has already been described. TAMs from *Rbpj*$^{i\Delta EC}$ mice and littermate controls were isolated and gene expression analysis was performed using the profile of TAMs during EOC tumor growth. Consistently, macrophages isolated from *Rbpj*$^{i\Delta EC}$ mice indicated weaker expression of the gene expression profile of TAMs compared to controls. This suggests that the TAM phenotype induced by TCs requires the presence of the transcription factor RBPJ in ECs. In addition, the number of cytotoxic T cells is increased in the peritoneal cavity of *Rbpj*$^{i\Delta EC}$ mice compared with control mice, and moreover the T cell population was more cytotoxic. Expression of CD74 on TAMs is important for the immunosuppressive phenotype and correlates with poor prognosis in patients with ovarian cancer. In recruited TAMs from *Rbpj*$^{i\Delta EC}$ mice, CD74 was lower expressed than in TAMs from control animals. As a consequence, reduced tumor burden was observed in *Rbpj*$^{i\Delta EC}$ mice compared to littermate controls.

In conclusion, endothelial Notch signaling plays an important role in the recruitment and activation of TAMs within the TME.

Zusammenfassung

Bösartige Tumorerkrankungen sind immer noch eine der häufigsten Todesursachen weltweit und das epitheliale Ovarialkarzinom (EOC) ist eine der tödlichsten gynäkologischen Krebsarten für Frauen. In der Krebsforschung wird heutzutage den Stromazellen innerhalb des Tumorgewebes (Tumor-Mikroumgebung; TME) eine wichtige Rolle für das Tumorwachstum zugeschrieben. Tumor-assoziierte Makrophagen (TAM) sind die bedeutendste Immunzellpopulation innerhalb des TME von EOC und spielen eine äußerst wichtige Rolle für die Tumorprogression und Metastasierung.

Unsere Arbeitsgruppe hat bereits beschrieben, dass in Proben von Krebspatienten eine häufige Hyperaktivierung der Notch1-Signalkaskade in Endothelzellen (EC) zu beobachten ist, welche die Infiltration von Immunzellen, die Transmigration von Tumorzellen (TC) und die Metastasierung fördert. Gewebeproben von Ovarialkarzinomen zeigten eine erhöhte Infiltration von myeloische Zellen im Primärtumor mit erhöhter Notch1-Aktivierung. Ziel dieser Arbeit ist es daher, den Mechanismus hinter der Rekrutierung und Aktivierung von myeloischen Zellen durch die Notch1-Signalkaskade in EC besser zu verstehen.

Um die Rolle der endothelialen Notch-Signalkaskade im Mausmodell zu evaluieren, wurde ein EC-spezifisches induzierbares *gain-of-function* Modell (ecNICD-Mäuse), welches die intrazelluläre Notch1-Domäne (N1ICD) überexprimiert verwendet. Im korrespondierenden *loss-of-function* Modell wurde eine EC-spezifische induzierbare Deletion des Transkriptionsfaktors RBPJ (*Rbpj*$^{i\Delta EC}$-Mäuse) vorgenommen. Darüber hinaus wurden zwei verschiedene Tumormodelle verwendet.

Die Experimente zeigten, dass der Verlust der Notch-Signalaktivität in EC zu einer signifikanten Reduktion der Anzahl an Makrophagen in einem subkutanen Tumormodell mit gleichzeitig erhöhter Gefäßdichte führt. Um die verminderte myeloische Zellinfiltration in einem Angiogenese-unabhängigen Modell während des Tumorwachstums zu validieren, wurde die Tumorprogression und die myeloische Zellinfiltration im metastasierten EOC-Modell untersucht. Hierbei war eine verstärkte Infiltration von aus Monozyten differenzierten Makrophagen in das Peritoneum von ecNICD-Mäusen zu beobachten, wohingegen im *Rbpj*$^{i\Delta EC}$-Modell eine signifikant verringerte Rekrutierung dieser Zellen auftrat. Um die Frage zu beantworten, welche Rolle ECs dabei spielen wurden angiokrine Faktoren identifiziert, welche durch die Notch-Signalkaskade reguliert werden. Die Analyse ergab CXCL2 als ein neues kanonisches Notch-Zielgen. Interessanterweise korreliert der CXCL2-Spiegel bei Patientinnen mit Ovarialkarzinom mit einer schlechten Prognose sowie mit der Infiltration myeloischer Zellen. Darüber hinaus, sind TCs in der Lage infiltrierende Makrophagen zu ihren Gunsten zu aktivieren um das Tumorwachstum zu unterstützen und es wurde bereits ein Genexpressionsprofil von diesen TAMs während des EOC beschrieben. TAMs aus *Rbpj*$^{i\Delta EC}$- und Kontrolltieren wurden isoliert und eine Genexpressionsanalyse mit dem Profil von TAM während EOC durchgeführt. Übereinstimmenderweise zeigten aus *Rbpj*$^{i\Delta EC}$-Mäusen isolierte Makrophagen eine schwächere Expression des Genexpressionsprofil von TAM an. Dies deutet daraufhin, dass der durch Tumorzellen induzierte TAM-Phänotyp die Anwesenheit von RBPJ in ECs erfordert. Passend dazu ist die Anzahl von zytotoxischen T-Zellen in der Bauchhöhle von *Rbpj*$^{i\Delta EC}$-Mäusen im Vergleich zu Kontrollmäusen erhöht und die T-Zellpopulation ist stärker zytotoxisch. Die Expression von CD74 auf TAM ist wichtig für den immunsuppressiven Phänotyp und korreliert mit einer schlechten Prognose bei Patientinnen mit Ovarialkarzinom. In rekrutieren TAM aus *Rbpj*$^{i\Delta EC}$-Mäusen war CD74 geringer exprimiert als in TAM aus Kontrolltieren. Als Konsequenz wurde auch ein verringertes Tumorwachstum in *Rbpj*$^{i\Delta EC}$-Mäusen im Vergleich zu Kontrollmäusen beobachtet.

Zusammenfassend lässt sich sagen, dass die Notch-Signalkaskade in EC eine wichtige Rolle bei der Rekrutierung und Aktivierung von TAM spielt mit einem Effekt auf die gesamte Tumorumgebung.

Table of content

List of abbreviations

ADAM	Disintegrine and metalloprotease
%	Percentage
Ang2	Angiopoetin2
APC	Antigen presenting cell
ApoE	Apolipoprotein E
ARG1	Arginase 1
AVM	Arteriovenous malformations
b-FGF	basic Fibroblast growth factor
BMDM	Bone marrow derived-macrophages
CCC	Clear-cell carcinoma
CCL	CC-chemokine ligand
CCR	CC-chemokine receptor
CD	Cluster of differentiation
CFSE	Carboxyfluorescein succinimidyl ester
CM	Conditioned medium
CMP	Common myeloid progenitor
COX-2	Cyclooxygenase-2
CSC	Cancer stem cell
CSF	Colony-stimulating factor
CSL	Suppressor of hairless
CTLA-4	Cytotoxic T-lymphocyte-associated protein 4
CXCL	C-X-C motif ligand
CXCR	C-X-C motif receptor
DNA	Desoxyribonukleinacid
DC	Dendritic cells
DLL	Delta like proteins
EC	Endothelial cell
ECM	Extracellular matrix
ECM	Extracellular matrix
ecN1ICD	Endothelial specific overexpression of N1ICD
ELIspot	Enzyme linked immuno spot assay
EMC	Endometrioid carcinoma
EOC	Epithelial ovarian cancer
FACS	Fluorescence Activated Cell Sorting
FALC	Fat-associated lymphoid cluster
FCS	Fetal calf serum
FGF	Fibroblast growth factor
FGFR	fibroblast growth factor receptors
FIGO	International federation of gynaecology and obstetrics
GM-MCSF	Granulocyte-macrophage colony-stimulating factor
GMP	Granulocyte-monocyte progenitors
GO	Gene Ontology
GSEA	Gene set enrichment analysis
HA	Hyaluronic acid

HDLEC	Human dermal lymphatic endothelial cells
Hes	Hairy/Enhancer of split
Hey	Hes-related proteins
HGSC	High-grade serious carcinoma
HNSCC	Head and neck squamous cell carcinoma
HPC	Hematopoietic progenitor cells
HRP	Horseradish peroxidase
HUVEC	Human umbilical vein endothelial cells
i.p.	Intra peritoneal
ICAM	Intercellular adhesion molecule
ICAM	Intercellular adhesion molecule 1
ICD	intracellular domain
IL	Interleukine
IMC	Immature myeloid cells
iNOS	Inducible nitric oxide synthase
intPM	Intermediate peritoneal macrophages
IPA	Ingenuity pathway analysis
Jag	Jagged
JAM	Junctional adhesion molecule 1
KO	Knock-out
LAG-3	Lymphocyte-activation gene 3
LDH	Lactate dehydrogenase
LEC	Lymphatic endothelial cell
LGSC	Low-grade serious carcinoma
LLC	Lewis lung carcinoma
LPM	Large peritoneal macrophages
LYVE1	Lymphatic vessel endothelial receptor 1
MAML	Mastermind-like
MC	Mucinous carcinoma
MCEC	Murine cardiac endothelial cell line
MCP-1	monocyte chemoattractant protein-1; also called CCL2
M-CSF	Macrophage colony stimulating factor
MDSC	Myeloid derived-suppressor cells
MHC	Major histocompatibility complex
MIF	Migration inhibitory factor
MMP	Matrix metalloproteinases
mRNA	Messenger RNA
N.A.	Not applicable
N1ICD	Notch1 intracellular domain
NECD	Notch extracellular domain
NF-κB	Nuclear factor kappa-B DNA binding subunit
NK	Natural killer cells
OC	Ovarian cancer
OD	Optical density
PBMC	Peripheral blood nuclear cells
PCAM	Platelet endothelial cell adhesion molecule; also called CD31
PD-1	Programmed cell death 1

PDAC	Pancreatic ductal adenocarcinoma
PDGFR	Platelet-derived growth factor receptor
PD-L1	Programmed cell death ligand 1
PDX	Patient-derived xenografts
PMN	polymorphonuclear
PNDN	Podoplanin
PROX1	Prospero homeobox 1
Rbpj	CBF1-Suppressor of Hairless-LAG1, also called CSL
Rbpj[iΔEC]	Endothelial specific deletion of *Rbpj*
RNA	Ribonucleic acid
RT-qPCR	Real time-quantitativ PCR
s.c.	Subcutenous
SD	Standard deviation
SDF-1	Stromal cell-derived factor 1, also called CXCL12
shRNA	Small hair pin RNA
siRNA	Small interfering RNA
SPM	Small peritoneal macrophages
TAM	Tumor-associated macrophages
TAN	Tumor-associated neutrophils
TC	Tumor cells
TGF	Transforming Growth Factor
Th	T helper cells
TIM	T cell immunoglobulin and mucin domain-containing protein
TIME	Tumor immune microenvironment
TMA	Tissue microarray
TME	Tumor microenvironment
TNF	Tumor necrosis factor
Treg	Regulatory T cell
VAP	Vascular adhesion protein
VCAM	Vascular adhesion molecule
VEGF	Vascular endothelial growth factor
VEGFR	Vascular endothelial growth factor receptor

List of figures

List of tables

1   Introduction

1.1   Tumor and tumor progression

Cancer incidence nowadays is 442,4 per 100.000 women and men per year and is still a leading cause of death worldwide. Most prominent cancer types are breast, lung, bronchus, prostate, colon and rectum, melanoma, bladder, non-Hodgkin lymphoma, kidney, endometrial, leukemia, pancreatic, thyroid and liver cancer (NIH, 2020). This list also highlights the diversity of the diseases as well challenges in treatment options. On top of that, with respect to increased lifespan-expectations cancer incidence is further increasing (Bray *et al.*, 2018).

Cancerous cells develop from different origin; epithelial, mesenchymal or hematopoietic cells due to DNA mutations leading to an aberrantly proliferation and numerous other cellular alterations. Risk factor are genetic predisposing as well as environmental factors; like smoking, alcohol, obesity, UV light exposure and viral infection (Colditz, Sellers, & Trapido, 2006).

The focus of cancer research has changed from the tumor cells (TC) itself towards the tumor microenvironment (TME). Although, cancer is a highly heterogeneous and complex disease, Hanahan and Weinberg defined the hallmarks of tumor progression, which also highlights the important role of the TME. The first version of the hallmarks of cancer included evading apoptosis, self-sufficiency in growth signals, insensitivity to anti-growth signals, sustained angiogenesis, limitless replicative potential and tissue invasion and metastasis. Moreover, the updated version of the hallmarks of cancer also includes the metabolic deregulation and tumor immunology, like tumor promoting inflammation and avoiding immune distraction also called cancer immunoediting (Hanahan & Weinberg, 2011).

1.1.1   Cancer immunoediting

For a successful tumor progression, malignant tumor cells have to escape from the immune system and this process is called cancer immunoediting. In more detail, cancer immunoediting can be divided into three phases: elimination, equilibrium, and escape leading to a successful shielding of malignant cells (**Fig. 1.1**). In the first phase cancerous cells get recognized by the immune system due to the presentation of tumor-antigens and secretion of pro-inflammatory cytokines from the tissue of origin, allowing the immune system to kill TCs. Next, TCs which were able to survive this elimination phase undergo genetic and epigenetic changes (equilibration phase) to escape the immune system and start to proliferate. In the final escape phase, TCs create an immunosuppressive TME including the accumulation of immune suppressive cytokines, like Interleukin (IL)-4, IL6, IL10 and transforming growth factor (TGF) β as well recruiting immunosuppressive immune cells like, tumor-associated macrophages (TAM), myeloid-derived suppressor cells (MDSC) and regulatory T cells (Treg). Consequently, the anti-tumor function of effector cells, like natural killer (NK) and cytotoxic T cells is impaired. Emphasizing, again the importance of the TME for the formation and outgrowth of tumors (Kim, Emi, & Tanabe, 2007; Schreiber, Old, & Smyth, 2011).
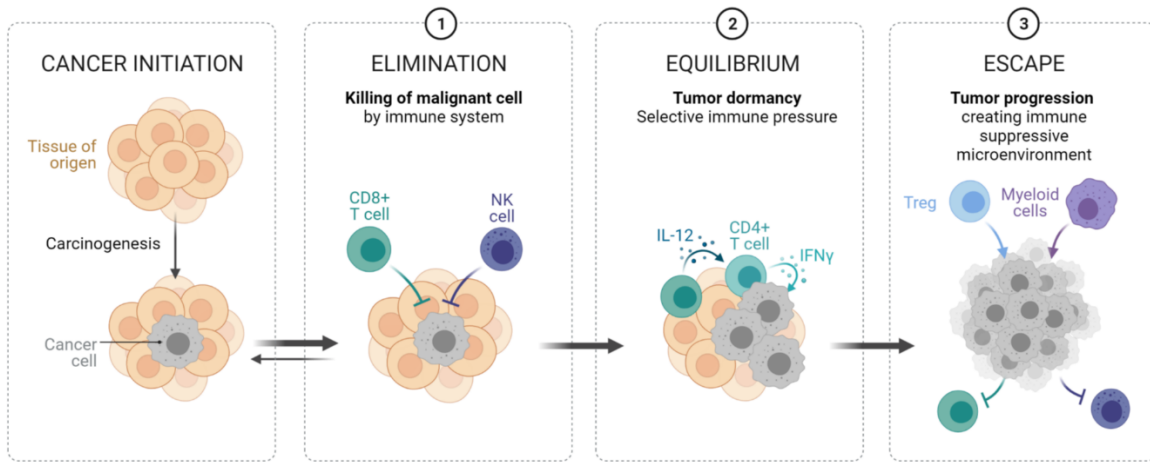
Figure 1.1: Cancer immunoediting divided in three different phases. After cells acquire malignant phenotype they get recognized by the immune system leading to a cancer cell killing by cytotoxic (CD8^{+}) T cells and natural killer cells (NK). Cancer cells, which were able to escape start to proliferate during equilibrium phase. In the escape phase, cancer cells create an immunosuppressive microenvironment secreting pro-tumorigenic cytokine and recruiting immune suppressive myeloid cells as well as regulatory T cells (Treg).

1.1.2   Metastasis and pre-metastatic niche

Metastasis is the most frequent cause of tumor-related death worldwide and is also considered as an utmost hallmark of cancer progression. Not only TCs themselves are implicated in the invasion and metastasis of tumors but also stroma cells of the TME play an important role (Hanahan & Coussens, 2012).

Metastasis is a complex process including the basic steps of local invasion of TCs from the primary tumor, intravasation into the blood stream, survival in circulation, extravasation from the blood stream, and finally colonization to distance site (Massague, Batlle, & Gomis, 2017). During these steps the TC disseminates from the primary tumor to distance organs, pass the blood stream and in the final step malignant cells home in the metastatic site (Valastyan & Weinberg, 2011). Additionally, metastasis is a multi-step process depending of the cell origin, acquisition of different mutations resulting in a successfully invading of distant organs. The process of metastasis also highlights again the important role of the TME. Until nowadays, the timeline of tumor metastasis is still poorly understood (Massague et al., 2017).

Dormancy of disseminated TCs is highly dependent on the microenvironment. The metastatic site (also called metastatic niche) can actively suppress TCs homing by immune cell-mediated killing, as already discussed. Therefore, the successful homing of TCs is also partly driven by the environment within the metastatic niche (Quail & Joyce, 2013). Already in 1889 Steven Paget hypothesized the "seed and soil"-theory, proposing that the TCs, the seed, interacted with the metastatic niche, the soil (Akhtar, Haider, Rashid, & Al-Nabet, 2019). Therefore, additional studies have already shown that the tissue where metastasis takes place is not passively or randomly chosen by the circulating TCs, rather than that the organ of metastasis is actively selected and primed before metastatic spread (Peinado *et al.*, 2017). TCs prepare a specialized microenvironment, the pre-metastatic niche, by secreting TC-derived factors to educate the metastatic distant site and promote TCs homing, colonization and tumor growth (Akhtar *et al.*, 2019).

1.2 Tumor microenvironment

As already mentioned, the TME is highlighted in the famous hallmarks of cancer and it also plays a critical role when it comes to specificity and effectivity of therapies. Unlike TCs, stromal cells within the microenvironment where the tumor starts to seed, are relatively stable genomically (Quail & Joyce, 2013). Interaction between TCs and stromal cells from the microenvironment plays an important role in tumor progression from the initiation to the extravasation and metastasis of TCs. The stromal cells from the TME include several different cell types; like cancer-associated fibroblast, which main function is the remodeling of the extracellular matrix (ECM); ECs, which build the tumor vasculature and the tumor immunity by infiltration immune cells (**Fig. 1.2**).
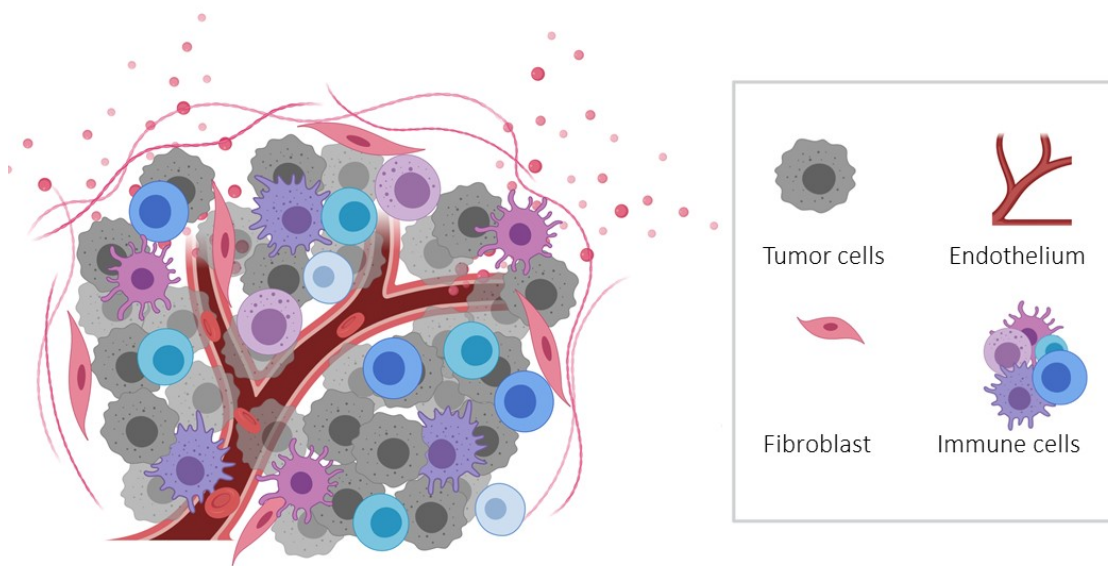
Figure 1.2: Tumor microenvironment consisting of tumor cells and stroma. Tumor stroma consists on endothelial cells building the tumor vasculature, fibroblast generating extracellular matrix and immune cells, which are important for the immunosuppressive microenvironment.

1.2.1 Tumor vasculature

In the last decades, cancer research on ECs revealed their crucial role for nourishing the tumor (Bagley, 2016) but the last years revealed that ECs play many additional roles to promote tumor progression (Alsina-Sanchis, Mülfarth & Fischer, 2021) . ECs are specialized cells, which are implicated in organ homeostasis as well as tumor progression due to their role in regulating oxygen exchange. Moreover, they play an essential role in the TME being responsible for the supply with nutrients and oxygen as well regulating the extravasation of TCs and infiltration of immune cells. Hypoxia, is characterized by a low oxygen level which is an initiator of tumor angiogenesis, the formation of new vessels from preexisting ones (Marcelo, Goldie, & Hirschi, 2013; Teleanu, Chircov, Grumezescu, & Teleanu, 2019). Therefore, tumor progression is an angiogenesis-depended process, which involves interaction with multiple different cell types. As a result, every cell has an approximately 100 to 150 µm distance to a vascular channel and the formation of new blood is essential for tumor growth and proliferation of primary tumors (Pasquier *et al.*, 2020). Highlighting the utmost role of ECs as major component of the TME because of their important role in supplying the TC with nutrients, being the border for metastatic spread and playing a role in the immunosuppressive microenvironment by regulating the immune cell

infiltration. Moreover, the role of ECs in regulating several tumor-related processes beyond tumor-angiogenesis have been described (Alsina-Sanchis, Mülfarth & Fischer, 2021).

1.2.1.1 Blood versus lymphatic vasculature

The vasculature systems consist of a circularly and lymphatic system. The circulating system consist of with three different blood vessel major classes; capillaries, veins and arteries. The main function of the blood circulation is the transport of blood throughout the whole body. The blood contains and transports oxygen, nutrients, hormones to every cell and returns unwanted material. Together with the heart, which is responsible for the flowrate of the circulation, the blood forms the circulating system of an organism. Capillaries are small caliber vessels, which connect veins and arteries, providing nutrient and oxygen exchange. Arteries transport the oxygen-loaded blood from the heart to the organs, whereas veins return the blood back to the heart. All vessels consist of ECs, which form the inner layer of blood vessels (Potente & Makinen, 2017).

On the other hand, the lymphatic system is a network of lymphatic vessels, lymphatic ECs (LEC) and lymphatic organs. Similar to the blood circulation, the lymphatic system also consists of lymphatic capillaries and bigger lymphatic vessels with distinct different functions compared to the blood circulation system (Oliver, Kipnis, Randolph, & Harvey, 2020). The main function of the lymphatic system is the transport of draining fluid from the tissue in the blood circulation to prevent accumulation of fluid and swelling of the tissue. Moreover, the lymphatic system also plays a role in the immune defense by filtering the body for pathogens, producing immune cells and antibodies (Potente & Makinen, 2017). Therefore, the lymphatic system is also connected to the lymph nodes of the organism (Oliver *et al.*, 2020).

The ECs of the particular vasculature are also specialized for the specific need of the respective tissue. Therefore, also the development of lymphatic or blood vessels is precisely regulated. During development EC progenitors differentiate from mesoderm into first embryogenic blood vessels leading further to an expansion of the vascular network through angiogenesis. After establishing the blood vasculature, LEC develop from venous ECs generating the lymphatic vasculature during early development. The differentiation of LEC from vein blood EC involves the transcription factor prospero homeobox protein 1 (Prox1) (Yang *et al.*, 2012). Furthermore, interaction of the angiocrine factor vascular endothelial growth factor (VEGF) with the receptor 3 (VEGFR3) promotes the migration of LEC from vein EC resulting in a first lymphatic structure (lymph sacs) (Karkkainen *et al.*, 2004). During adulthood, not only the origin of the ECs but also the microenvironment play an important role in regulation of the specifications of blood and lymphatic ECs. This leads also to the concept that ECs heterogeneity and specification are due to the tissue of origin. However as already mentioned, blood and lymphatic ECs have distinct functions. For instance, blood ECs are mostly building a barrier function whereas, lymphatic ECs are permeable to allowed fluid uptake (Potente & Makinen, 2017).

1.2.1.2 Angiocrine factors

ECs are not only building a passive barrier function but are also known to secrete angiocrine factors. The term "angiocrine" factors was generated to highlight the importance of EC-secreted growth factors, cytokines, chemokines, extracellular matrix components, exosomes and others. These factors can have different functions depending on the organ of origin and organ state (Alsina-Sanchis, Mülfarth, & Fischer, 2021; Pasquier *et al.*, 2020; Rafii, Butler, & Ding, 2016). Especially, in the tumor context, cancer-associated ECs interact with different cell types and tumor-induced angiocrine factors are able to shape the TME by influencing TC proliferation, cancer stem cell (CSC) properties, ECM remodeling, tumor

invasiveness and metastasis as well as immune cell recruitment and activation (Alsina-Sanchis, Mülfarth, & Fischer, 2021) Thereby, ECs influence the direct microenvironment as well as distant organ homeostasis and pre-metastatic niches (Fig. 1.3).

Angiocrine factors are not restricted to secreted factors but also include membrane-bound proteins like EC adhesion proteins, for example intercellular adhesion molecule 1 (ICAM1), vascular cell adhesion molecule 1 (VCAM1) as well as E-selectin and P-selectin. These membrane-bound angiocrine factors are involved in the recruitment of leukocytes and transmigration of cancer cells across the vessel wall. On the other hand, ECs are also able to secrete soluble angiocrine factors like, cytokines and chemokines for example IL-8 (also known as C-X-C motif ligand (CXCL) 8), monocyte chemotactic protein 1 (MCP1; also known as CC-chemokine-ligand (CCL) 2), stromal cell-derived factor 1 (SDF1; also known as CXCL12). TC-dependent secretion of soluble factors by ECs influence the recruitment and polarization of immune cells, impact on TCs and therefore shape the phenotype on the TME (Alsina-Sanchis, Mülfarth, & Fischer, 2021).
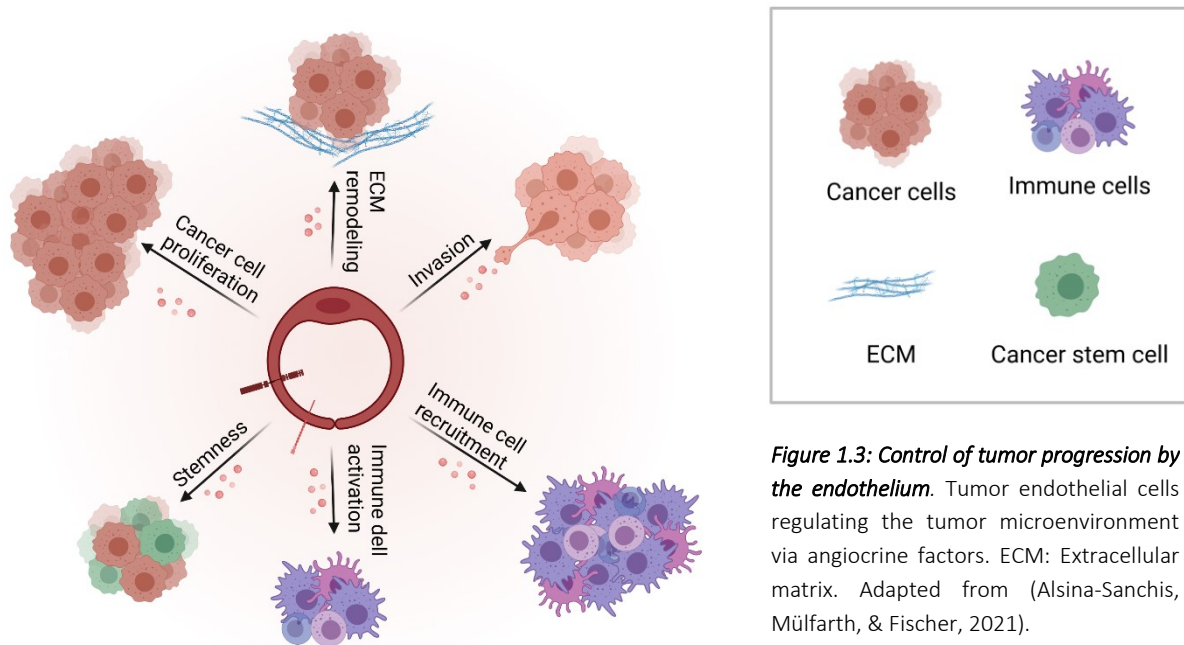
Figure 1.3: Control of tumor progression by the endothelium. Tumor endothelial cells regulating the tumor microenvironment via angiocrine factors. ECM: Extracellular matrix. Adapted from (Alsina-Sanchis, Mülfarth, & Fischer, 2021).

1.2.1.3 Endothelial Notch signaling

Endothelial Notch signaling (Fig. 1.4) is a cell-to-cell communication system and it further plays an important role in vascular morphology, vessel stability and cell quiescence. During embryonal development Notch signaling is a key regulator of angiogenesis and arterio-venous specification but also in the endothelium of adult mice Notch still regulates maintenance of junctional stability and endothelial homeostasis (Mack & Iruela-Arispe, 2018). The two receptor domains are generated by posttranslational cleavage of the 300kDa full length Notch receptor in the Golgi apparatus by furin-like convertases (S1 cleavage). The resulted Notch extracellular (NECD) and intracellular domain (NICD) noncovalently coupled Notch receptor complex is located at the cell membrane (Logeat *et al.*, 1998). Additional posttranslational modifications like glycosylation modify the ligand-specificity of the receptor.

Introduction

The Notch receptor family consist of four transmembrane Notch receptor (Notch1, Notch2, Notch3 and Notch4) which are located on the signal receiving cell. Upon stimulation from the signal-sending cell via Notch ligands like Delta like proteins (DLL; DLL1, DLL3 and DLL4) or Jagged (JAG; JAG1 and JAG2), the Notch receptor gets activated on the signal receiving cell. The Notch receptor undergoes two cleavages generating an extracellular and an activated intracellular signaling domain. S2 proteolytic cleavage by disintegrine and metalloprotease (Gale *et al.*, 2004) family member at juxtamembrane region results in a NECD, which becomes trans-endocytosis and reused by the signal sending cells (Brou *et al.*, 2000; Gordon, Arnett, & Blacklow, 2008). The subsequent S3 cleavage by γ-secretase/presenilin complex results in an activate NICD which translocates into the nucleus for signal transduction (Takasugi *et al.*, 2003). Translocation into the nucleus leads to formation of a transcriptional activator complex through NICD binding to recombination signal binding protein for immunoglobulin kappa J region (Rbpj; also called CBF1-Suppressor of Hairless-LAG1 (CSL)) on DNA to activate the transcription of Notch target genes like Hairy/Enhancer of Split (Hes1 and Hes5), Hes-related proteins (Hey1 and Hey2), and others. Rbpj binding to DNA together with co-regulators functions as a transcriptional repressor which gets inactivated upon NICD binding (Chillakuri, Sheppard, Lea, & Handford, 2012).

TCs and blood vessels communicate through direct interactions via Notch1 receptor. Wieland *et al.* could show that activated Notch1 receptors are frequently expressed in EC of human tumors (Wieland *et al.*, 2017). This study also showed that TCs stimulate EC Notch1 signaling and sustain activation of the cleaved Notch1 intracellular domain (N1ICD) in EC within the microenvironment. In addition, EC Notch signaling induced EC senescence, expression of cytokines and VCAM1 on ECs. This promotes infiltration of immune cells, transmigration of TC and increase metastasis.
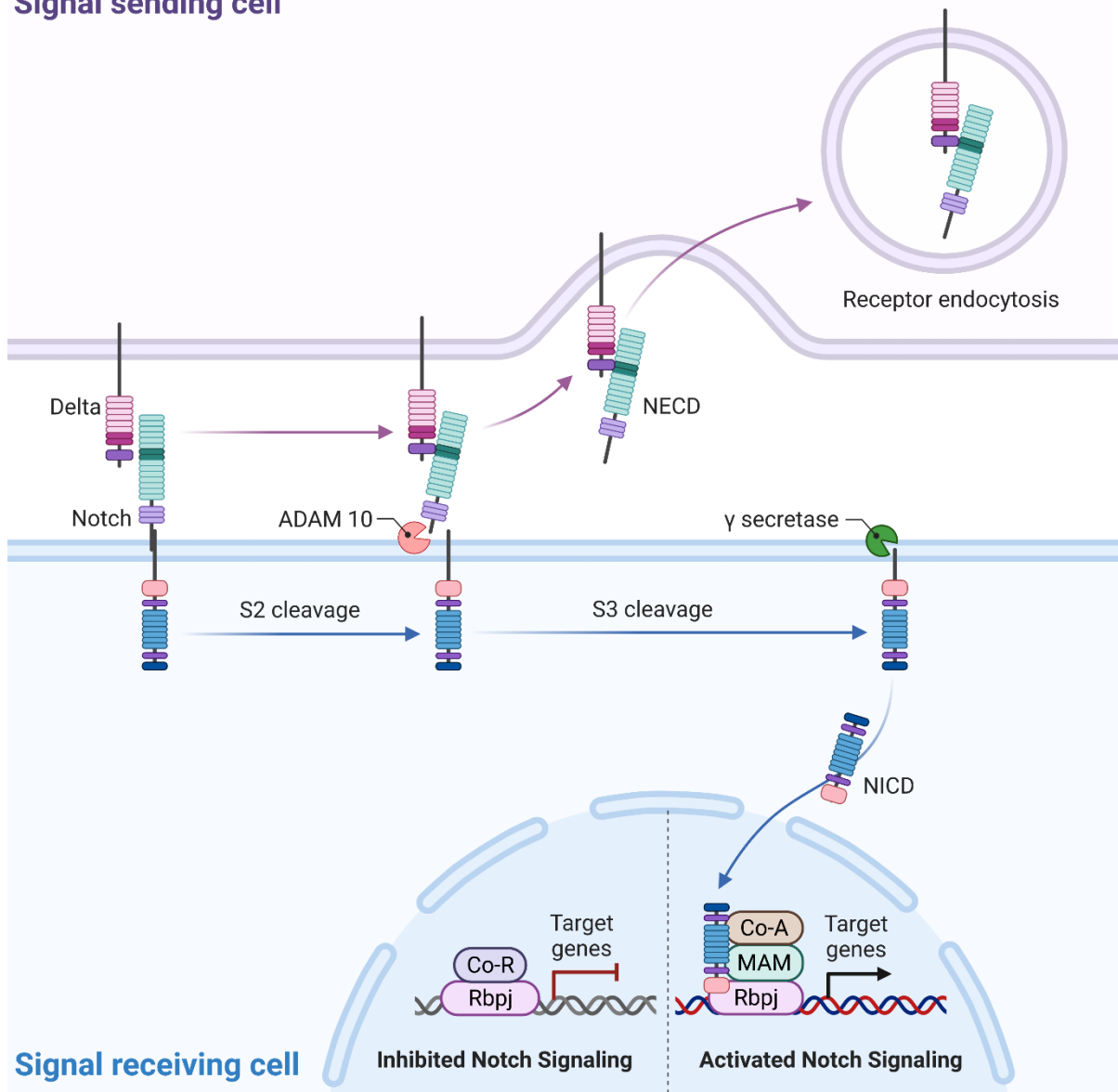
Figure 1.4: Canonical Notch signaling. Signal sending cell activate Notch receptor on signal receiving cell via the expression of Notch ligand on their cell surface. Upon Notch activation the receptor gets cleaved and translocate into the nuclei to activate transcription of target genes. N1ICD: Notch1 intracellular domain; Rbpj: Recombining binding protein suppressor of hairless.

Notch-dependent angiocrine factors like VCAM1 have already described (Nus *et al*., 2016; Verginelli *et al*., 2015; Wieland *et al*., 2017). The study from Wieland *et al*., provides a list of cytokines upregulated in human ECs overexpressing N1ICD, for example *CCL1, CCL21* and *CXCL2*. Moreover, the alarmin IL33 is also reported to be a target gene of Notch signaling in senescent ECs (Sundlisaeter *et al*., 2012).

Targeting endothelial Notch signaling in non-inducible transgenic mouse models leads to a lethal phenotype during midgestation (Duarte *et al*., 2004; Fischer, Schumacher, Maier, Sendtner, & Gessler, 2004; Gale *et al*., 2004; Krebs *et al*., 2004; Limbourg *et al*., 2005). In more details, EC specific depletion of *Notch1* and *Rbpj* leads to arteriovenous malformations (AVM) and typical AV shunts which is also observed in forced Notch1 expression in ECs (Krebs, Starling, Chervonsky, & Gridley, 2010; Nielsen *et al*., 2014). As a result, inducible mouse models are used to study the role of endothelial Notch signaling without affecting the embryogenic development and *de novo* angiogenesis. For example, the ligand

independent gain-of-function model (ecNICD mice) overexpressing Notch1 intracellular domain (N1ICD) and the EC-specific and inducible deletion of *Rbpj* in the loss-of-function (*Rbpj*$^{i\Delta EC}$) mouse model.

1.2.1.4   Anti-angiogenic cancer therapy

Anti-angiogenic cancer therapy designed to clock tumor-induced angiogenesis was one of the first approaches to target the stromal cells in the TME. As a consequence of angiogenesis-dependent tumor growth (Bagley, 2016), targeted therapies against VEGF was developed (Bussolino, 2017). Secretion of VEGF by TCs and certain immune cells within the TME leads to angiogenesis after binding to the VEGFR on the endothelial tip cell, which is the leading cell of the sprout for angiogenesis, inducing migration and sprouting (Teleanu *et al.*, 2019). Studies blocking VEGF in human tumor cell lines showed *in vitro* as well as *in vivo* to reduce TC proliferation. Furthermore, preclinical studies on clinical dosing showed that intraperitoneal application of monoclonal VEGF antibodies in tumor-bearing mice significantly reduce tumor growth with efficient plasma concentrations (Mordenti *et al.*, 1999). Combination of anti-angiogenesis therapy with chemotherapy showed in clinical studies to reduce side-effects in different cancer types, like gastrointestinal, non-small cell lung, breast and ovarian cancer (Yonucu, Yiotalmaz, Phipps, Unlu, & Kohandel, 2017). In 2004 the food and drug administration (FDA) approved bevacizumab, a humanized monoclonal antibody to target VEGF in the TME, leading to about 20% improved survival in metastatic colorectal cancer compared to standard therapy (Koukourakis & Sotiropoulou-Lontou, 2011). Bevacizumab binds and inhibits VEGF binding to its receptor leading to an inhibition of angiogenesis and consequently, reduced tumor growth. Moreover, also small molecule inhibitors are approved to target angiogenesis, for example sunitinib and pazopanib, which target mainly VEGFR, PDGFR, FGFR and other receptors to inhibit tumor vascularization (Teleanu *et al.*, 2019). In more detail, combined therapy of bevacizumab and paclitaxel (chemotherapy) or carboplatin (chemotherapy) in non-squamous non-small cell lung cancer improved patients outcome resulting in a FDA approval of as first line-treatment (Socinski *et al.*, 2018). Additionally, combination of anti-angiogenesis in combination with immunotherapy improved patient survival, for example the combination of VEGF-therapy with programmed cell death protein (PD-1)/programmed cell death ligand (PD-L1) immunotherapy (Teleanu *et al.*, 2019). Especially, the IMBrave study from 2020 demonstrated that this combination not only lead to a normalization of the tumor vasculature but it also impacted immune cell infiltration into the TME improving overall survival rate. In the clinical phase III study of hepatocellular carcinoma, therapies of standard care by sorafenib, a kinase inhibitor, was compared with the combined targeted therapy of bevacizumab and atezolizumab, immune checkpoint therapies against PD-L1. The results of this study showed an increased overall as well as progression free survival in the combined therapy approach compared to the standard treatment with sorafenib (Finn *et al.*, 2020). In addition, patients with metastatic renal cell carcinoma treated with anti-PD-1 antibodies (pembrolizumab) in combination with VEGFR inhibitors (axitinib) therapy showed increased progression-free survival compared towards the single and standard therapy leading to FDA approval (Rini *et al.*, 2019). In summary, the combined targeted therapy showed an improved patient outcome. However, anti-angiogenic therapies are facing their limitations due side-effects and acquisition of resistance mechanisms (Teleanu *et al.*, 2019). Thus, targeting the cross-talk of ECs and immune cells within the TME by combining vascular targeted and immunotherapies showed to enhance cancer immunity. For this reason, study the cross-talk between EC and immune cells is of utmost importance and would elucidate new possible targeted therapies.

1.2.2 Tumor immunology

The function of immune cells is to protect the organism from disease. Generally, the immune system is divided in two main groups: the innate and adaptive immune response. The adaptive immune response is specific towards pathogens, which includes mainly B- and T cells whereas, the innate immune system comprise a broad and unspecific immune response including myeloid cells.

Tumor progression and metastasis highly depend on the infiltration of immune cells into the TME. Therefore, the tumor immune microenvironment (TIME) shapes the phenotype of a tumor. The secretion of chemotactic chemokines and cytokines as well as growth factors promote and influence the activation of immune cells as well as shield the tumor against the immune response (Franklin & Li, 2016; Ostuni, Kratochvill, Murray, & Natoli, 2015; Qian *et al.*, 2011). With a focus on immunotherapies like checkpoint-blocking and adaptive cell transfer, the interest in the TIME increased in the last decade.

The TIME consist of both the myeloid and lymphoid cell, innate and adoptive immune response, which promote tumor progression and survival by creating an immunosuppressive environment (Seliger & Massa, 2021).

1.2.2.1 Tumor-associated macrophages

TAMs are the most abundant immune cell population within most TME and their role in cancer-related inflammation is also considers as the seventh hallmark of cancer (Mantovani, Allavena, Sica, & Balkwill, 2008). Macrophages play an important role in organ homeostasis but also in the response to pathological diseases like cancer (Franklin & Li, 2016; Wynn, 2013). Macrophages are myeloid immune cells which infiltration into the TME often correlates with a poor prognosis for cancer patients. TAMs can be derived from infiltrating monocytes into macrophages present different phenotypes on the microenvironment (Lawrence & Natoli, 2011; Xue *et al.*, 2014). Classically, two extreme and contrary phenotypes are distinguished by their different functions, inflammatory (M1) by the expression of the functional marker inducible nitric oxide synthase (iNOS) as well as anti-inflammatory (M2) macrophages, with an expression of the functional marker arginase 1 (ARG1) (Orecchioni, Ghosheh, Pramod, & Ley, 2019). Although in reality these represent two extreme of a spectrum and TAMs often present intermediate phenotypes (Beyer et al., 2012; Murray et al., 2014; Stoger, Goossens, & de Winther, 2010). Inflammatory macrophages are activated by Interferon gamma (Inf-γ) or Lipopolysaccharide (LPS) responses, which are predominately associated with an inflammation or early tumor stage. Inflammatory macrophages secrete inflammatory cytokines like IL1β, IL6 and tumor necrosis factor (TNF) α and are further associated with anti-tumorigenic T cell responses. Anti-inflammatory macrophages polarize upon stimulis like IL4, IL10 and IL13. However, these two macrophage phenotypes do not reflect the plastic behavior and phenotype of activated macrophages (Beyer *et al.*, 2012; Murray *et al.*, 2014; Stoger, Goossens, & de Winther, 2010). Macrophage education and activation during later stages of tumor development show a pro-tumorigenic (M2-like) phenotype. Moreover, for pro-tumorigenic macrophages serval marker beyond the classical activation marker, ARG1 are described. Several already well-described tumor-induced chemotactic cytokines (mainly CCL2 also called MCP-1, CCL11 and CCL16) are known to recruit immunosuppressive monocytes into the TME, which leads to a secretion of CCL2 by macrophages themselves to further recruit more myeloid cells. TAMs are further characterized by a secretion of pro-tumorigenic factors like CCL2, cyclooxygenase-2 (COX-2), basic fibroblast growth factor (bFGF), CXCL8, metalloproteases (MMPs), TNF as well as VEGF (Lewis & Pollard, 2006; Mantovani, Sozzani, Locati, Allavena, & Sica, 2002). Differentiation of TAMs showed to increases the markers cluster of differentiation (CD) 163, CD204 and CD206 in TME (Kubota *et al.*, 2017). Moreover, TAMs expressing CD163 and CD204 showed to secrete immune suppressive

molecules, like IL10 and PD-L1 and inhibit T cell function in *in vitro* co-culture experiments (Kubota *et al.*, 2017). As well as, expression of the mannose receptor, CD206 on TAMs correlates with poor prognosis for cancer patients in intrahepatic cholangiocarcinoma (Sun *et al.*, 2020). The immune responses of TAMs are associated with pro-tumorigenic T cell activation and impaired effector T cell function. Therefore, TAMs promote tumor growth by creating an immunosuppressive microenvironment and are further also associated with *de novo* tumor angiogenesis, tumor migration, invasion and metastasis (Franklin & Li, 2016).

Additionally, also tissue resident macrophages play a profound role in the organ homeostasis and tumor development. Resident macrophages developed from embryonic precursors with a self-renewal capacity. Thus, tissue resident macrophages already seed in the tissue before birth and have a decreased plasticity compared to monocyte-derived macrophages (Cotechini, Atallah, & Grossman, 2021). Moreover, tissue resident macrophages show a distinct gene signature and transcriptome profile depending on their tissue of origin (Orecchioni *et al.*, 2019). Leading to a sentinel function by presenting antigens to the adaptive immune system to keep organ homeostasis. During cancer progression, tissue resident macrophages play a major role in the seeding in metastatic TCs. In the last decades, studies have been performed to unravel how resident macrophages interact with infiltrating TCs using modern technics like refined fate-mapping tools in combination with specifically genetic engineered mouse models (Cotechini *et al.*, 2021). For example, in mouse models of ovarian cancer and pancreatic ductal adenocarcinoma (PDAC), depletion of resident peritoneal macrophages by intraperitoneal injection of clodronate prior tumor inoculation impaired tumor growth and reduced metastasis. Moreover, omental tissue resident macrophages help the TCs to colonize the tissue by providing a microenvironment, which further promotes also the metastatic spread into the peritoneum (Etzerodt *et al.*, 2020). Additionally, resident macrophages within the peritoneal cavity have also been described to play a profound role in the effectiveness of immunotherapy (Rodriguez & Ruffell, 2021). Peritoneal resident macrophages can inhibit effector cell function in a TME (DeNardo & Ruffell, 2019). Therefore, Rodriguez and Ruffel describe the role of T cell immunoglobulin and mucin domain containing 4 (Tim4) receptor only expressed on resident or long-term recruited peritoneal macrophages preventing the effector function of T cells in peritoneal metastatic tumors to immunotherapy (Rodriguez & Ruffell, 2021). On the contrary, the depletion of resident alveolar macrophages did show any effect on mammary carcinoma-derived cells in an experimental metastasis model (Orecchioni *et al.*, 2019). Taking together, the contribution of resident macrophages on the tumor progression highly depend on the tissue of origin, microenvironment and pre-metastatic niche.

1.2.2.2 Tumor-associated neutrophils

Neutrophils are the major immune cell population of the blood stream under steady state conditions. The main function of neutrophils is to patrol the organism to detect foreign particles. Under inflammatory or tumorigenic conditions, neutrophils leave the blood stream to phagocytose pathogens. During tumor growth, neutrophils are also classified as anti-tumorigenic (N1) and pro-tumorigenic (N2), with different activation and polarization phenotypes, like macrophages (Fridlender *et al.*, 2009). N1 tumor-associated neutrophils (TAN) show an increased expression of TNFα, CCL3, ICAM-1 and activate of T-, B-, neutral killer (NK) cell and dendritic cells (DC). Whereas, N2 TANs increase pro-tumorigenic chemokines like CCL2, CXCL1, CXCL2 and CXCL8, as well as enzymes to modulate the extracellular matrix promoting metastasis (Masucci, Minopoli, & Carriero, 2019). Therefore, infiltration of neutrophils into a solid tumor correlates with increased lymph node metastasis as well an increased neutrophil-to-leukocyte ratio is further correlated with bad prognosis for prostate, gastric as well as pancreatic cancer

patients (J. Cao, Zhu, Zhao, Li, & Xu, 2016; J. Chen, Hong, Zhai, & Shen, 2015; Giakoustidis *et al*., 2018; L. Wu, Saxena, Awaji, & Singh, 2019).

1.2.2.3 Myeloid-derived suppressor cells

Myeloid-derived suppressor cells (MDSC) are immunosuppressive immature myeloid cells including different heterogonous cell populations like monocytic MDSCs, polymorphonuclear (PMN) MDSCs and granulocytic MDSCs immune cells (Mabuchi & Sasano, 2021). The immunosuppressive function of MDSCs is due to their ability to inhibit T cells and NK cell activity. Under physiological conditions, myeloid progenitor cells from the bone marrow niche differentiate into mature myeloid cells like macrophages or DCs upon stimulation. While, in pathological conditions like cancer, myeloid progenitor cells differentiation is not efficient and leads to immature myeloid cells, like MDSCs. MDSCs secrete cytokines like CCL3, CCL4 and CCL5 to recruit T helper cells as well IL10 and TGFβ to induce their differentiation. In addition, the expression of immune checkpoint molecules inhibits T cell function and proliferation by MDSC (Groth *et al*., 2019). Accumulation of MDSCs correlates with poor prognosis and overall survival in several different tumor entities (Ai *et al*., 2018).

1.2.2.4 Dendritic cells

DCs develop as well from the myeloid linage. The main role of DCs within the TME is the presentation of tumor-associated antigens to T cells. Therefore, DCs prime the anti-tumorigenic immune response. However, in an immunosuppressive microenvironment DCs become dysfunctional. As a consequence of this, DCs promote tumor growth by inefficient antigen-presentation to the effector T cells due to a downregulation of major histocompatibility complex (MHC) class molecules, immune checkpoint molecules like CD80 and CD86 on DCs. Furthermore, immunosuppressive cytokines like VEGF, TGF-β, IL1β, and prostaglandins may lead to a differentiation into TAMs or MDSCs (Fu & Jiang, 2018; Veglia & Gabrilovich, 2017).

1.2.2.5 Tumor-infiltrating lymphocytes

NK cells are located in the blood, bone marrow niche as well in lymphoid tissue. Moreover, NK cells develop from lymphoid progenitors and get educated to successfully eliminate virus-infected as well as cancerous cells. The main function of NK cells within the TME is the independent killing of TCs, and therefore NK cells are considered as the main effector cells of the innate immunity. Activation of NK cells is balanced between the expression of inhibitory molecules, like MHC class I-binding receptors and activation receptors on the cell surface. TCs downregulate MHC class I during early stages of tumor progression, therefore NK cells get activated if the inhibitory stimuli are missing. Activated NK cells lead to a lysis of targeted cell by granule-mediated cell lysis (Meza Guzman, Keating, & Nicholson, 2020; Wu, Fu, Jiang, & Shao, 2020). NK cells also secrete inflammatory cytokines like INF-γ, to modulate the adaptive immunity (Wu *et al*., 2020). Therefore, increased numbers of NK cells within the TME correlates with a better outcome for cancer patients (Zhang *et al*., 2020).

Primary tumors frequently also home lymphocytes, like B and T cells in the TIME. Especially, T cells play an important role in anti-tumor immunity. Cytotoxic, CD8$^+$ T cells are able to kill cancerous cells by cytotoxic granules perforin and granzyme B delivery (Durgeau, Virk, Corgnac, & Mami-Chouaib, 2018). Therefore, cytotoxic T cells correlate with better patient outcome in several tumor identities (An *et al*., 2019; Vihervuori *et al*., 2019). On the other hand, T helper (Th) cells, CD4$^+$ T cells, secrete pro-inflammatory cytokines like IL2 and INFγ, stimulate antigen-presenting cells (APC) to prime cytotoxic T cells, inhibit activation-induced cell death and support memory formation (Kennedy & Celis, 2008). Helper T cells within the TME are still pivotally discussed depending on their role and functions.

Furthermore, the activation of T cells can be further determined by cell surface receptors. Most prominent receptors of T-cell immune checkpoint functions are PD-1 and cytotoxic T-lymphocyte-associated protein 4 (CTLA4) (Dong *et al.*, 2002; Iwai *et al.*, 2002). Expression of the receptor ligand by TCs or APC suppresses the immune response by lymphocytes. CTLA-4 binds the ligands CD80/CD86 on APC and inhibits T cell functions. PD-1 is upregulated after T cell activation and binds the ligands PDL-1/PD-L2 on APC. The expression of suppressive PD-1 on T cells is used as biomarker with contrary outcomes. In cervical and epithelial cancers, the expression of PD-1 correlates with poor prognosis whereas, in colorectal cancer and head and neck squamous cell carcinoma (HNSCC) PD-1 expression correlates with better outcome for the patients (Ishikawa *et al.*, 2020; Li *et al.*, 2016; Schneider *et al.*, 2018; Zhang *et al.*, 2015).

B lymphocytes are cells from the humoral immunity. Their implication in cancer progression is rarely described but mostly assigned to a regulation of immune responses as well (Guo & Cui, 2019).

1.3   Myeloid cell recruitment

As already mentioned, myeloid cells belong to the innate immunity consisting of granulocytes, macrophages and DCs. During myelopoiesis, hematopoietic progenitor cells (HPC) from the bone marrow niche differentiate into common myeloid progenitor cells (CMP) and further into granulocyte/macrophage progenitor cells (GMP) also called immature myeloid cells (IMC). In the following steps of myelopoiesis, IMC differentiate into monocytic/dendritic progenitor cells (MDP) and further into DCs/macrophages as well as myeloblasts (MB) into neutrophils. The differentiation of myeloid cells is driven by chemokines, like granulocyte-macrophage colony-stimulating factor (GM-CSF), granulocyte colony-stimulating factor (G-CSF), and macrophage colony-stimulating factor (M-CSF). Furthermore, expression and secretion of chemotactic cytokines also lead to a recruitment of myeloid cells into TME or inflamed tissue (Groth *et al.*, 2019).

1.3.1   Chemokines and chemokine receptors

Myeloid cell infiltration is tightly regulated by chemokine gradient as well cell-surface receptors for cell interactions. Nowadays, 50 different chemokines and 20 chemokine receptors have been described concluding that each receptor interact with several chemokines (except six), for example CXCR2 binds CXCL1-3 and CXCL5-8. Chemokines are small chemotactic cytokines, which can be classified into four different groups; C, CC, CXC, CX_3C depending of their first two cysteine residue in the conserved cysteine motif in the amino acid sequence. Chemokines can be produced and secreted by several different cell types; like immune cells, fibroblasts, epithelial cells, ECs and TCs with a main function to recruit immune cells. Although, chemokine receptors are expressed mainly on immune cells they are also expressed on ECs and TCs. The interaction of chemokines with the receptors leads to a binding to the transmembrane heterotrimeric G-protein-coupled receptors on the cell surface and G protein coupling followed by an activation of downstream pathways. Moreover, studies on the complexity of chemokine-chemokine receptor interactions also unravel the specific activation depending on chemokine binding (Gorbachev & Fairchild, 2014). Most common downstream mediators are Rac, Rho, and Cdc42 resulting in a migration towards the chemokine gradient. Chemokines are also secreted under homeostasis conditions, like CCL14, CCL19, CCL20, CCL21, CXCL12, and CXCL13 to maintain leukocyte homing. During inflammation leukocyte recruitment and activation is mediated due to pro-inflammatory cytokines (like IL1, TNF or IFN) damage signals or responses of tissue damage (Gorbachev & Fairchild, 2014; Kohli, Pillarisetty, & Kim, 2021).

1.3.2 Regulating myeloid cell recruitment

As already mentioned, myeloid cells from the innate immune system consist of a variety of different cell types with different functions (Groth *et al.*, 2019). It includes macrophages, differentiated from monocytes to phagocytose pathogens and neutrophils, which patrol the blood stream and induce inflammatory response. Neutrophils and monocytes enter the blood stream from the bone marrow niche to detect inflammatory stimuli. The process of recruitment of innate immune cells towards the inflammation is strongly controlled by chemokines and their receptors on the cell surface. Under homeostasis conditions, the blood stream is the major compartment for neutrophils, whereas CX_3CR1^+ monocytes can also distribute to organs under steady state conditions and differentiate to resident, tissue macrophages. During inflammation neutrophils and $CCR2^+$ monocytes exit the blood stream towards a chemokine gradient (**Fig. 1.5**). This indicates that the stimuli not only affects the recruitment of immune cells but also their activations and phenotype (Sokol & Luster, 2015).

Furthermore, the recruitment of immune cells also involves interaction with ECs. Immune cells are in close contact to ECs within the blood stream, which build a barrier towards inflamed tissue. To exit the blood stream, immune cells need to interact with ECs, which requires also cell-to-cell interactions via selectins and integrins, which get upregulated upon inflammatory stimuli (Pober & Sessa, 2007). This process of migration is divided in serval steps; rolling, adhesion and transmigration (**Fig. 1.5**) (Nourshargh, Hordijk, & Sixt, 2010). The first step involves the interaction of EC receptors, P- and E selectin and their ligands expressed on immune cells. This step of rolling is reversible until the cell adheres to the EC barrier. In the next step, the adhesion is mediated by endothelial integrins, like VCAM and ICAM as well the surface expression of integrins on immune cells. The expression of integrin Mac-1, also called CD11b on myeloid cells also induce adhesion and crawling on the endothelium (Wetzel et al., 2004). In the final step, the immune cells transmigrate into the inflamed tissue. The transmigration involves again the expression of surface receptors, like PCAM and JAM on ECs and PCAM, integrins and CD11b on immune cells (Al-Soudi, Kaaij, & Tas, 2017).
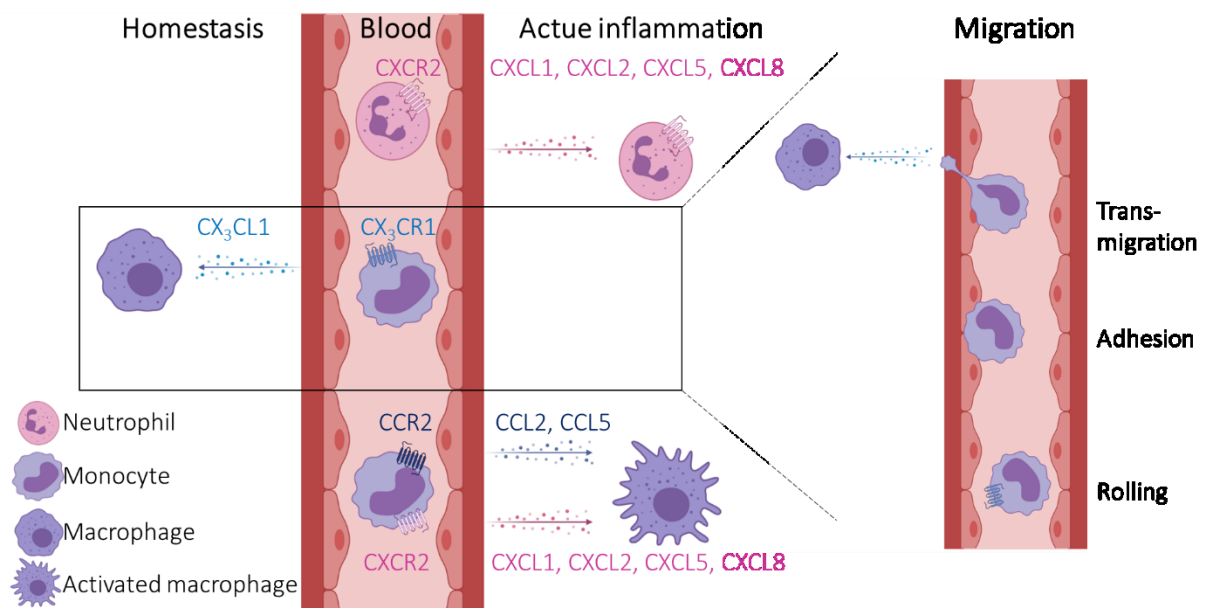
Figure 1.5: Myeloid cell recruitment controlled by chemokines and cell-to-cell interactions with the endothelium. Left: Myeloid cell recruitment towards inflammation or homeostasis (monocytes) depends of chemokine gradient. CXCL: C-X-C motif ligand, CXCR: C-X-C motif receptor, CCL: CC-Chemokine-ligand, CCR: CC-Chemokine receptor. Right: Migration of immune cells by interaction with endothelial cells divided into rolling, adhesion and transmigration. Modified from (Sokol & Luster, 2015).

1.3.3 Myeloid cell recruitment in the tumor microenvironment

Several studies back in the 1850's (Virchow) and later in the early 2000's (Fibrig and Yamagiwa) showed that chronic inflammation can induce cancer (Balkwill & Montavini, 2001). Tumors are also considered as "wounds that do not heal" (Dvorak, 1986). Therefore, it is evident that immune cell recruitment is implicated in the tumor progression (Franklin & Li, 2016; Ostuni *et al.*, 2015; Qian *et al.*, 2011). As previously exposed, immune cell infiltration is regulated by chemokine gradients which induce a directed migration of cells. In more detail, chemokines within the TME can be divided in to three different groups, pro-tumorigenic, anti-tumorigenic and dual-role chemokines. Pro-tumorigenic chemokines, like CXCL2, CXCL12 and CCL1, promote the recruitment of immunosuppressive cells. However, anti-tumorigenic chemokines like CXCL10, CXCL14 or CXCL16 leads to a recruitment of effector cells. Moreover, dual-function chemokines, like CCL2 and CCL21 show both functions depending on the tumor stage and the TME. Remarkably, chemokines within the TME are not only expressed by TCs themselves. Stromal cells also secrete chemokines and cytokines amplifying the TC-induced response. Infiltrating immune cells are also a main source of chemokines contributing to the chemokine network of the TME. In turn, tumor-infiltrating immunosuppressive myeloid cells, TAMs and MDSCs produce and secrete for example CCL20 and CCL22 to recruit regulatory T cells into the TME (Gorbachev & Fairchild, 2014).

The role of immunosuppressive myeloid cells is widely described to promote tumor growth by creating an immune suppressive phenotype of the TME. Especially, the cytokine CCL2 is necessary to induce extravasation of $CCR2^+$ monocytes into TME (Ostuni *et al.*, 2015; Serbina & Pamer, 2006). Confirmed by *in vivo* tumor studies on *Ccr2* knock-out mice leading to a reduced infiltration of immunosuppressive MDSCs and decreased tumor growth and metastasis (Chen *et al.*, 2016; Ren *et al.*, 2012; Yang *et al.*, 2020). Also, increased production of CCL2 by the TME correlating with increased infiltration of monocytes and macrophages in mouse models of several different tumor types (Gorbachev & Fairchild, 2014). In line with this, studies on human melanoma patients showed an increased infiltration of $CCR5^+$ MDSCs compared to healthy controls, which was validated in a spontaneous skin melanoma mouse model (Blattner *et al.*, 2018). In ovarian and bladder cancer patients, serum levels of CXCL2 correlate with myeloid cell infiltration into the TME, whereas blocking CXCR2 decreased myeloid cell infiltration and tumor progression in mouse model of pancreatic cancer (Katoh *et al.*, 2013; Taki *et al.*, 2018; Zhang *et al.*, 2017). Moreover, also CXCL12 is able to recruit immunosuppressive myeloid cells via CXCR4 into the TME of ovarian cancer patients (Obermajer, Muthuswamy, Odunsi, Edwards, & Kalinski, 2011). Moreover, the human cytokine IL8 (CXCL8) was able to induce chemotaxis of immune suppressive myeloid cells *ex vivo* (Alfaro *et al.*, 2016). Also, hypoxic conditions induce CCL26 expression by TCs, which recruits CX_3CR1 immunosuppressive myeloid cells within the TME (Chiu *et al.*, 2017).

1.3.4 Recruitment of myeloid cells into peritoneal cavity

The peritoneal cavity allowed to study infiltration kinetics as well to isolate different immune cell population after stimulation like tumor inoculation or inflammation. The peritoneal cavity of mice mainly contain B and T cells as well as large peritoneal macrophages (LPM), which originate from embryonic progenitors and have renewal capacity. Murine macrophages are characterized by an F4/80 expression, which is low expressed on monocyte-derived macrophages and shows a strong expression on tissue resident and long-term recruited macrophages (**Fig. 1.6**). LPMs express high levels of F4/80 and Tim4, which is a marker of long-term macrophages. Under tumorigenic and inflammatory conditions small peritoneal macrophages (SPMs) infiltrate the peritoneal cavity to clear the contamination. SPM are characterized by a high CCR2 and MHCII expression as well as low F4/80

expression. During tumor progression within the peritoneal cavity, SPMs further develop into intermediate PM (intPM) and become the main macrophages population within the TME (Ghosn *et al.*, 2010; Goossens, *et al.*, 2019; Okabe & Medzhitov, 2014).

Visceral fat tissue, omentum within the peritoneal cavity is a vascular rich tissue. Therefore, it is hypothesized that immune cells from the blood stream reach the peritoneum by passing the vasculature of the omentum. Furthermore, the omentum itself is rich of leukocyte aggregations, which are as well known to expand during inflammation (further discussed in 1.4.2 Omentum) (Platell, Cooper, Papadimitriou, & Hall, 2000).
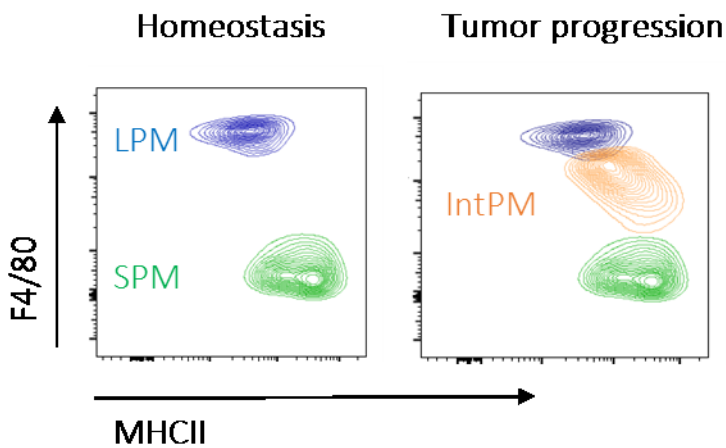
Figure 1.6: Population of monocyte-derived macrophages in peritoneal cavity of mice. Characterization of myeloid cells (CD45$^+$ CD11b$^+$) into monocyte-derived macrophages by F4/80 and MHCII expression. During homeostasis, the peritoneum is mainly populated by large peritoneal macrophages (LPM) and a minor population of small peritoneal macrophages (SPM). During tumor progression, peritoneal macrophages promote tumor growth and recruit (SPM) into the tumor microenvironment which develop into intermediate PM (IntPM).

1.3.4.1 Myeloid cell recruitment during peritoneal inflammation

Upon peritoneal inflammation, neutrophils are the first line of immune response within the first hours, followed by an increased infiltration of monocytes and macrophages into the peritoneal cavity after 24 hours after inflammatory stimulation. Monocytes and macrophages become the most prominent population after three to six days after inflammatory stimuli. Macrophages have a longer lifespan compared to neutrophils. Therefore, macrophages have a stronger impact on clearance via phagocytosis (Gautier, *et al.*, 2013). The experimental model of thioglycolate peritonitis is used to study the myeloid cell infiltration into an acute inflamed peritoneum (Cook, Braine, & Hamilton, 2003). Thioglycolate broth is a medium primary used to cultivate aerobe and anaerobe microorganism. The intraperitoneal (i.p.) injection of thioglycolate into mice also allows to study kinetics of leukocyte infiltration. In this case, the role of resident macrophages is minor for the recruitment of myeloid cells towards the inflamed tissue. Studies have shown that depletion of macrophages in the peritoneal cavity does not influence the neutrophil recruitment (Gautier *et al.*, 2013). However, the resident macrophages are the first once to clear the infection and disappear (Leijh, van Zwet, ter Kuile, & van Furth, 1984). Lymphocyte infiltration starts after four days of injection (Gautier *et al.*, 2013).

1.4 Epithelial ovarian cancer

Worldwide, ovarian cancer is one of the most lethal cancers for women with a 5-years survival rate below 45 % (Webb & Jordan, 2017). Ovarian cancer is mostly diagnosed in patients older than 40 years, with a peak for women with an age of 70 years. Therefore, with an increased lifespan expectation also the number of ovarian cancer patients is increasing. Additionally, several risk factors like family history of ovarian cancer, endometriosis and smoking have been identifies in different studies (Webb & Jordan, 2017).

In healthy women, the ovaries are located within the abdominal cavity. Besides their role in producing ova, the ovaries produce and secrete hormones and function as an endocrine gland (Webb & Jordan, 2017).

Ovarian carcinoma can develop from different cell identities. A minor percentage of ovarian carcinoma develops from germ or stromal cells. Whereas, most common carcinomas are classified as epithelial ovarian cancer (EOC) due to their epithelial histology. However, there is still a lack of knowledge about the exact origin of the malignant cells. It was assumed that the malignant cells derive from the ovarian surface epithelium but nowadays there is increased evidences that ovarian cancer can also derive from other pelvic organs, like fallopian tube and primary peritoneal cancer. Therefore, EOC is a heterogeneous group, which can be further histological classified as Low-Grade Serious Carcinoma (LGSC), High-Grade Serious Carcinoma (HGSC), Endometrioid Carcinoma (EMC), Clear-Cell Carcinoma (CCC) and Mucinous Carcinoma (Webb & Jordan, 2017).

1.4.1 Tumor progression of epithelial ovarian cancer

EOC is the most diagnosed ovarian cancer type with around 90 % of the cases (Webb & Jordan, 2017). Due to a lack of screening methods and preclinical symptoms, it is mostly diagnosed in a late and metastatic stage, which significantly reduce the survival rate. Therefore, EOC correlates with poor prognosis and high mortality rate (Baci *et al.*, 2020).

The *Fédération Internationale de Gynécologie et d'Obstétrique* (International Federation of Gynaecology and Obstetrics, FIGO) classifies the different stages of ovarian cancer (**Fig. 1.7**). The progression of ovarian cancer is divided in four main stages with different sub-groups. The stage I is limited to the primary tumor. The malignant cells are confined to the ovarian or fallopian tube without major population of malignant cells in the pelvic region. In the stage II, the tumor involves both ovaries or fallopian tubes with spread into pelvic region and intraperitoneal tissue. Due to the lack of anatomical barriers, ovarian cancer cells can easily spread to other organs within the pelvis and the abdominal cavity including the omentum (peritoneal visceral fat tissue). In the next stage, stage III, the tumor spreads to both ovaries or fallopian tubes, the pelvic region and intraperitoneal tissue with spread to the peritoneal outside pelvis and metastasis to retroperitoneal lymph nodes. Most patients get diagnosed in these metastatic stage III (around 70%). The last stage of tumor progression in EOC is stage IV, where the tumor cells metastasize beyond the abdominal cavity to distant sites.
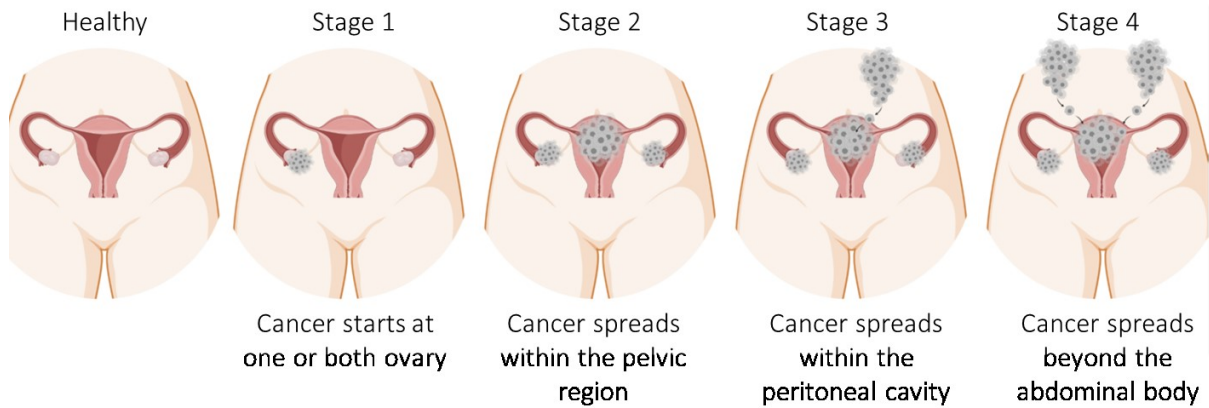
Figure 1.7: Tumor progression of epithelial ovarian cancer with different stages of classification. In the first stage, malignant cells starts to proliferate at ovary followed by a spread in the pelvic region (stage 2). In metastasis stages (stage 3 and 4) cancer cells spread within the peritoneal cavity and beyond the abdominal body including the omentum.

1.4.2   Omentum

Depending of the cell type of origin different malignant cells prefer different organs to invade for metastasis (Nieman *et al.*, 2011). In the case of metastatic EOC the malignant cells spread in the peritoneum and home in the peritoneal visceral fat tissue called omentum. One important cause of the homing of TCs to the omentum is the immunological niche and adipocytes, which provide fatty acids to TCs for proliferation (Nieman *et al.*, 2011). The omentum is a visceral adipose tissue located between the stomach and the spleen of mice (**Fig. 1.8**), whereas, in humans the omentum covers the whole peritoneal wall. Nevertheless, it has the same function in the different species independent of the localization and structure. The greater omentum develops from the dorsal mesogastrium. This results in a lose adipose tissue which is connected by mesothelial layers with a vascular-rich structure. Omental ECs and mesothelial cells are specialized for the transmigration of cells within the peritoneal cavity and omentum. Human omental microvascular ECs express surface markers like E- and P- Selectin which helps to distinguish from mesothelial cells (Platell *et al.*, 2000).

1.4.2.1   Function of omentum

The main function of the omentum is to limit infection and inflammation within the peritoneal cavity. Firstly, the rapid clearance of contaminations within the peritoneal cavity and secondly, supply leukocyte to the peritoneum. Therefore, the omentum consists of leucocyte aggregates, which are called fat-associated lymphoid clusters (FALCs) or milky spots (Jackson-Jones *et al.*, 2020). These leukocyte aggregations consist of mainly macrophages with different stages of maturation, B- and T cells, mast cells and stromal cells. The milky spots protect the peritoneum against contaminations being the first immunological response. (Platell *et al.*, 2000) Moreover, the discontinuous endothelium or the fenestration containing ECs within the milky spots allows rapid transmigration of leukocytes (Platell *et al.*, 2000).

The macrophages within the milky spots are playing a major role in the immune response of the omentum. They are independent of bone-marrow derived monocytes (BMDM) and rather develop from monocytic precursors within the milky spots (Etzerodt *et al.*, 2020; Platell *et al.*, 2000). During peritoneal inflammation the macrophages in the omentum start to proliferate and differentiate into phagocytic cells triggered by the M-CSF- produced in the milky spots. During peritoneal inflammation, omental macrophages migrate to the peritoneal cavity to absorb and clear the local contamination. In addition,

immune cells and especially neutrophils can also migrate though the omental ECs and pass the vascular network of the omentum (**Fig. 1.8**). However, the increase of B- and T cells in the milk spots upon inflammation is not clear yet. Therefore, the omental vascular system is the main source of recruited immune cells towards peritoneal inflammation. The third function of the omentum in the immune response is the encapsulation of contaminations. Cells within the omentum produce fibrin, which adhere the area of contamination leading to an encapsulation, blood vessel development and fibroblast recruitment within few days. Moreover, the contaminated area will be also encapsulated with collagen to generate a dense adhesion. Therefore, it is not surprising that the removal of the omentum, so called omentectomy leads to an increased incidence of postoperative sepsis. This effect was observed due to a decreased number of immune cells in the peritoneum resulting in an impaired peritoneal immune response (Platell *et al.*, 2000).

In summary, the omentum is important for the peritoneal immunity because of its high absorptive and immune cell reservoir function.
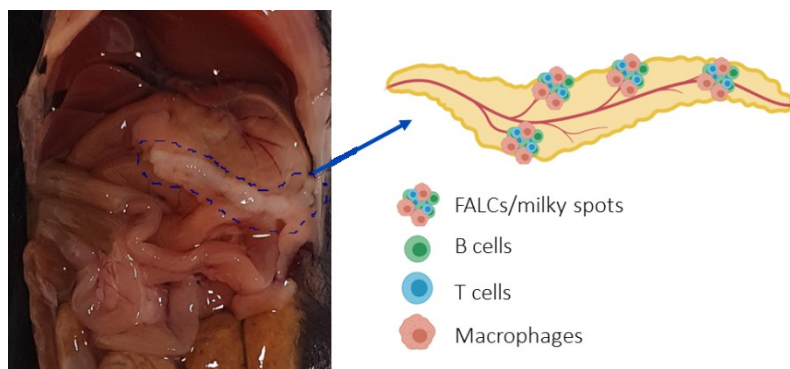
Figure 1.8: Location and structure of omentum in mice. Omentum is located between spleen and stomach. The visceral adipose tissue consist of leukocyte aggregations of macrophages, B- and T cells. FALCs: fat-associated lymphoid clusters, also called milky spots.

FALCs/milky spots

B cells

T cells

Macrophages

1.4.2.2   Omentum as pre-metastatic niche

TCs frequently disseminated on the omentum during peritoneal metastasis. In different tumor models, malignant cells preferentially seed in the peritoneal adipose tissue and colonize in the milky spots. Therefore, the omentum is the main distant metastasis site of peritoneal carcinomatosis (Platell *et al.*, 2000). Especially, ovarian cancer is characterized by a metastatic spread of TCs within the peritoneum and colonization of the omentum. A specific role in the colonization of ovarian cancer cells is described for CD163$^+$ and Tim4$^+$ omental macrophages. The TCs, which seed in the omentum acquire a stem cell-like phenotype (CSC) initiated by resident macrophages from the omentum (Etzerodt *et al.*, 2020). This metabolic switch allows the cells to be more plastic and further adapt to the microenvironment within the peritoneum. Removing the omentum as well as depleting resident omental macrophages lead to decreased survival of TCs within the peritoneum (Etzerodt *et al.*, 2020; Krishnan *et al.*, 2020). Therefore, in the case of EOC omentectomy is often combined with debulking of the tumor material to reduce metastasis.

1.4.3 Tumor immune microenvironment in epithelial ovarian cancer

EOC tumor growth highly depends on the immune context and is associated with a chronic inflammation (Clendenen *et al.*, 2011). Immune cell infiltration in EOC correlates with worse patient prognosis. Major components of the EOC TIME are macrophages, neutrophils, T cells as well as NK cells, which could have a tumor promoting or suppressing role within the TIME (Baci *et al.*, 2020). The infiltration of pro-tumorigenic TAMs into the TME of EOC is of striking importance for the immunosuppressive microenvironment and tumor progression (Bingle, Brown, & Lewis, 2002; Lewis & Pollard, 2006). Therefore, the contribution of other leukocytes for the progression of EOC is limited to clinical studies evaluating the overall survival as well as progression free survival with the infiltration of neutrophils, T and B cells.

The different immune cell populations, like macrophages, monocytes, neutrophils, B- and T cells can be distinguished by their expression of different surface markers within the peritoneal cavity in mice (**Table 1.1**).

Table 1.1: Cell surface markers of immune cells in peritoneal cavity of mice. CD: cluster of differentiation; MHC: major histocompatibility complex; LPM: Large peritoneal macrophages; IntPM: intermediate PM; SPM: Small PM; NA: not applicable.

Cell type	Subset	Marker
Macrophages		$CD45^+$; $CD11^{high}$; $F4/80^+$
	LPM	$CD45^+$; $CD11^{high}$; $F4/80^{high}$; $MHCII^{low}$
	IntPM	$CD45^+$; $CD11^{high}$; $F4/80^{int}$; $MHCII^{int}$
	SPM	$CD45^+$; $CD11^{high}$; $F4/80^{low}$; $MHCII^{high}$
Monocytes	N.A.	$CD45^+$; $CD11^{high}$; $Ly6C^+$
Neutrophils	N.A.	$CD45^+$; $CD11^{high}$; $Ly6G^+$
T cells	CD4	$CD45^+$; $CD3^+$; $CD4^+$
	CD8	$CD45^+$; $CD3^+$; $CD8^+$
B cells		$CD45^+$; $CD19^+/B220^+$; $MHCII^{high}$; $CD11b^{low}$

1.4.3.1 Immunosuppressive myeloid cells in epithelial ovarian cancer

TAMs are the most prominent immune cell population within the TME of EOC, which are up to 30 % of the total tumor ascites (Bingle *et al.*, 2002; Lewis & Pollard, 2006). As already mentioned, macrophages are plastic cells, whose activation and polarization is context dependent. TCs education of TAM induce an anti-inflammatory phenotype and therefore they promote tumor growth with an immunosuppressive microenvironment (Franklin & Li, 2016).

Co-culture *in vitro* experiments of TAMs with ovarian cancer cells increased the proliferative capacity of the TCs indicating an important pro-tumorigenic role of TAMs in this metastatic cancer (Carroll, Kapur, Felder, Patankar, & Kreeger, 2016). Further, *in vivo* studies on EOC, showed that the polarization of TAMs towards a pro-tumorigenic phenotype is promoted by the cholesterol depletion (Goossens, *et al.*, 2019) (**Fig. 1.9**). TCs educate TAMs towards an anti-inflammatory phenotype by secreting high molecular weight hyaluronic acid (HA). Binding of HA on surface receptors in TAMs, like CD44 and LYVE1 leads to cholesterol efflux resulting in a hypersensitivity towards IL4. This hypersensitivity further increases their immunosuppressive role and promotes tumor progression. The same study also highlights the role of recruited monocyte-derived macrophages over resident LPMs in the progression of EOC (Goossens, *et*

al., 2019). Using transgenic CX$_3$CR1 mice the authors could unravel the utmost role of newly recruited monocyte-derived macrophages in the tumor progression of EOC. This goes in line with the impact of CCR2-dependent recruitment of monocytes into the peritoneal cavity (Lee *et al*., 2009). Interestingly, the immunosuppressive phenotype was observed 21 days after TCs inoculation. Earlier time-points rather show an inflammatory gene signature with goes in line with the first phase of cancer immunoediting (Goossens, *et al*., 2019).
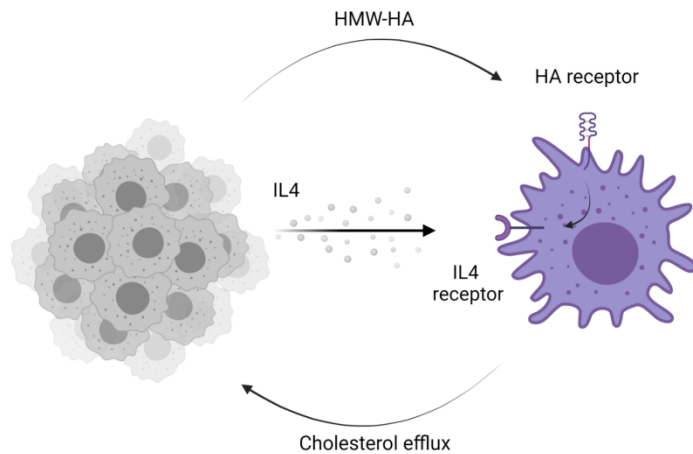
Figure 1.9: Re-education of tumor associated macrophages by epithelial ovarian cancer cells. Epithelial ovarian cancer cells secrete high molecular weight hyaluronic acid (HMW-HA), which gets recognized by HA receptors on surface of tumor-associated macrophages. These effects results in a hypersensitivity towards IL4, also secreted by EOC tumor cells as well increased in cholesterol efflux promoting tumor growth. Adapted from (Goossens, *et al*., 2019).

One of the genes described by several studies *in vitro* and *in vivo* to play an important role in macrophage polarization towards the anti-inflammatory, pro-tumorigenic phenotype is the invariant chain of MHCII complex (CD74) and its ligand macrophage migration inhibitory factor (MIF) (Bernhagen *et al*., 2007; Ghoochani *et al*., 2016). Expression of CD74 in TAM is important for the immunosuppressive TME and correlates with poor prognosis for ovarian cancer patients (Cortes *et al*., 2017). In addition, mouse studies on targeting CD74 on APC in melanoma showed to decrease immunosuppressive function and thereby increased T cell activation with a benefit on overall survival (Figueiredo *et al*., 2018). Nevertheless, there is still a lack of a better understanding of the TME and macrophage infiltration in ovarian cancer.

1.4.3.2   Tumor infiltrating lymphocytes in epithelial ovarian cancer

As already mentioned, the contribution of lymphocytes in the progression of EOC is limited to clinical studies. Lymphocytes and especially infiltration of tumor-associated T cells into the highly immunogenic TME of EOC is generally associated with better patient outcome (Wang, Zou, & Liu, 2018). Although, the consequence of infiltration of T cells and cytotoxic T cells is not clear. Infiltration of cytotoxic T cells in HGSC correlates with decreased disease-free survival (Yildirim *et al*., 2017), whereas the amount of cytotoxic T cells within epithelial tumor islets in the omentum does not increase overall survival of EOC patients (Wang *et al*., 2018). The tumor-infiltrating T cells express several immune checkpoint molecules, like PD-1, lymphocyte-activation gene 3 (LAG-3), T-cell immunoglobulin and mucin domain 3 (Tim-3) and CTLA-4 in EOC (Salas-Benito *et al*., 2020).

Only few studies in B lymphocytes and their role in EOC are reported, but there is evidence that infiltration of B cells into the tumor areas of omental metastasis are associated with worse prognosis for ovarian cancer patients (Lee & Wang, 2020).

1.4.4 Treatment options of epithelial ovarian cancer

The classical therapeutically approach include the debulking of the tumor mass by removing the tumor tissue combined with chemotherapy depending on the stage of the tumor (Wang *et al.*, 2018). Current therapy approaches also include anti-angiogenesis therapy, poly-ADP-ribose polymerase (PARP) inhibitors, inhibition of growth factor signaling, folate receptor inhibitors and immune therapy to improve the therapeutic outcome (M. Yousefi, 2020). Anti-angiogenesis therapy using monoclonal blocking antibodies of VEGF (bevacizumab) (Park & Choi, 2016) in combination with chemotherapy improved patient survival in clinical phase III studies (Conteduca *et al.*, 2014). In EOC, VEGF expression is a clinical marker, which is related to tumor burden and stage of the disease. VEGF may increase vascular permeability within the peritoneal cavity and play a role in the formation of ascites in metastatic tumor stages (Chambers, MacDonald, Schmidt, Morris, & Groom, 2000; van Baal *et al.*, 2018; Weidle, Birzele, Kollmorgen, & Rueger, 2016). Moreover, bevacizumab is the only approved anti-angiogenesis therapy approach but more agents are under consideration. For example, peptide-based anti-angiogenesis molecules (aflibercept, AMG-706) as well as small molecule inhibitors targeting as well receptor tyrosine kinases like VEGFR.

As described before, immune cells play an important role in EOC progression which is characterized by a predominant infiltration of monocyte-derived macrophages. Therefore, monocyte-derived macrophages promote the tumor growth, invasion and metastasis by creating an immunosuppressive microenvironment. Several studies on immunotherapy in EOC showed positive effects to increase patient survival. Combination of immune check blockade with classical therapies are promising.

1.4.4.1 Targeting tumor-associated macrophages in epithelial ovarian cancer

Several immunotherapy approaches targeting TAMs are already translated from *in vivo* mouse models into clinical trials. TAMs are the predominant immune cell population and therefore, targeting specifically monocyte-derived macrophages in EOC could improve standard care in the treatment of ovarian cancer. There are three different main routes to target TAMs in EOC progression. Firstly, targeting the infiltrations of monocyte-derived macrophages in the TME, second targeting the phenotype of TAMs and lastly, targeting the interaction with effector cells, like PD-1/PD-L1 interactions.

Inhibition of colony-stimulating factor 1 (CSF1) receptor not only impact on the TAM phenotype it also showed a reduction of infiltrating TAM in the TME. Small molecule inhibitor and antibodies targeting the receptor of CSF1 on macrophages showed reduced monocyte-derived macrophage infiltration in the TME of EOC improving patients outcome (Nowak & Klink, 2020). However, targeting TAMs using CSF1 in brain tumors, showed that TCs could overcome this inhibition and re-educated TAM (Quail & Joyce, 2017). Therefore, studies on BRCA-mutated breast cancer showed that combined therapies of PARP inhibition CSF1 blocking impact on the immunosuppressive phenotype of TAM (Mehta *et al.*, 2021). Several mouse studies showed that monocyte recruitment into the TME of EOC is CCR2-dependent (Goossens, *et al.*, 2019). Moreover, blocking CCR2 in kidneys of hypertensive rats (Alsheikh *et al.*, 2020) as well as in PDAC (Sanford *et al.*, 2013) reduced the number of infiltrating immune cells and led to increased anti-tumor immune response. Taken together, blocking monocyte recruitment could be a promising pharmacological approach in treatment of EOC. In this regard, several clinical studies on antibodies against CCR2 in combination with chemotherapies already show some beneficial effects on patients in advanced tumor stages. In line with the *in vivo* mouse models, which showed decreased infiltration of monocyte-derived macrophage infiltration into the TME of EOC (Nowak & Klink, 2020).

Targeting polarization of TAM in *ex vivo* mouse model studies showed that isolated pro-tumorigenic TAMs could be polarized with LSP towards anti-tumorigenic TAMs with decreased immunosuppressive capacity (Nowak & Klink, 2020). Moreover, neutralization of IL4, a common anti-inflammatory and pro-tumorigenic factor is a reasonable approach to target re-polarization of TAMs. Unfortunately, humanized anti-IL4 monoclonal antibody, pascolizumab treatment showed only minor benefits in clinical studies of asthma patients (Gibeon & Menzies-Gow, 2012). However, using the approach of blocking the receptor of IL4 showed beneficial effects in atopic dermatitis patients (Beck *et al*., 2014). Similar approach is used to inhibit IL4R+ cells in ovarian cancer using a drug which fused IL4 to a *pseudomonas* exotoxin (MDNA55) to target TCs. Pro-tumorigenic TAM also express PD-L1 promoting an immune suppressive TME. Recently, also the expression of the receptor for phosphatidylserine (PS), Tim4 on peritoneal resident macrophages is identified to inhibit effector T cell function and effecting immunotherapy in carcinomas. Tim4 is only expressed by long-term peritoneal macrophages and blocking of Tim4 could be a new therapeutically approach to targeting regulatory activity within the TME (Rodriguez & Ruffell, 2021). Therefore, using immune checkpoint inhibition by blocking PD-1/PD-L1 T cell-macrophage interaction could be a beneficial approach in chemotherapy resistance patients (Nowak & Klink, 2020).

Moreover, a more specific treatment approaches use nanoparticles to target TAMs. Nanoparticles are small compounds ≤100 nm, which are designed to deliver drugs with reduced side effects. It has been recently published, that nanoparticles get selectively absorbed by TAMs after i.p. administration. *In vivo* mouse studies on ovarian cancer showed that nanoparticles accumulated efficiently in TAMs resulting in new strategies to target selectively TAMs within the TME (Haber *et al*., 2020; Klichinsky *et al*., 2020).

1.5   Aim

The overall goal of this PhD project was to analyze the crosstalk between ECs, TCs and immune cells with a strong focus on endothelial Notch signaling. Notch signaling is a conserved cell-to-cell communication system which is frequently deregulated in human malignancies. Notch ligands are present on ECs, immune and TC. ECs are a major component of the TME not only because of their important role in angiogenesis. Our group could show that activated Notch1 receptors (N1ICD) are frequently expressed in ECs of human tumors and that sustained activation of N1ICD in ECs induced EC senescence, expression of chemokines and VCAM1 to promote infiltration of immune cells, transmigration of TCs and metastasis (Wieland *et al*., 2017). The hypothesis of this thesis is that TCs induce Notch signaling in ECs to shape the immunosuppressive phenotype of the TME. Therefore, the subject of my PhD thesis is to further analyze and characterize the myeloid cell infiltration into the TME mediated by endothelial Notch signaling and, in more detail, to unravel the role of endothelial Notch signaling behind the recruitment and activation of monocyte-derived macrophages.

2   Results

2.1   Role of endothelial Notch signaling on myeloid cell infiltration in tumors

2.1.1   Notch1 activation associates with myeloid cell in human primary ovarian cancer

Human tumors frequently have activated Notch1 receptors in tumor endothelial cells (ECs) (Wieland *et al.*, 2017). To focus further on the effect of Notch1 activation on immune cell recruitment I analyzed human tissue microarrays (TMA) of ovarian cancer samples which were stained for cleaved Notch1, a marker for Notch1 activation, and CD33, a marker for human myeloid cells. While analyzing 50 different TMA samples, I observed that the only few samples that showed low cleaved Notch1 expression also showed a mild CD33$^+$ cell infiltration. In contrast, in the groups of intermediate and high cleaved Notch1 expression the amount of CD33$^+$ cell density was substantially higher (**Fig. 2.1**). This analysis suggested, that TCs lead to an activation of Notch1 in ECs with an impact on the myeloid cell infiltration in human primary ovarian cancer patient samples.
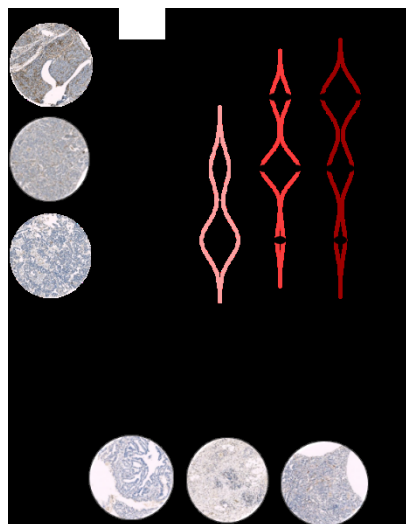
Figure 2.1: Levels of cleaved Notch1 show a positive association with myeloid cell infiltration in tissue microarray samples from ovarian cancer patients. Representative hematoxylin and eosin (H&E) staining and analysis of cleaved Notch1 expression (low, intermediate (int) and high) with representative images correlating with infiltrating myeloid cells, stained with CD33 and classified as 1 (low), 2 (intermediate) and 3 (high). (n=50)

2.1.2   Loss of endothelial Notch signaling leads to decreased myeloid cell recruitment into the tumor microenvironment in mice

Activation of endothelial Notch1 signaling by TCs correlates with increased immune cell infiltration as well as increased metastatic potential in a mouse model (ecN1ICD mice) (Wieland *et al.*, 2017). Furthermore, I observed a relationship between cleaved Notch1 and infiltrating myeloid cells into human ovarian cancers (**Fig. 2.1**). Therefore, I investigated the role of endothelial Notch signaling on myeloid cell infiltration using a subcutaneous (s.c.) model of LLC tumor growth in a loss-of-function (*Rbpj*$^{i\Delta EC}$) model. These mice allow tamoxifen-induced inhibition of canonical Notch signaling in ECs by deleting its nuclear transducer RBPJ. TCs were injected one week after tamoxifen administration (**Fig. 2.2A**) because previous data from the group showed an effect on tumor volume at later time points. Moreover, tumor volume decreased in ecN1ICD mice, which was most likely due to disturbed angiogenesis (Appendix **Fig. 5.1**). Consequently, I analyzed the primary tumors and infiltration of myeloid cells at a time point where no difference in tumor volume was observed to ensure the effects of angiogenesis did not impact on the TME (**Fig. 2.2.B**). Nevertheless, at that early time point after tumor inoculation I observed an increased vessel density by immunohistochemistry of CD31$^+$ cells (**Fig. 2.2.D**) as well by flow cytometry staining of CD31$^+$ cells (**Fig. 2.2.E**) in *Rbpj*$^{i\Delta EC}$ compared to control mice. I also observed a significant increase of vessel coverage quantified by Desmin$^+$ cells covering ECs (**Fig 2.2.G**).

In summary, loss of endothelial Notch signaling affects the tumor vasculature already at early time point of tumor progression.
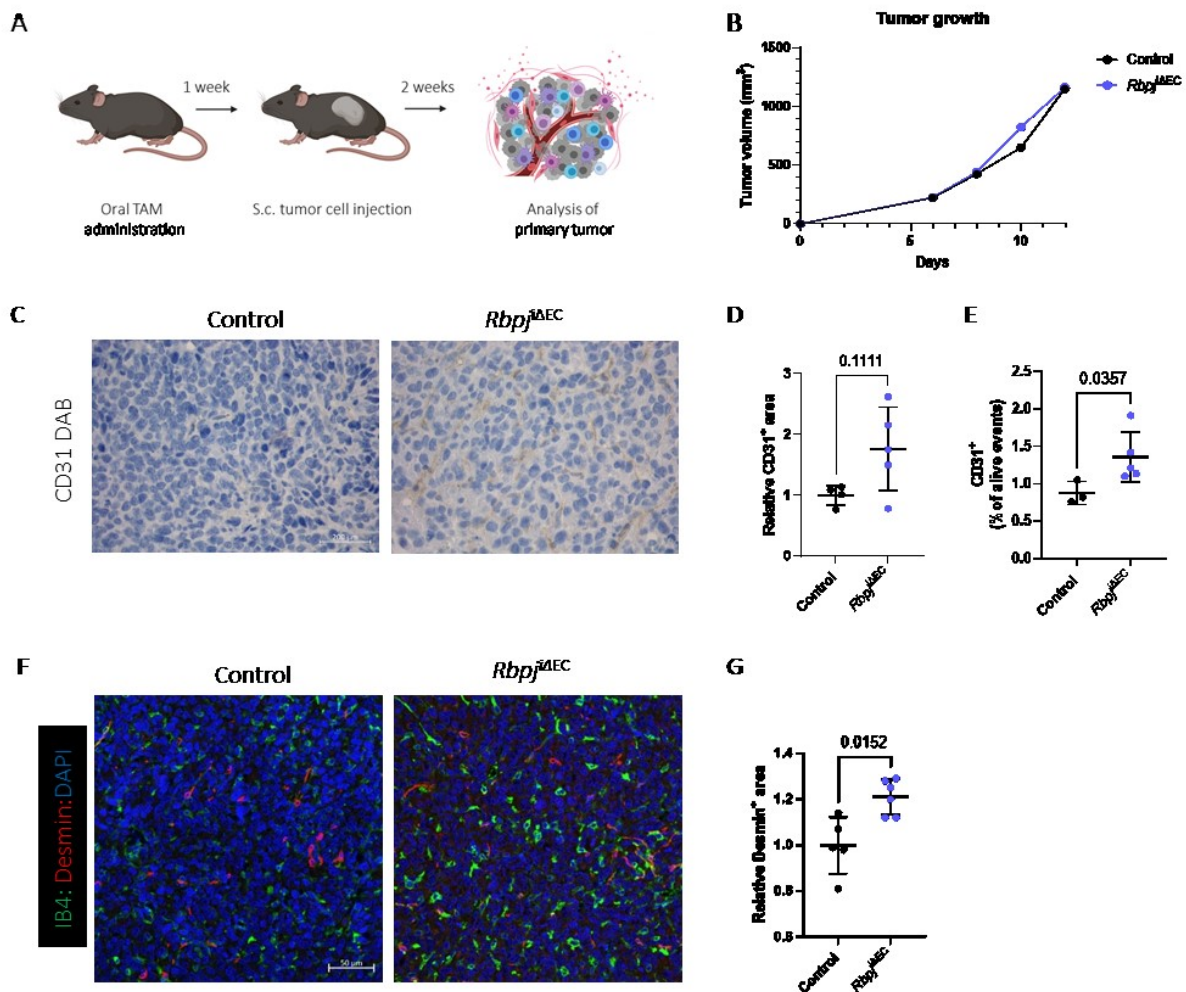
Figure 2.2: Loss of endothelial Notch increases vessel density in a subcutaneous tumor model. **A** Workflow of subcutaneous (s.c.) LLC tumor model. One week after gene recombination induced by tamoxifen, tumor cells were injected and tumor growth was monitored. **B** Tumor growth of LLC tumors in loss-of-function (*Rbpj*$^{i\Delta EC}$) and control mice (n=5; mean). **C** Analysis of tumor endothelium by of CD31$^+$ DAB staining with representative images and quantification (**D**). **E** Flow cytometer analysis of CD31$^+$ cells relative to alive cells. **F** Representative images of vessel coverage by immunohistochemistry staining of isolectin (IB4; green) and Desmin (red) analysis and quantification (**G**) (n=5; mean±SD; two-tailed, unpaired Mann-Whitney U-test).

To further address the question if loss of endothelial Notch signaling impact on the myeloid cell infiltration into the TME, I analyzed the immune cell composition of the s.c. LLC tumor model. Remarkably, even though I detected an increase in vessel density, I observed decreased immune cell infiltration in the primary tumor (**Fig. 2.3.A**). Depletion of endothelial Notch signaling resulted in a significantly decreased infiltration of myeloid cells (**Fig. 2.3.B**) into the TME, which were further characterized as monocyte-derived macrophages (**Fig. 2.3.C**). Therefore, the data suggest that inhibition of TC-induced education of the tumor vasculature by Notch1 activation, reduce the recruitment of myeloid cells into the TME.
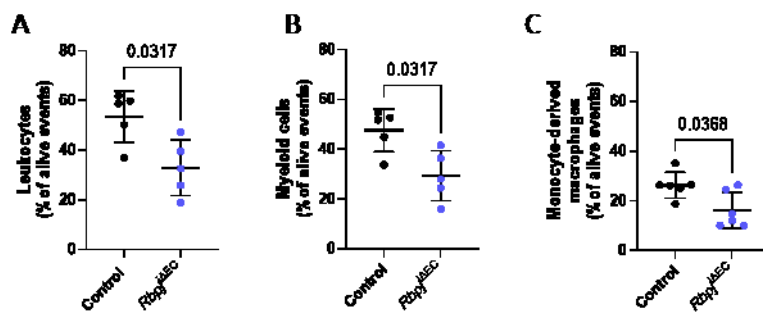
Figure 2.3: Loss of endothelial Notch siganling decreases myeloid cell infiltration into the tumor microenvironment. Analysis of immune cells characterized by CD45$^+$ (**A**), myeloid cells (**B**), characterized by CD45$^+$ and CD11b$^+$ expression and monocyte-derived macrophages (**C**), characterized by CD45$^+$, CD11b$^+$, F4/80$^+$ and CCR2$^+$ expression within the tumor microenvironment of *Rbpj*$^{i\Delta EC}$ mice compared to controls (n=5; mean±SD; two-tailed, unpaired Mann-Whitney U-test).

2.2   Effects of Notch1 activation on the endothelial cell phenotype

2.2.1   Endothelial Notch1-regulate secretion of angiocrine factors

Immune cell recruitment is tightly regulated by chemokine expression, for example by inflamed tissue or TCs, to recruit immune cells into the microenvironment. Activation of endothelial Notch signaling leads to the secretion of angiocrine factors (Wieland *et al*., 2017). Therefore, to understand how the activation of Notch in ECs could impact on the recruitment of immune cells I evaluated chemokine expression upon Notch1 activation. I infected human umbilical vein ECs (HUVECs) with adenovirus constructs to overexpress N1ICD or GFP, as control. HUVECs with an overexpression of N1ICD showed a significant increase of classical Notch target genes, *HEY1, HES1* and *HES5* (**Fig. 2.4.A**) as well as several chemokines and cytokines, like *CCL1*, *CCL21*, *CXCL2* and *IL33* on mRNA level (**Fig. 2.4.B**). Analysis of the chemokine expression via chemokine profiler (**Fig. 2.4.C to D**), enzyme-linked Immunosorbent assay (ELISA; **Fig. 2.4.E**) and western blot (**Fig. 2.4.F**) validated the induction of CCL1, CXCL2, CXCL12 and IL33 on protein level. The induction of *Cxcl2* by endothelial Notch was further validated in whole tissue lysates from gain-of-function mice compared to their littermate control. In contrast, the expression of the other chemokines and cytokines such as *Ccl1, Ccl21, Cxcl12* and *Il33* did not show significant changes in these conditions (**Fig. 2.4.E**). Taking together, results indicate that the activation of Notch1 in ECs is able to induce cytokine and chemokine expression.
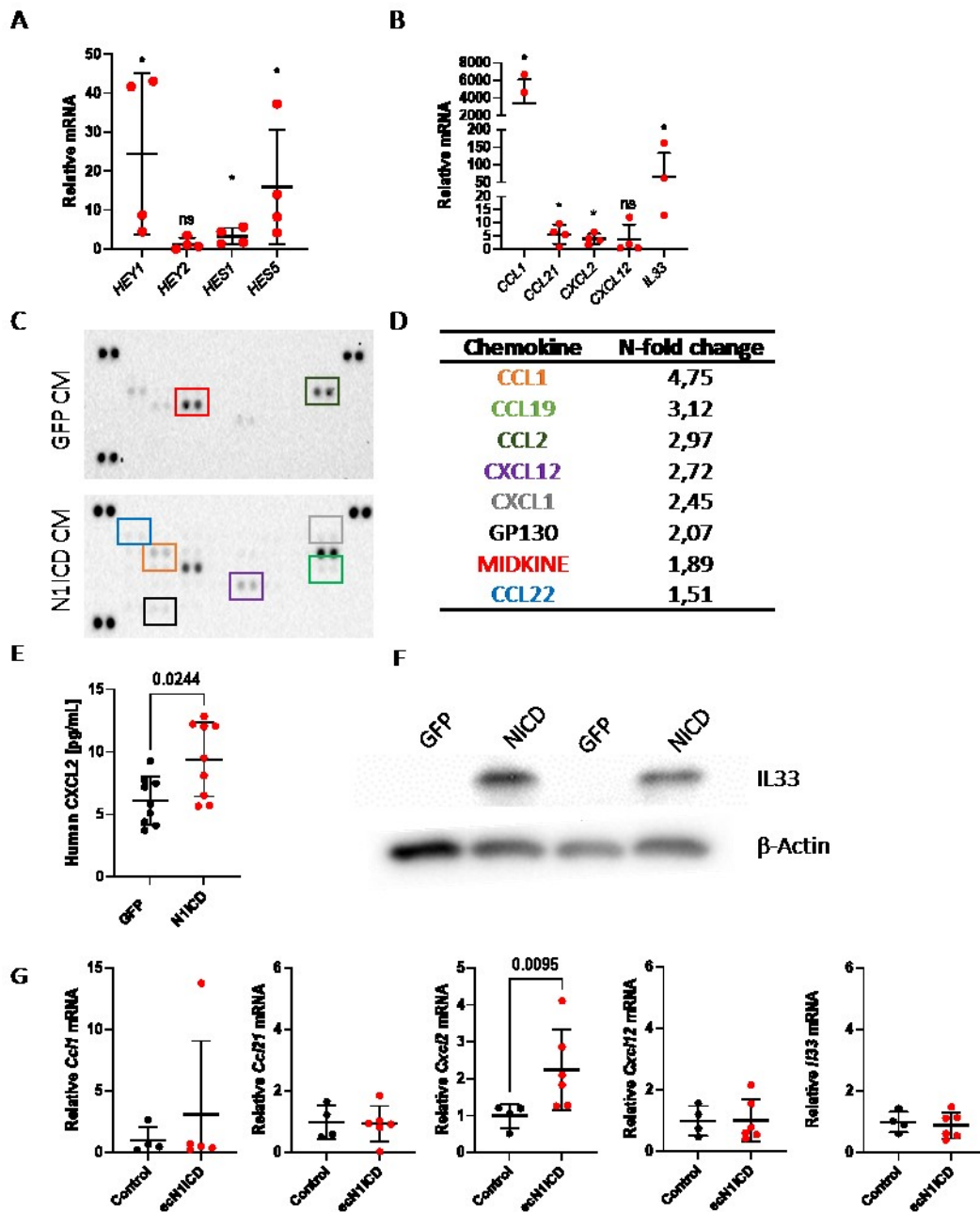
Figure 2.4: Overexpression of N1ICD induces cytokine and chemokine expression in human primary endothelial cells. Analysis of classical Notch targets genes (**A**) and several cytokines (**B**) via RT-qPCR (n=4; mean±SD; two-tailed, unpaired students T-test; *p≤0.05) in human umbilical vein endothelial cells (HUVEC). **C** Chemokine profiling assay of cell culture supernatant (CM: conditioned medium) of HUVEC infected with N1ICD and GFP, as control and quantification of increased chemokines (n=2) (**D**). **E** Enzyme-linked immunosorbent assay (ELISA) of CXCL2 of cell culture supernatant from HUVEC infected with N1ICD and GFP as control (n=9; mean±SD; two-tailed, unpaired Mann-Whitney U-test). **F** Western blot of IL33 and actin (as control) in HUVEC infected with N1ICD or GFP as control (n=2). **G** mRNA expression in whole peritoneal fat tissue from ecN1ICD and control mice (n≥4; mean±SD; two-tailed, unpaired Mann-Whitney U-test).

To further investigate if the regulation of chemokines by N1ICD is canonical through RBPJ, or non-canonical, I performed a CRISPR-Cas9 mediated knock-out of *RBPJ*. First, I confirmed the successful depletion of RBPJ on protein level (**Fig. 2.5.A**). Regulation of chemokines via RBPJ was analyzed with a gene expression cytokine array, which showed a downregulation of several genes including *CXCL2* (**Fig. 2.5.B**). The decrease of *Cxcl2* expression upon *Rbpj* depletion in ECs was further validated with whole tissue lysates from loss-of-function (*Rbpj*$^{i\Delta EC}$) mice compared to their littermate controls (**Fig. 2.5.C**). Again, the chemokines and cytokines *Ccl1, Ccl21, Cxcl12* and *Il33* did not show changes in mRNA expression. These obtained results suggest, that CXCL2 could be a novel canonical Notch1 target gene regulated by the N1ICD/RBPJ-axis in ECs.

Relative mRNA	N-fold change
STAT3	1,74
CXCL1	0,62
HIF1A	0,62
C5	0,62
MYD88	0,56
CXCL2	0,53
GDF5	0,50
JAK2	0,41
IL8	0,41
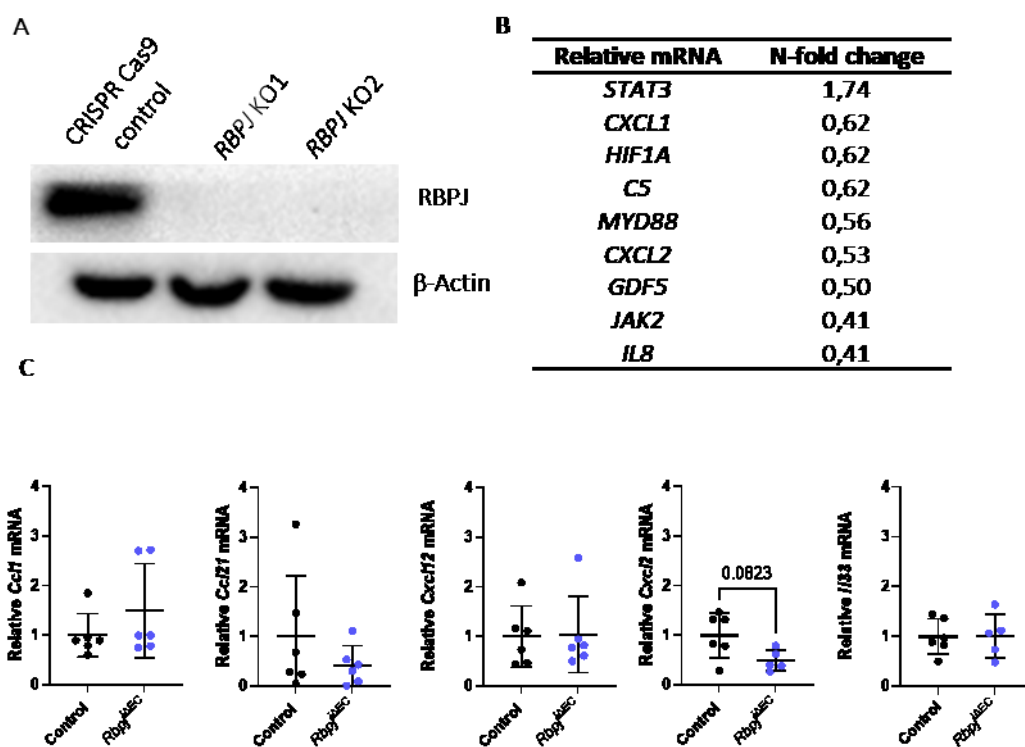
Figure 2.5: RBPJ knock-out in human umbilical vein endothelial cells decreases chemokine expression. **A** Western blot of RBPJ and actin (as control) in human umbilical vein endothelial cells (HUVECs) with CRISPR-Cas9 mediated knock-out (KO) of two different constructs and control. **B** Chemokine expression array of HUVEC with *RBPJ* KO compared to control (n=2). **C** mRNA expression in whole peritoneal fat tissue from *Rbpj*$^{i\Delta EC}$ and control mice (n≥4; two-tailed, unpaired Mann-Whitney U-test).

In order to analyze the regulation of CXCL2 by RBPJ-mediated Notch signaling, I performed a knock down of *CXCL2* in HUVECs and analyzed the protein expression upon N1ICD induction in ECs. Knock down of *CXCL2* by two different shRNA eliminated the induced chemokine expression by N1ICD (**Fig. 2.6.A**). To investigate and validate whether CXCL2 is a canonical Notch target gene, I performed *in silico* analysis of the promoter region. I found several RBPJ binding sites in the human and murine promoter regions of CXCL2 (**Fig. 2.6.B**). Moreover, N1ICD-induced *CXCL2* overexpression was abolished in *RBPJ* KO HUVECs quantified by RT-qPCR (**Fig. 2.6.C**). CXCL2 has serval functional homologs like CXCL1, CXCL5 and CXCL8, which also all bind to the same receptor, CXCR2. Therefore, I also analyzed if the expression of CXCL2 analogs is mediated by endothelial Notch signaling. I could not observe any Notch1/RBPJ-dependent gene expression in any of these chemokines (**Fig 2.6.D**). I further also analyzed the induction of *CCL1, CCL21, CXCL12, IL33* as well as *CCL2* upon N1ICD expression and *RBPJ* depletion in HUVEC. Several of

the cytokines of interest showed as well canonical Notch-RBPJ regulation, for example *CCL1, CXCL12* and *IL33* (**Fig. 2.6.E**). However, *CCL2* is induced by N1ICD (**Fig. 2.4.D**) but did not show any regulation by RBPJ (**Fig. 2.6.F**). Taken together, I could identify and validate several novel canonical Notch1 angiocrine factors, especially CXCL2 is one of the most regulated.
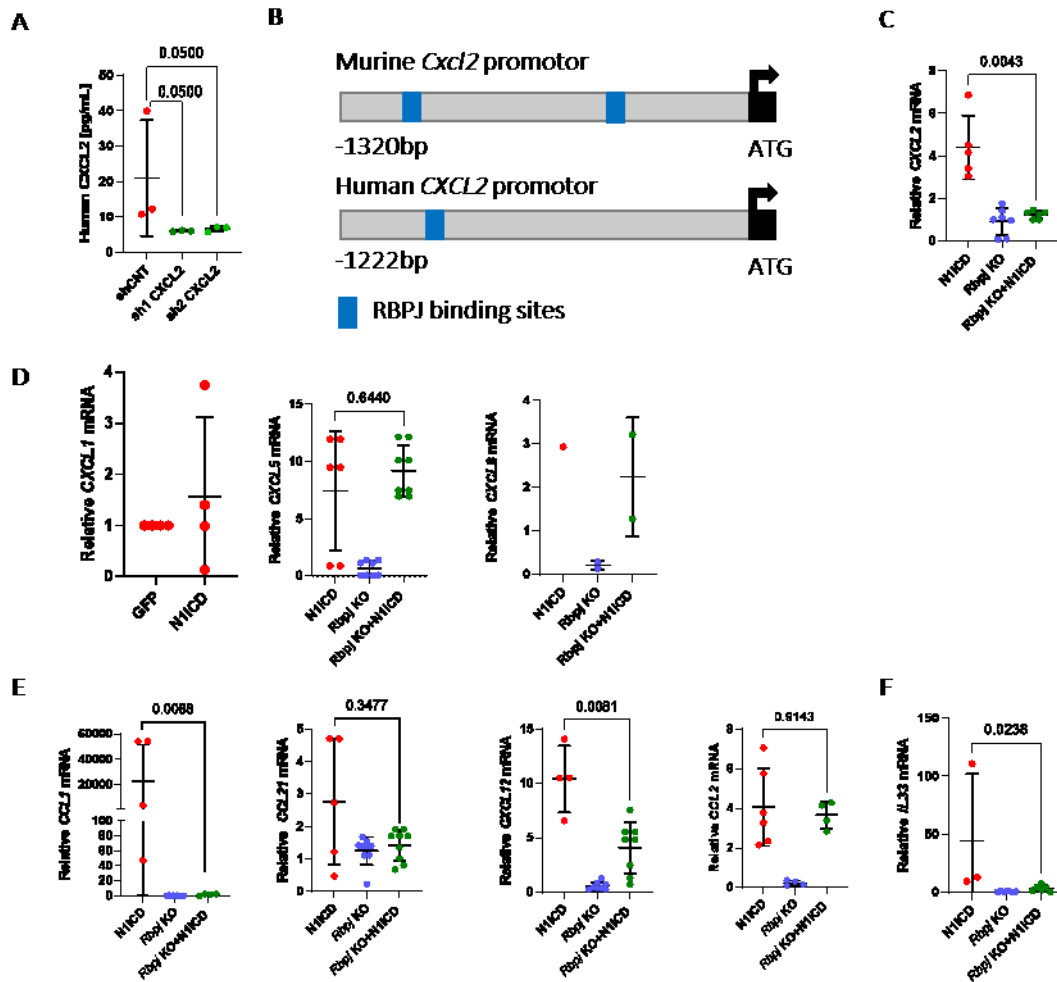
Figure 2.6: Endothelial Notch1 regulates CXCL2 expression. **A** CXCL2 Enzyme-linked immunosorbent assay (ELISA) of cell culture supernatants of two different *CXCL2* knock down construct infected with N1ICD and GFP, as control in human umbilical vein endothelial cells (HUVEC) (n=3; mean±SD; two-tailed, unpaired Mann-Whitney U-test). **B** Scheme of RBPJ binding in CXCL2 promotor region in murine and human genome. **C-F** mRNA of CXCL2 (**C**); CXCL1, CXCL5, CXCL8 (**D**); CCL1, CCL21, CXCL12; IL33 (**E**) and CCL2 (**F**) expression upon NICD overexpression, knock-out of *RBPJ* and combination in HUVEC (n≥3; mean±SD; two-tailed, unpaired Mann-Whitney U-test).

2.2.2 Effects of Notch activation on lymphatic endothelial cells

Chemokine expression by ECs is mainly associated with the lymphatic vasculature. Lymphatic EC (LEC) secrete chemokines to guide immune cells through the lymphoid organs (Lucas & Tamburini, 2019). For this reason, I investigated whether endothelial Notch signaling affects the phenotype of lymphatic ECs. I studied the phenotype of the tumor vasculature within tumors s.c. injected in ecNICD gain-of-function mice and I could not detect any differences in vessel density by CD31$^+$ staining (**Fig. 2.7.D**). Interestingly, I observed a significant increase of PROX1, a classical LEC marker in the TME of ecN1ICD mice compared to littermate controls (**Fig. 2.7.A**), whereas the other LEC markers, VEGFR3 and LYVE1, showed no differences (**Fig. 2.7.B to G**). Even through PROX1 is report to be a key regulator of LEC cell fate it is not only expressed by LEC. Moreover during tumor progression expression of PROX1 is changed within the TME because for example also some TCs are expressing PROX1 (Rudzinska & Czarnocka, 2020). Therefore, the observations suggest that the overall number of cells, which express PROX1 is increased in the TME upon overactivation of N1ICD in endothelium. However, the obtained results are not sufficient enough to make any conclusion regarding the LEC population within the TME of mice overexpressing N1ICD in the endothelium.
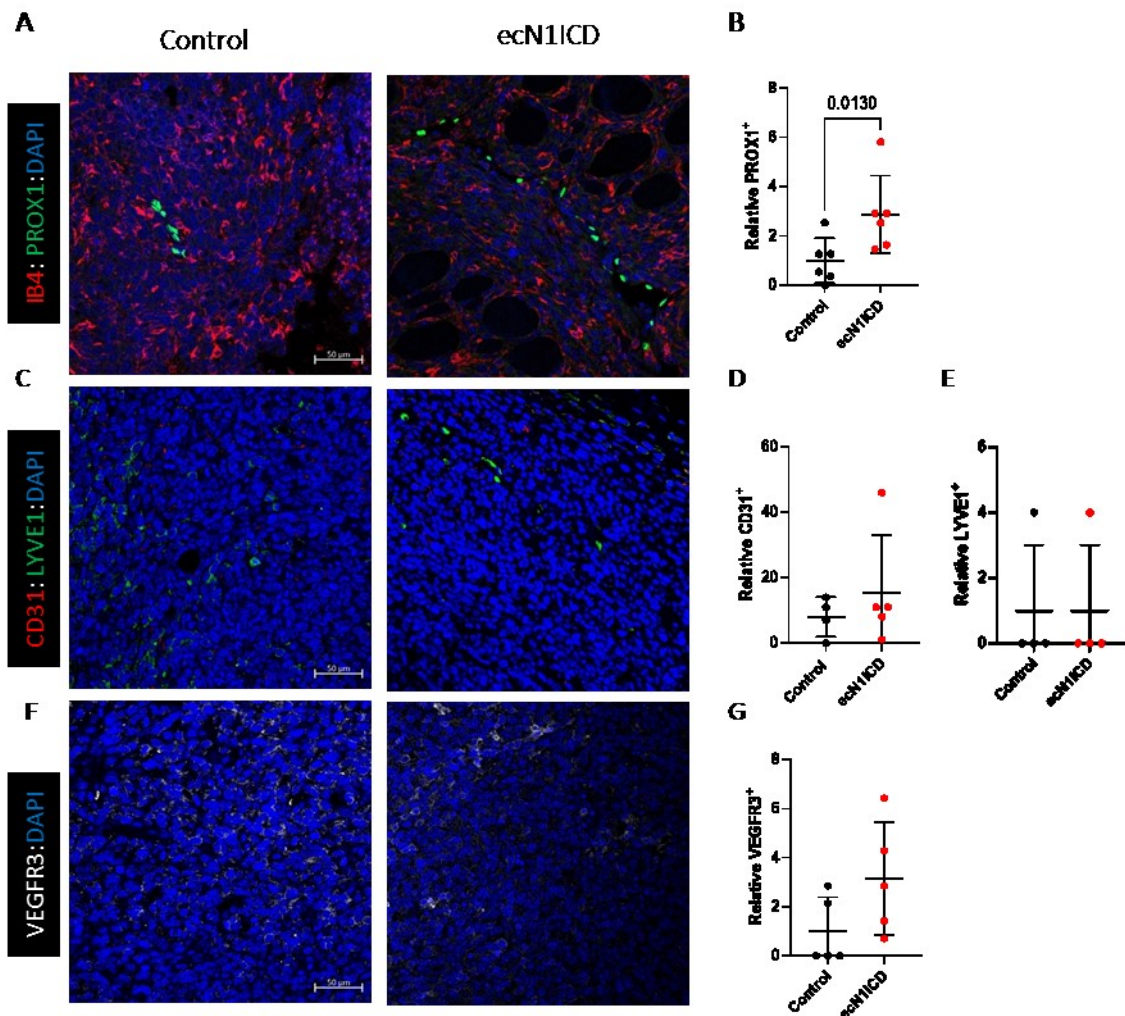
Figure 2.7: Increased Notch activation in tumor endothelium increases lymphatic endothelial cell marker PROX1 in subcutaneous tumor. Analysis of tumor endothelium in s.c. LLC model from gain-of-function mice compared to control using immunohistochemistry staining of PROX1, CD31, LYVE1 and VEGFR3. Representative images (**A**) and quantification of PROX1 (**B**). Representative images (**C**) and quantification of CD31 (**C**) and LYVE1 (**E**). Representative images (**F**) and quantification of VEGFR3 (**G**); (Tumor tissue kindly provided by Dr. Elfriede Wieland; n=5; mean±SD; two-tailed, unpaired Mann-Whitney U-test).

To further investigate, if N1ICD overexpression in ECs is sufficient to change the phenotype of blood EC towards LEC, I analyzed the expression of lymphatic EC markers in HUVEC upon N1ICD induction. I could observe an increase mRNA expression of *VEGFR3, LYVE1, PROX1* and *VEGFc* mRNA expression, (**Fig. 2.8.A**). Additionally, all LEC markers showed a correlation with N1ICD activation in HUVECs (**Fig. 2.8.B** to **D**). Taking together, I can conclude that the expression of the homeobox gene *PROX1* by an overexpression of N1ICD is not sufficient to acquire an accurate LEC phenotype in blood ECs.
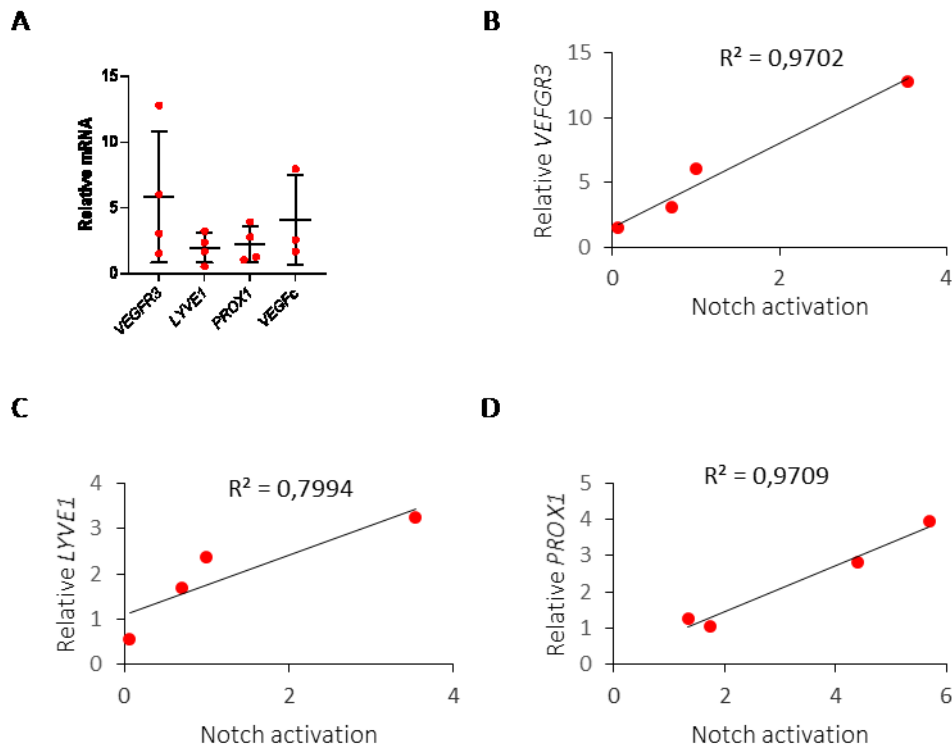
Figure 2.8: Activation of endothelial Notch signaling induces lymphatic endothelial cell marker PROX1. **A** Overexpression of N1ICD in human umbilical vein endothelial cells (HUVEC) and analysis of *VEGR3, LYVE1*, *PROX1* and *VEGFc* mRNA fold change relative to control (n=4; mean±SD; two-tailed, unpaired students T-test; *p≤0.05) and correlation of mRNA induction to Notch1 activation (Hey2/Hes1) (**B** to **D**; n=4).

It is worth noting, that recombination and overexpression of N1ICD in the gain-of-function mouse model is induced by tamoxifen administration only in cells, which express VE-Cadherin. VE-Cadherin is a broad ECs specific marker, which is not only expressed by blood ECs but also by LEC (Hagerling *et al*., 2018). To address the question of whether PROX1 staining is increased due to an increased proliferation of LEC after recombination and overexpression of N1ICD, I also investigated the effects of N1ICD overexpression on cultured LEC. Human dermal lymphatic ECs (HDLECs) showed an increase of the chemokines, *CCL1, CCL21*, *CXCL2, CXCL12* and the cytokine *IL33* (**Fig. 2.9.B**) upon successful induction of N1ICD signaling (**Fig. 2.9.A**). I further analyzed the consequence of the depletion of the transcription factor *RBPJ* using CRISPR-Cas9 mediated knock-out on HDLEC and I observed a significantly decrease of those same genes with both different *RBPJ* KO CRISPR-Cas9 constructs (**Fig. 2.9.C**). Interestingly, analyzing the mRNA expression of proliferation marker of LEC (Ducoli *et al*., 2021; Yang *et al*., 2017), I indeed observed changes between the different groups. The expression of *KLF4* and *LYMPHOTOXIN b* (*LTb*) was significant increased upon N1ICD induction (**Fig. 2.9.D**) and decreased in HDLEC with *RBPJ* KO (**Fig. 2.9.E**). However, additional work will have to be performed to elucidate and characterize these implications on the blood as well as the lymphatic blood system.
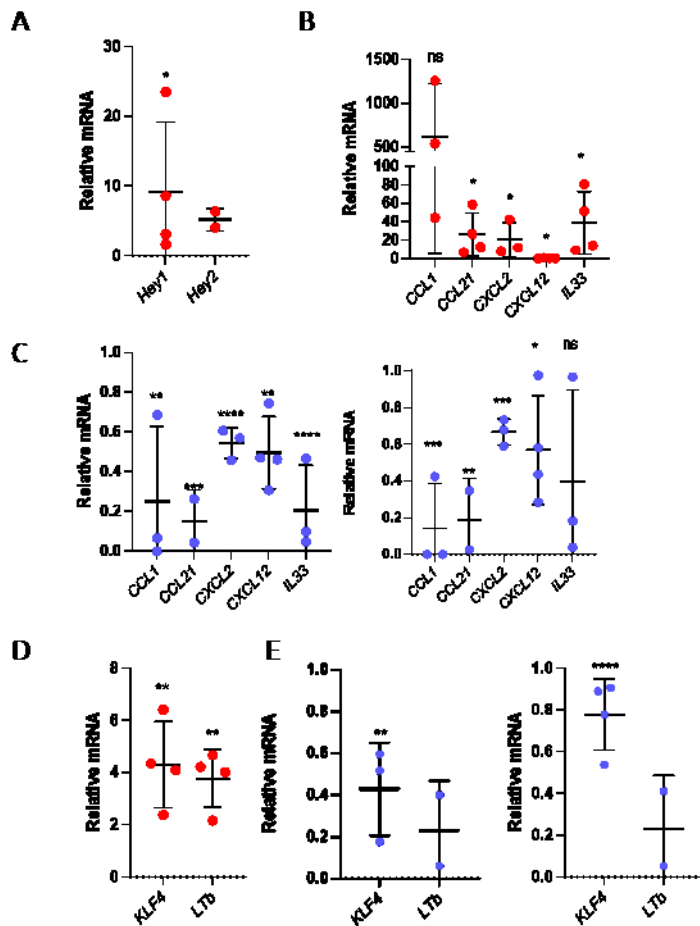
Figure 2.9: Overexpression of N1ICD in human lymphatic cell induces increased expression of cytokines and survival factors. **A** RT-qPCR analysis of Notch target genes (*HEY1* and *HEY2*) after N1ICD overexpression relative to control in chemokine and cytokine expression in human dermal lymphatic endothelial cells (HDLEC) (**B**). **C** Analysis of chemokine and cytokine expression (*CCL1, CCL21, CXCL2, CXCL12* and *IL33*) in HDLEC with *RBPJ* KO with two different CRISPR-Cas9 constructs relative to control. **D-E** Analysis of survival markers (*KLF4* and *LYMPHOTOXIN b* (*LTb*)) of HDLEC overexpressing N1ICD (**D**) and *RBPJ* KO (**E**) relative to control. (n≥2; mean±SD; unpaired, two-tailed students T-test).

2.3   Endothelial Notch signaling impacts on metastatic tumor growth

As mentioned before, endothelial Notch1 activation promotes metastasis (Wieland *et al.*, 2017), whereas loss of endothelial Notch results in reduced metastatic potential in a s.c. metastatic melanoma model (Donovan *et al.*, 2019). Therefore, I used the model of metastatic EOC by injecting murine ID8 cells i.p. to study the role of endothelial Notch1 signaling on tumor progression and immune cell recruitment in a well-established model of metastatic tumor growth. This model allows the analysis of the effect of endothelial Notch signaling on tumor progression and immune cell recruitment which is largely independ of tumor angiogenesis in this particular model. After three weeks of tamoxifen administration TCs were injected in the peritoneum of the mice and tumor burden as well as immune cell infiltration was evaluated after four weeks of tumor growth (**Fig 2.10.A**). When EOC cells invade the peritoneum during metastatic spread, they settle on the omentum (**Fig. 2.10.B**) and interact with different cells types within the microenvironment resulting in an increased tumor growth rate (Etzerodt *et al.*, 2020).
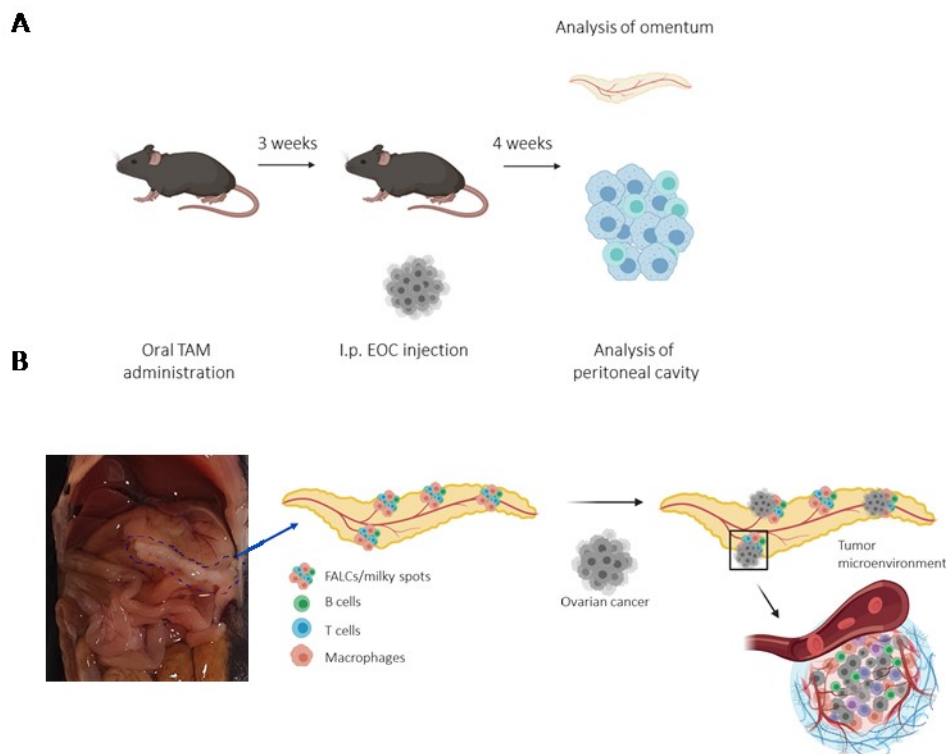
Figure 2.10: Model of metastatic epithelial ovarian cancer. **A** Workflow of metastatic epithelial ovarian cancer. **B** Localization of the omentum in the peritoneal cavity of mice (blue line) and model of spreading and proliferation of epithelial ovarian cancer cells.

2.3.1 Endothelial Notch signaling pre-conditions a metastatic niche for epithelial ovarian cancer

To determinate the contribution of the tumor endothelium on tumor progression, I analyzed the omental vasculature with and without the presence of an abdominal tumor in the gain-of-function as well as loss-of-function model compared to corresponding controls. Firstly, analyzing the vessel density in the omentum with and without tumor in the gain-of-function (ecN1ICD) model did not show any differences in vessel density quantified by CD31$^+$ cells (**Fig. 2.11.B**). Interestingly, when I had a closer look, I observed an increased expression of VCAM1$^+$ ECs. This is in line with the fact that VCAM1 is a known Notch1 target gene in ECs (Nus *et al.*, 2016; Verginelli *et al.*, 2015; Wieland *et al.*, 2017). There is a tendency of more VCAM1$^+$ omental ECs in the gain-of-function model compared to their littermate controls (**Fig. 2.11.C**). Additionally, I also observed an increase of VCAM1$^+$ ECs in tumor-bearing mice, control or ecN1ICD, compared to mice without tumor, indicating that tumor growth is enough to induce this gene in ECs, probably through Notch activation (**Fig. 2.11.C**). Taking together, the data show that tumor-mediated Notch activation in omental endothelium leads to the induction of Notch-induced VCAM1 expression.
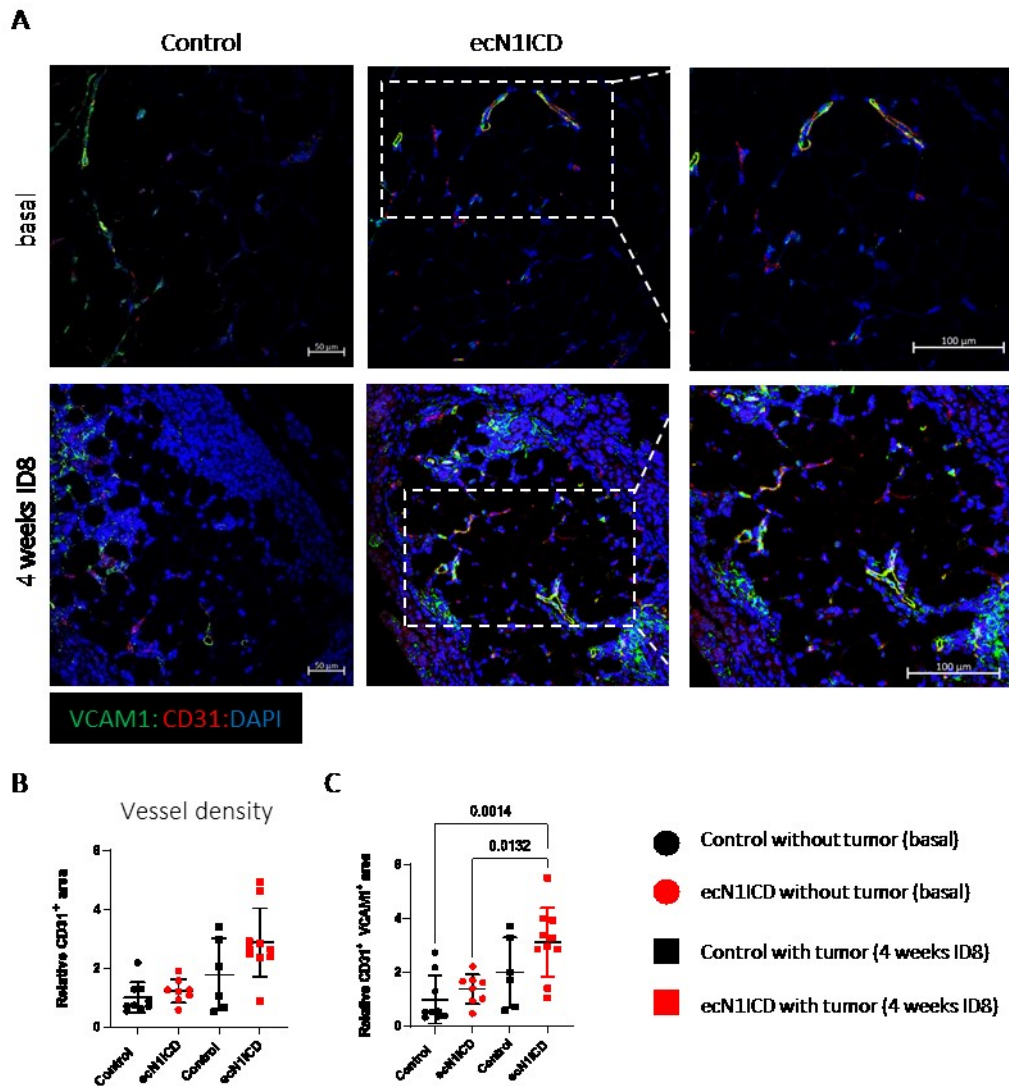
Figure 2.11: Vasculature of the metastatic niche in the omentum with and without tumor in the gain-of-function model. A Representative images and increased magnification of immunohistochemistry staining for VCAM1 (green), CD31 (red) and DAPI (blue) in omentum of EC-specific Notch gain-of-function and control mice with and without tumor. Quantification of vessel density (**B**) and VCAM1+ endothelial cells (**C**); (n≥5; two-way Anova, multiple comparison).

TC educate the endothelium by activating Notch1, which canonical signaling pathway is mediated by RBPJ binding. Therefore, I also analyzed the contribution of loss of endothelial Notch signaling on the endothelium in the metastatic niche. Analyzing the vessel density in omentum of *Rbpj*$^{i\Delta EC}$ mice with and without tumor injection, I could observe a significant increase of vessel density in tumor-bearing mice of *Rbpj*$^{i\Delta EC}$ compared to control mice (**Fig. 2.12.B**). However, I could not detect any changes in vessel density in the omentum of mice without tumor neither in VCAM1+ ECs in any condition in the loss-of-function model compared to littermate controls (**Fig 2.12.B and C**). The analysis of vessel coverage by αSMA+ also showed no difference in tumor-bearing mice (**Fig. 2.12.E**). In summary, TCs induced-education of the tumor vasculature cannot take place if *Rbpj* is lacking in the ECs.
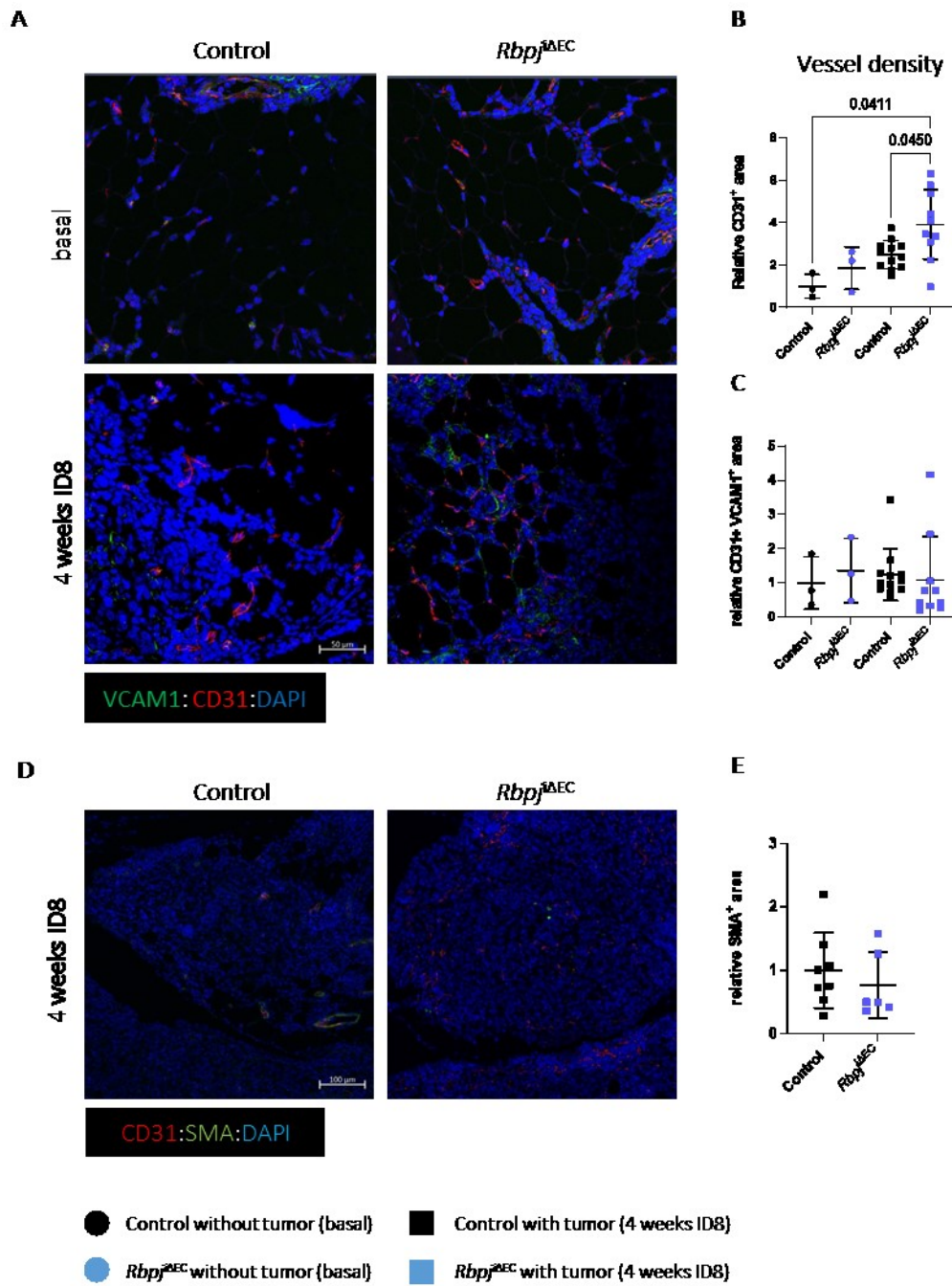
Figure 2.12: Vasculature of metastatic niche in the omentum with and without tumor in loss-of-function model. A Representative images of immunohistochemistry staining for VCAM1 (green), CD31 (red) and DAPI (blue) in omentum of loss-of-function and control mice with and without tumor. Quantification of vessel density (B) and VCAM1+ endothelial cells (C) (n≥3; mean±SD; two-tailed, unpaired Mann-Whitney U-test). D-E Representative images of immunohistochemistry staining for CD31 (red), αSMA (green) and DAPI (blue) as well quantification (E) in loss-of-function mice compared to control after four weeks of tumor growth (n=6; mean±SD; two-way Anova, multiple comparison).

2.3.2 Loss of endothelial Notch reduces tumor burden in metastatic niche

As already mentioned, TCs initially seed in the omentum during metastasis of EOC (Etzerodt *et al.*, 2020). Therefore, I firstly evaluated tumor burden in the omentum of our loss-of-function model by quantifying cytokeratin staining in the omentum. I observed a significantly decreased tumor burden in the $Rbpj^{i\Delta EC}$ compared to littermate controls (**Fig. 2.13.A**). This result cannot be explained by impaired angiogenesis and nutrient perfusion due to the observed increased vessel density in tumor-bearing mice (**Fig 2.12.B**).
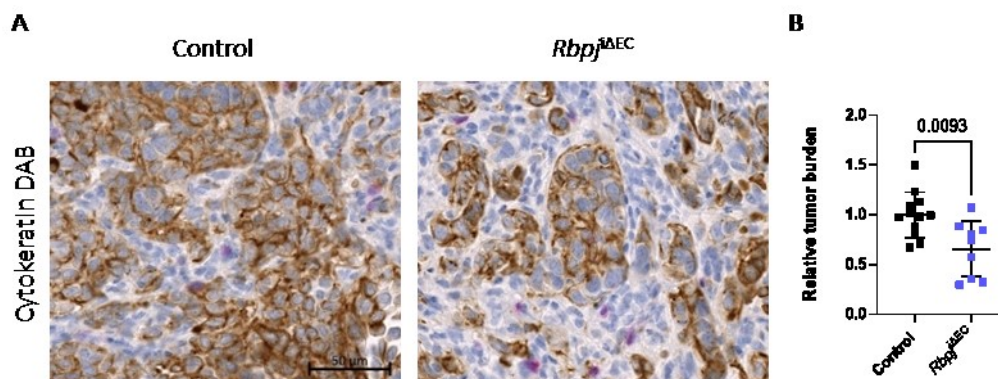
Figure 2.13: Reduced tumor burden in omentum of loss-of-function mice. **A** Representative images of diaminobenzidine (DAB) Cytokeratin staining and quantification (**B**) (n≥9; mean±SD; two-tailed, unpaired Mann-Whitney U-test).

Immune cells and especially, omental macrophages play an essential role for the colonization of the peritoneal cavity and promote the metastatic potential of the TCs (Etzerodt *et al.*, 2020). Consequently, I analyzed the role of immune cells for the reduced tumor burden, I characterized the tumor nodule (determined by anti-luciferase staining) of the omentum by whole mount staining of freshly isolated omentum after four weeks of tumor growth. I detected a decrease of infiltrating immune cells (CD45^{+}) in the $Rbpj^{i\Delta EC}$ compared to littermate controls (**Fig. 2.14.B**). For further characterization, I analyzed the infiltration of myeloid cells (CD11b^{+}) into the tumor areas. I could observe a tendency of decreased infiltrating myeloid cells into the tumor areas quantified by CD11b^{+} nearby cytokeratin^{+} staining (**Fig. 2.14.E**). This observation indicates that loss of endothelial Notch signaling decreases the infiltration of myeloid cells (even though vessel density is increased) leading to a decreased tumor burden in the metastatic niche of EOC metastatic tumor growth.

A

CD45:Luciferase:DAPI

B

C

D

Cytokeratin DAB: CD11b AP
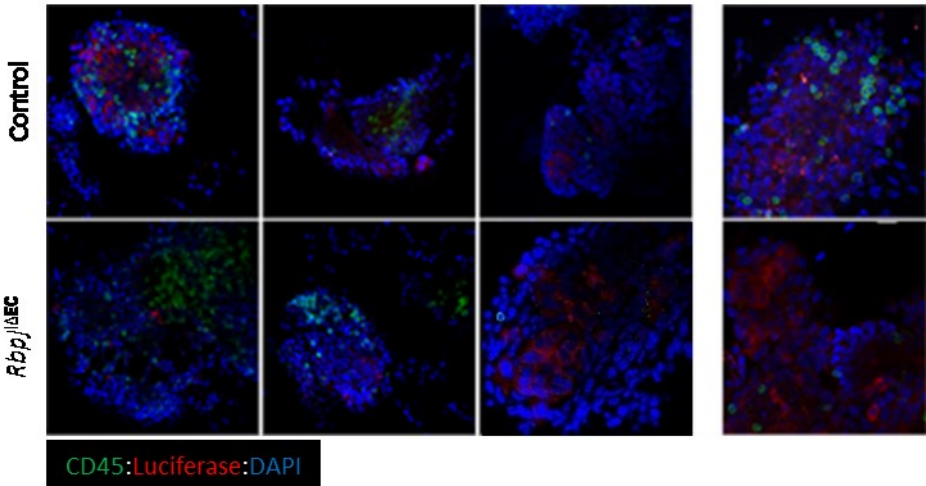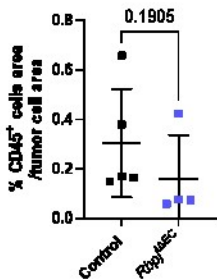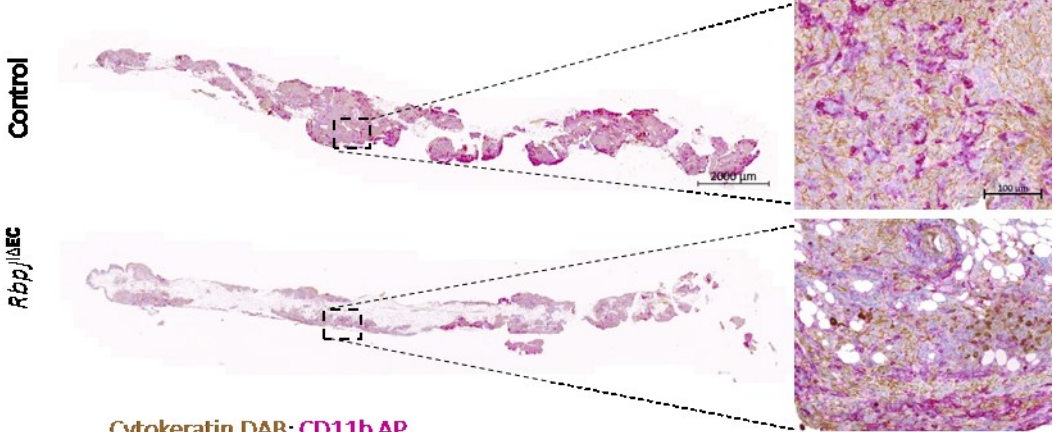
E
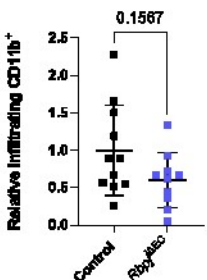
Figure 2.14: Analysis of immune cell infiltration in metastatic niche of epithelial ovarian cancer. **A** Representative images of whole mount staining of tumor nodules of the omentum for luciferase (red), CD45 (green) and DAPI (blue) four weeks after tumor injection in *Rbpj*[iΔEC] and control mice. **B** Quantification of infiltrating immune cells (CD45^{+}) (n≥4; mean±SD; two-tailed, unpaired Mann-Whitney U-test). **C** Representative images of whole omentum and increased magnification (**D**) of tumor infiltrating myeloid cells (CD11b^{+}) in tumor areas (cytokeratin) from *Rbpj*[iΔEC] and control mice four weeks after tumor injection and quantification (**E**) (n≥10; mean±SD; two-tailed, unpaired Mann-Whitney U-test).

As already mentioned, omental macrophages have been suggested to be responsible for successful peritoneal spread of TCs (Etzerodt *et al.*, 2020). Therefore, I further analyzed the infiltration of CD163^{+} cells into the omentum of ecN1ICD as well as *Rbpj*[iΔEC] tumor-bearing mice. Quantifying the whole omental anti-inflammatory macrophages I could not observe any change in the different groups, ecN1ICD as well as *Rbpj*[iΔEC] compared to their controls (**Fig. 2.15**). Moreover, further investigation is needed to determinate the myeloid cell population affecting the tumor progression in the metastatic niche.
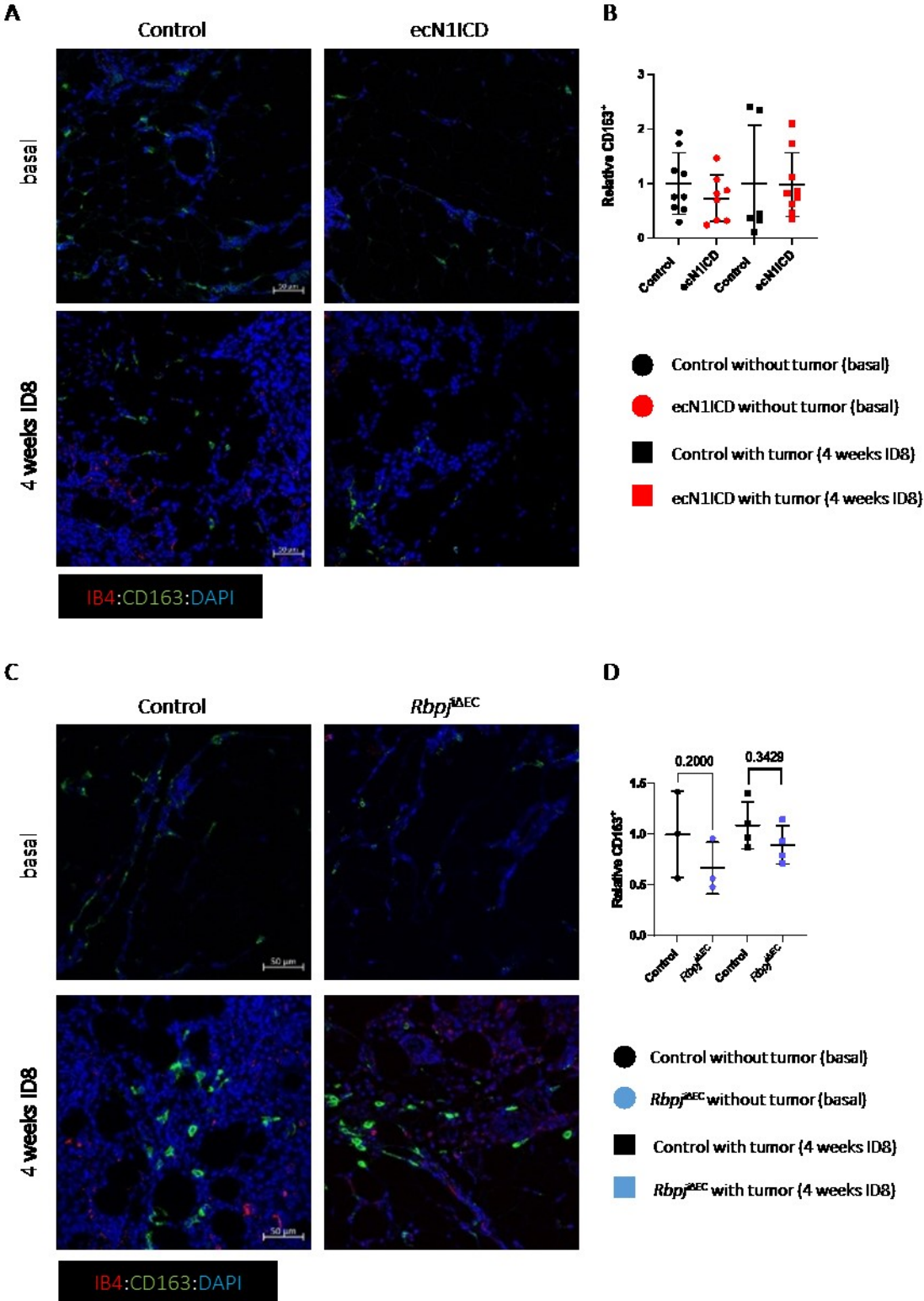
Figure 2.15: Analysis of omental macrophages in metastatic niche of epithelial ovarian cancer. **A** and **C** Representative images of macrophages (CD163+, green) and endothelium (IB4, red) in omentum from gain-of-function (**A**; n≥6), loss-of-function (**B**; n≥3) mice compared to control and quantifications (**B** and **D**) (mean±SD; two-way Anova, multiple-comparison).

2.3.3 Loss of endothelial Notch reduces metastatic spread of epithelial ovarian cancer

During tumor progression and metastasis of EOC, TCs colonize the omentum as well spread though the peritoneal cavity. I already detected a significant reduced tumor burden in the omentum, the metastatic niche in EOC of *Rbpj*[iΔEC] compared to control mice (**Fig. 2.13.B**). Therefore, I decided to also evaluate the tumor burden in the peritoneal fluid by quantifying the luciferase activity of cells collected from the peritoneal cavity. Peritoneal spread of TCs (determined by *ex vivo* luciferase activity) was significantly reduced in *Rbpj*[iΔEC] mice after four weeks of tumor growth (**Fig. 2.16.B**). Whereas, no differences were observed in tumor-bearing ecN1ICD mice compared to littermate controls (**Fig. 2.16.A**). In summary, loss of endothelial Notch signaling impact on the tumor burden in the metastatic niche resulting in a decreased metastatic spread of TCs in EOC model.
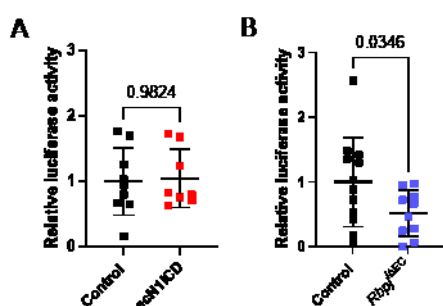
Figure 2.16: Loss of endothelial Notch reduces tumor burden in peritoneum.
Luciferase activity in peritoneal cavity of tumor-bearing mice four weeks after tumor injection in ecN1ICD (**A**) and *Rbpj*[iΔEC] mice (**B**) compared to control mice (n≥8; mean±SD; two-tailed, unpaired Mann-Whitney U-test).

2.4 Role of endothelial Notch signaling on myeloid cell recruitment and education in epithelial ovarian cancer

2.4.1 Endothelial Notch signaling regulates monocyte-derived macrophage recruitment in epithelial ovarian cancer

Immune cell infiltration plays a significant role in shaping the TME and more important the immunosuppressive phenotype of TAM supports tumor growth and metastasis (Schupp *et al.*, 2019). Additionally, during EOC progression the macrophage populations within the peritoneal cavity are shifting towards monocyte-derived macrophages (Goossens, *et al.*, 2019). Therefore, I analyzed the myeloid cell infiltration into the peritoneal cavity by flow cytometry to understand whether endothelial Notch signaling could have a role in their composition. I could not detect any B cell (CD19^{+} population) expressing high levels of CD11b in peritoneal lavage in the myeloid cell (CD45^{+} CD11b^{high}) gating strategy (Appendix **Fig. 5.2.A**). Analyzing the different myeloid cell populations within the peritoneal cavity, I observed no differences in myeloid cells, neutrophils and total macrophages in neither ecN1ICD nor *Rbpj*[iΔEC] tumor-bearing mice compared to control (**Fig 2.17.A and B**). During EOC tumor progression monocyte-derived macrophages infiltrate in the peritoneum, become the most prominent macrophage population and promote tumor progression (Goossens, *et al.*, 2019). Therefore, I analyzed the recruited monocyte-derived macrophage populations and I detected a significant increase of monocyte-derived macrophages, characterized by intermediate expression of MHCII and F4/80 (IntPM) after four weeks of tumor growth in ecN1ICD mice compared to littermate controls (**Fig 2.17.C**). In line with this, I observed a significant decrease of monocyte-derived macrophages, in more detail IntPM and SPM (characterized by high MHCII and low F4/80 expression) populations in tumor-bearing *Rbpj*[iΔEC] mice compared to littermate controls (**Fig. 2.17.D**). The obtained results suggest, that the recruitment of monocyte-derived macrophages into the TME is mediated by endothelial Notch1 signaling.
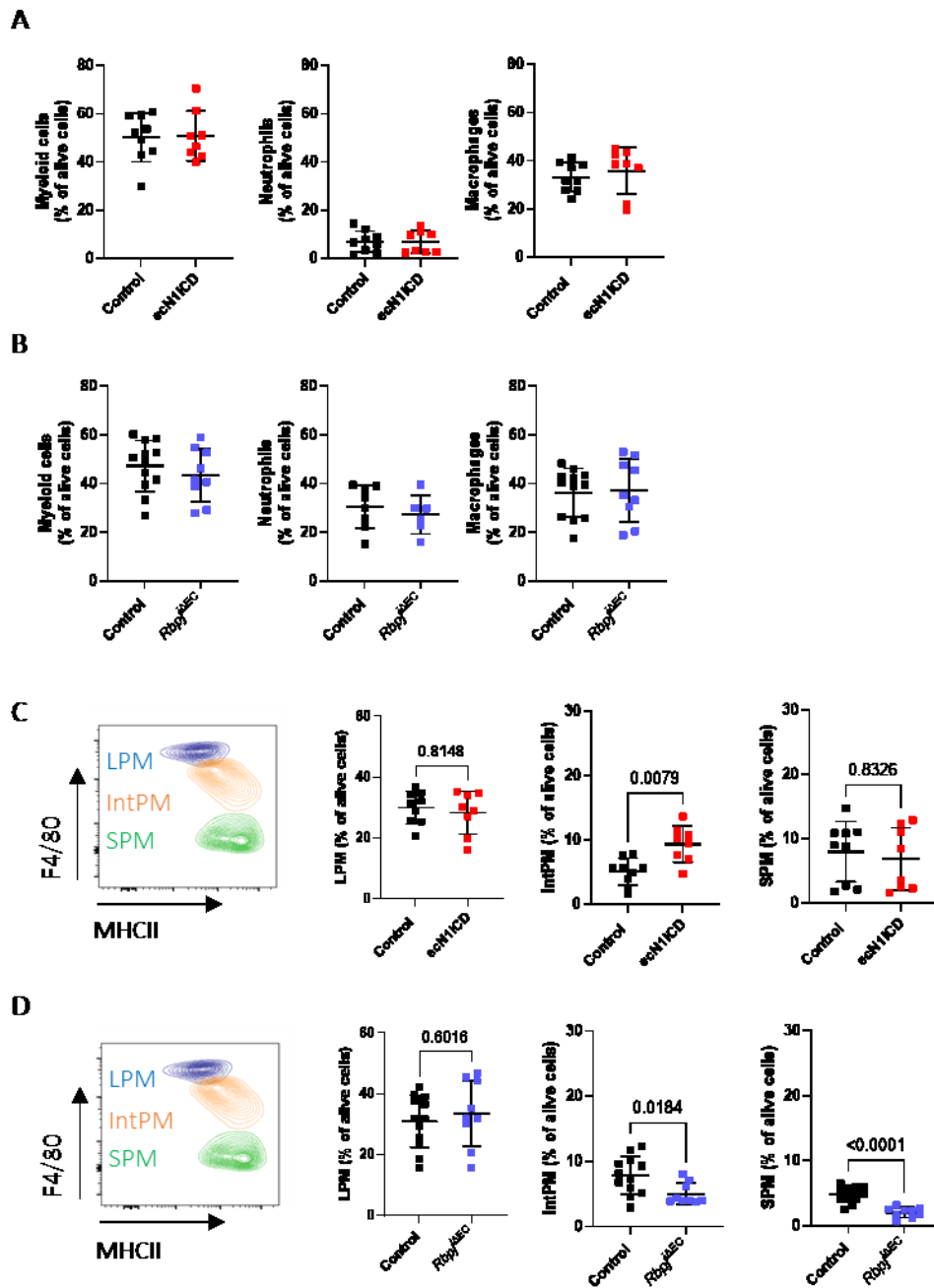
Figure 2.17: Endothelial Notch regulates monocyte-derived macrophage recruitment in metastatic epithelial ovarian cancer. Analysis of myeloid cells within the peritoneal cavity after four weeks of tumor growth. **A** Percentage (%) of myeloid cells (CD45$^+$, CD11b^{high}), neutrophils (CD45$^+$, CD11b^{high}, Ly6G$^+$) and macrophages (CD45$^+$, CD11b^{high}, F4/80$^+$) relative to alive (live/dead marker) cells in gain-of-function model (n=8; mean±SD; two-tailed, unpaired Mann-Whitney U-test). **B** Percentage of myeloid cells, neutrophils and macrophages relative to alive cells in loss-of-function model (n≥9; mean±SD; two-tailed, unpaired Mann-Whitney U-test). **C** Representative flow cytometer plot of monocyte-derived macrophages characterized by F4/80 and MHCII expression into large peritoneal macrophages (LPM), intermediate PM (intPM) and small PM (SPM) and their quantification in gain-of-function mice compared to control (n=8; mean±SD; two-tailed, unpaired Mann-Whitney U-test). **D** Representative flow cytometer plot of monocyte-derived macrophages characterization by F4/80 and MHCII expression into LPM, IntPM and SPM in in loss-of-function mice compared to control and their quantification (n≥9; mean±SD; two-tailed, unpaired Mann-Whitney U-test).

The observed changes in the myeloid cell population were limited to monocyte-derived macrophages which are recruited through the blood. For this reason, I also analyzed the myeloid cell population in the blood of tumor-bearing mice and I observed a significant increase of CD11b$^+$ myeloid cells as well as neutrophils in ecN1ICD mice compared to littermate controls (**Fig 2.18.A**). Mobilization and egress of myeloid cell into the blood and peritoneal cavity as well as migration through the blood stream is mediated by a chemokine gradient and CXCL2 is described to recruit neutrophils as well monocytes (Sokol & Luster, 2015). Therefore, the observed increase of myeloid cells and neutrophils in the gain-of-function model goes in line with the previous described regulation of CXCL2 by RBPJ/Notch1 in ECs (2.2.1 Endothelial Notch1-regulate secretion of angiocrine factors). Moreover recent studies, suggest that overexpression of endothelial Notch has a role in the stress response within the bone marrow niche impacting on HPC (Vanderbeck & Maillard, 2019). However, if overactivation of endothelial Notch signaling by TCs could also implicated in the increased recruitment of myeloid cells from the progenitor compartment in our model of metastatic EOC, needs further investigation of the bone marrow niche. Nevertheless, I could not detect any significant differences in the myeloid cell composition in the blood of *Rbpj*$^{i\Delta EC}$ mice compared to littermate controls (**Fig 2.18.B**). Taking together, that endothelial Notch signaling regulate infiltration of myeloid cells from the blood.
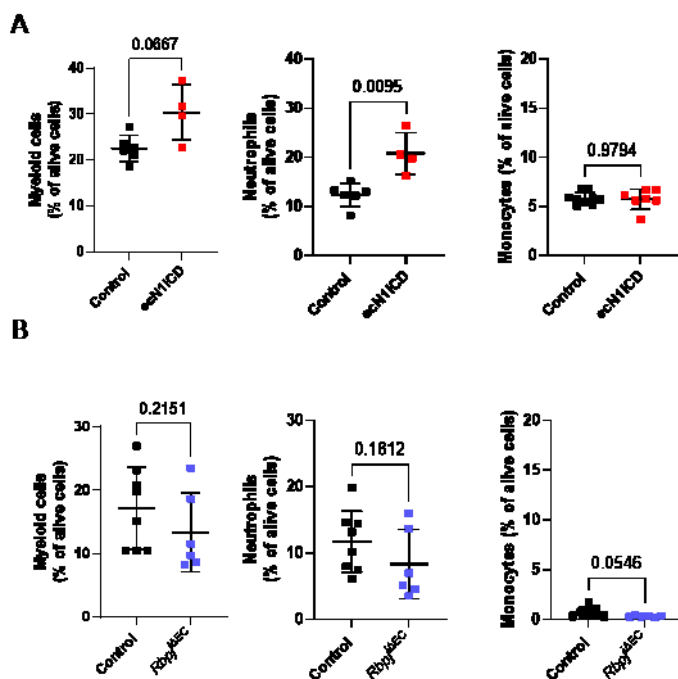
Figure 2.18: **Activation of endothelial Notch increases myeloid cells in blood of tumor-bearing mice.** Analysis of myeloid cells within in the blood after four weeks of tumor growth. **A** Percentage of myeloid cells (CD45$^+$, CD11b$^+$), neutrophils (CD45$^+$, CD11b$^+$, Ly6G$^+$) and monocytes (CD45$^+$, CD11b$^+$, Ly6C$^+$) relative to alive (live/dead marker) cells in gain-of-function model and loss-of-function (**B**) model compared to control (n≥4; mean±SD; two-tailed unpaired Mann-Whitney U-test).

The data presented so far indicate that monocyte-derived macrophage recruitment into tumors is regulated by endothelial Notch1 signaling. To proof this observation of EC-mediated monocyte migration also in a human *in vitro* setting, I analyzed the transmigration of human CD14$^+$ monocytes through a monolayer of ECs in a transwell insert. I cultured SKOV-3 human ovarian cancer cells on a plate and seeded a monolayer of HUVECs on transwell inserts (**Fig. 2.19.A**). Transmigration of human monocytes through the monolayer of ECs cells was analyzed with N1ICD overexpression in ECs compared to GFP controls (**Fig. 2.19.B**), as well as through HUVECs transfected with CRISPR-Cas9 mediated *RBPJ* KO compared to a scrambled gRNA (**Fig 2.19.C**). I could observe an increased rate of monocyte migration when ECs had been infected with N1ICD expression virus compared to control (**Fig 2.15.B**). Additionally, I observed that monocyte transmigration was significantly decreased when ECs

lack RBPJ (**Fig 2.19.C**). Even more interesting, when I knocked down *CXCL2*, the cytokine I found out to be a novel Notch1 target in ECs (2.2.1 Endothelial Notch1-regulte secretion of angiocrine factors), I could obtain a tendency of reduced migration of human monocytes towards the TME (**Fig 2.19.D**). Several studies indicate the important role that CXCL2 has on the recruitment of MDSC in the TME (Katoh et al., 2013), in particular in ovarian cancer (Taki et al., 2018). This suggests that ECs mediate monocyte recruitment could at least partially induced by TCs though the expression of CXCL2.
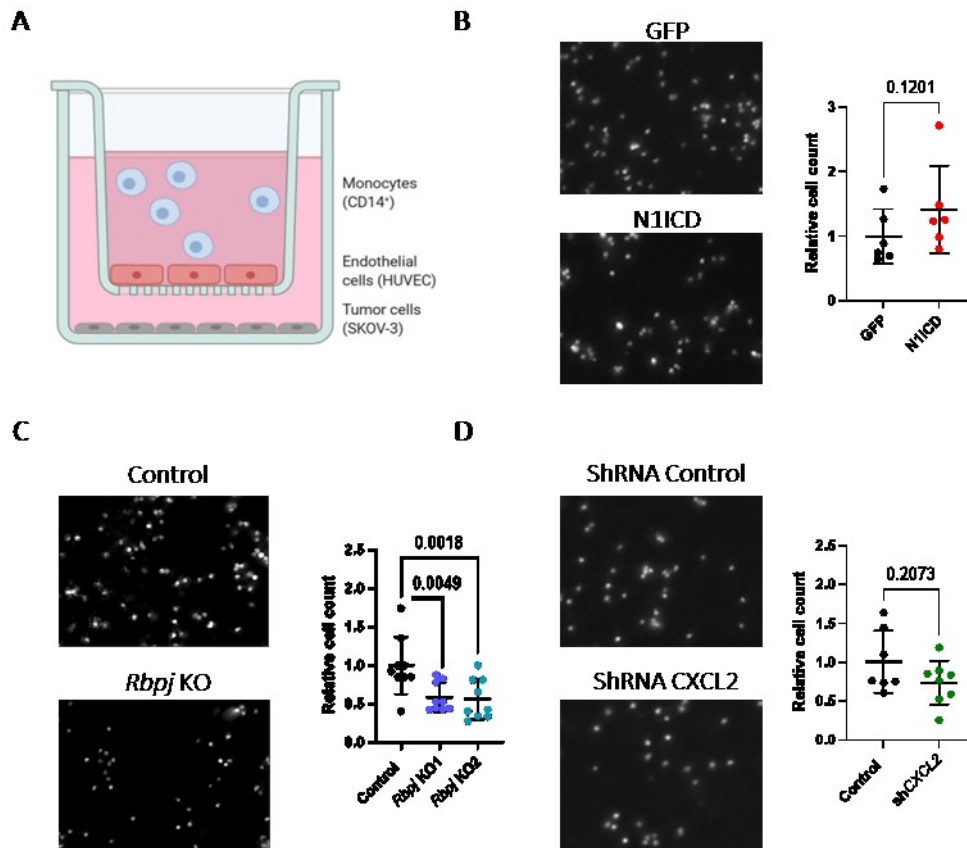
Figure 2.19: Loss of endothelial Notch reduces migration of monocytes in an in vitro transwell assay. **A** Scheme of transwell assay with human CD14+ monocyte through a monolayer of human umbilical vein endothelial cells (HUVEC) towards human ovarian cancer cells (SKOV-3). Analysis of cell tracer carboxyfluorescein succinimidyl ester (CFSE) stained migrated CD14+ monocyte through monolayer of HUVECs infected with N1ICD using microscopy (**B**), HUVECs with *RBPJ* KO (**C**) and HUVEC with knock down of *CXCL2* (**D**) (n≥7; mean±SD; two-tailed, unpaired Mann-Whitney U-test).

2.4.2   Loss of endothelial Notch signaling regulates hyaluronic acid receptors on monocyte-derived macrophages

Not only the recruitment of macrophages in the TME plays an important role in the progression of metastatic EOC but also their activation and polarization have an impact on the TME (Baek *et al*., 2020). Therefore, I decided to evaluate whether endothelial Notch signaling could have also an effect on the activation and polarization of monocyte-derived macrophages, besides mediating their recruitment. I isolated newly recruited macrophages (CD45$^+$, CD11b$^+$, F4/80$^+$, CCR2$^+$) four weeks after tumor injection, by fluorescence-activated cell sorting and performed microarray analysis (**Fig. 2.20.A**). To determine differentially regulated pathways in TAMs from *Rbpj*$^{i\Delta EC}$ mice and their littermate controls I performed Ingenuity pathway analysis (IPA) and Gene Ontology (GO) analysis. Among the pathways found to be differentially regulated, the cluster of cholesterol pathways for cholesterol metabolism was particularly interesting (**Fig. 2.20.B**). TAM isolated from *Rbpj*$^{i\Delta EC}$ mice showed significant downregulation of the cholesterol metabolism WP4346 (p= $4.5*10^{-12}$) and cholesterol biosynthesis WP103 (p= $8.57*10^{-10}$) pathways (**Fig. 2.20.C**). The education of TAMs by TCs can take place through the production and efflux of cholesterol. The depletion of cholesterol in TAM is mediated by TCs, through the secretion high molecular weight hyaluronic acid (HA) (Goossens, *et al*., 2019). Therefore, I evaluated whether EOC-induced cholesterol regulation was affected in macrophages using gene set enrichment analysis (GSEA). I compared a gene list for cholesterol homeostasis obtained from TAMs 21 days after tumor injection (Goossens, *et al*., 2019). This gene set for cholesterol homeostasis was significantly enriched in newly recruited macrophages coming from tumor-bearing control compared to *Rbpj*$^{i\Delta EC}$ mice (**Fig. 2.20.D**), indicating that EC-Notch signaling is required for cholesterol depletion in TAMs. HA gets recognized by HA receptors, such as LYVE1 or CD44, on macrophages and leads to cholesterol efflux through ABC transporter (Goossens, *et al*., 2019). Interestingly, when bone marrow-derived macrophages (BMDM) were incubated with conditioned medium (CM) from murine ECs with CRISPR-Cas9 mediated *Rbpj* KO, I observed a significant decrease of *Cd44* mRNA (**Fig. 2.20.E**). Activation of CD44 results in a release of the CD44 intracellular domain (ICD), which translocates into the nucleus where it binds to the promotor region of MMP9 and induces the mRNA expression. Indeed, MMP9 was also significantly downregulated in BMDM stimulated with CM from ECs lacking *Rbpj* (**Fig. 2.20.F**). This indicates, that endothelial RBPJ-mediated Notch signaling regulates the expression of the HA receptor CD44 levels in macrophages. Moreover, co-culture of HUVECs with *RBPJ* KO and human primary monocytes isolated from buffy coat showed a significant downregulation of CD44 quantified by flow cytometer analysis (**Fig. 2.20.H**). These investigations, suggest that endothelial RBPJ is necessary for the regulation of HA receptor expression and priming of newly recruited monocyte-derived-macrophages.
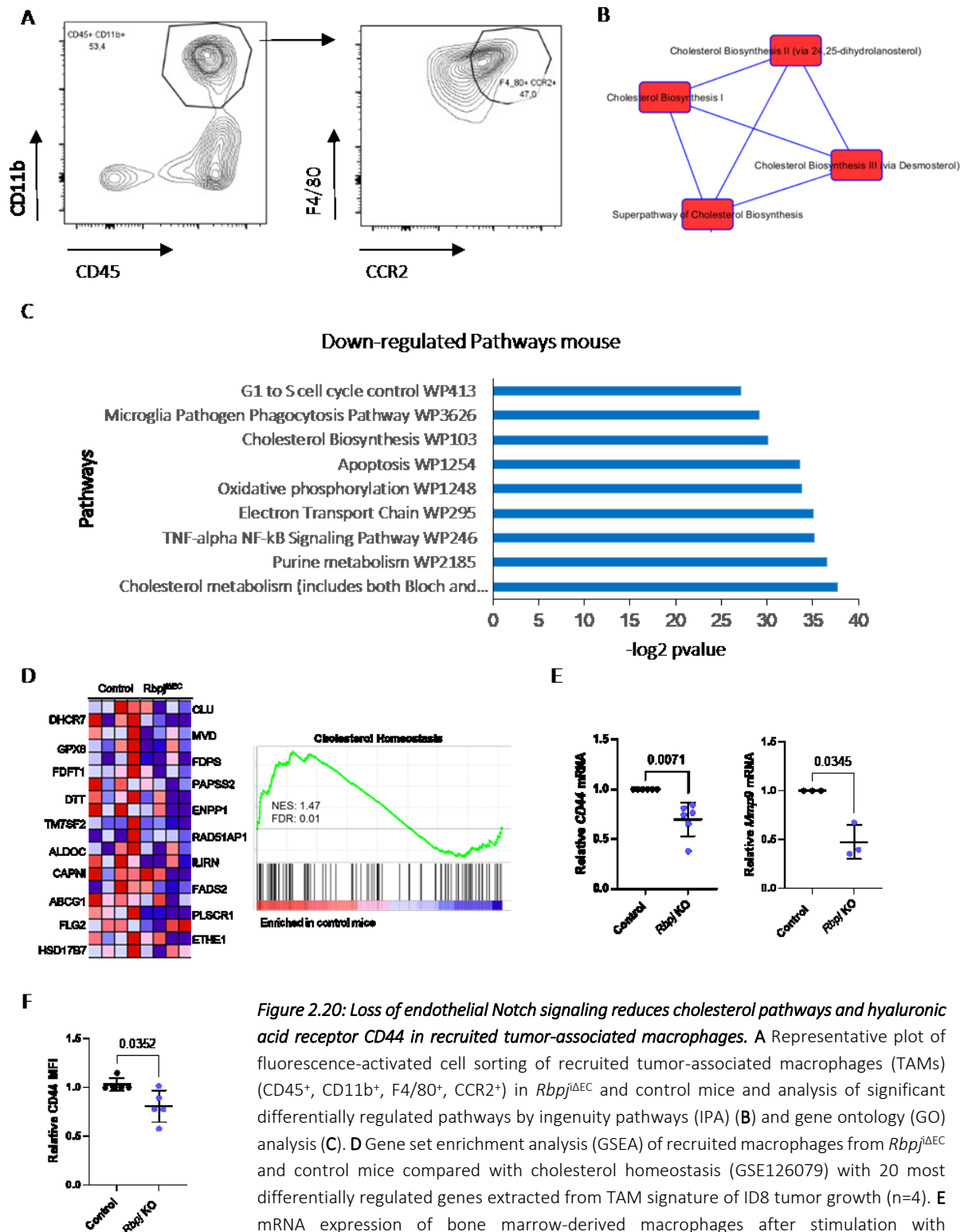
Figure 2.20: Loss of endothelial Notch signaling reduces cholesterol pathways and hyaluronic acid receptor CD44 in recruited tumor-associated macrophages. **A** Representative plot of fluorescence-activated cell sorting of recruited tumor-associated macrophages (TAMs) (CD45+, CD11b+, F4/80+, CCR2+) in *Rbpj*iΔEC and control mice and analysis of significant differentially regulated pathways by ingenuity pathways (IPA) (**B**) and gene ontology (GO) analysis (**C**). **D** Gene set enrichment analysis (GSEA) of recruited macrophages from *Rbpj*iΔEC and control mice compared with cholesterol homeostasis (GSE126079) with 20 most differentially regulated genes extracted from TAM signature of ID8 tumor growth (n=4). **E** mRNA expression of bone marrow-derived macrophages after stimulation with conditioned medium form immortalized mouse cardiac ECs (MCEC) with *Rbpj* KO and control (n≥3; mean±SD; two-tailed, paired students T-test). **F** Mean fluorescence intensity (MFI) of CD44 expression of human monocytes co-cultured with human ECs with *RBPJ* KO (n=5; mean±SD; two-tailed, unpaired Mann-Whitney U-test).

2.4.3 Loss of endothelial Notch inhibits immunosuppressive phenotype of monocyte-derived macrophages

Importantly, Goossens *et al.* not only described the important role of cholesterol in TAMs. Moreover, the cholesterol homeostasis in TAM has also an essential role in the development of their immunosuppressive phenotype in metastatic ovarian cancer (Goossens, *et al.*, 2019). This led to the hypothesis, that recruited monocyte-derived macrophages in *Rbpj*[iΔEC] do not only show inhibited cholesterol homeostasis but also an implication in the immunosuppressive phenotype of TAMs. In order to verify this, I performed GSEA to compare the expression profiles of newly recruited monocyte-derived macrophages from *Rbpj*[iΔEC] and control mice with a gene set of TAM signature. In the above-mentioned study, the expression profile of TAMs within metastatic EOC was characterized leading to the ID8 TAM signature of genes upregulated during ID8 tumor progression (Goossens, *et al.*, 2019). Apart from the increased cholesterol efflux, this profile showed a hypersensitivity towards IL4. This list includes 173 genes, which are upregulated by IL4 in TAMs during metastatic EOC at all stages of its development. When analyzing this TAM signature, I found that TAMs isolated from control mice showed a significant enrichment, compared to those from *Rbpj*[iΔEC], indicating that TC-induced macrophage education cannot take place if Notch signaling is inhibited in ECs (**Fig. 2.21.A**). Additionally, significantly downregulation of most differentially genes (*Slamf8* and *Slamf9*) were further validated by RT-qPCR in TAMs isolated from tumor-bearing mice (**Fig. 2.21.B**). Furthermore, IPA upstream regulator analysis showed that IL4, the top upstream regulator was inhibited in newly recruited macrophages form *Rbpj*[iΔEC] mice compared to littermate controls (**Fig. 2.21.C**). These results indicate that loss of endothelial RBPJ inhibits the TC-induced education of TAMs towards an immunosuppressive phenotype, by reducing HA responses on monocytes recruited to the TME.

Upstream Regulator		
Name	p-value	prediction
IL4	$4{,}67*10^{-24}$	inhibited
TGFB1	$1{,}15*10^{-22}$	inhibited
TP53	$1{,}47*10^{-20}$	no prediction
LPS	$4{,}89*10^{-20}$	inhibited
IFNG	$2{,}86*10^{-19}$	inhibited
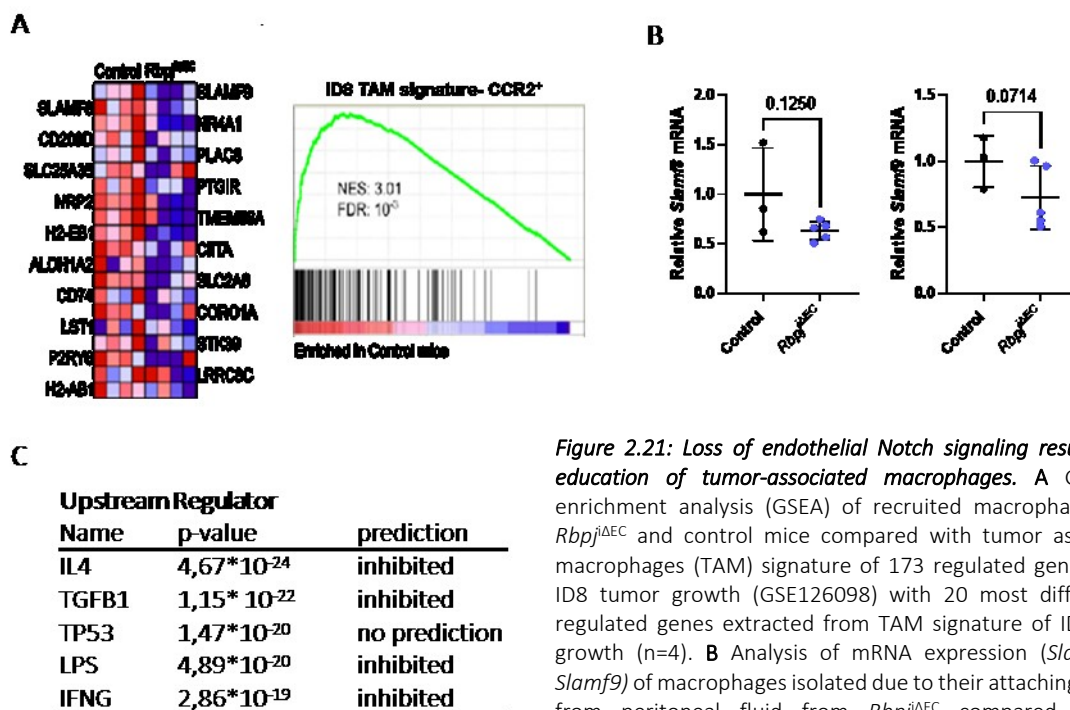
Figure 2.21: Loss of endothelial Notch signaling results in an education of tumor-associated macrophages. **A** Gene set enrichment analysis (GSEA) of recruited macrophages from *Rbpj*[iΔEC] and control mice compared with tumor associated-macrophages (TAM) signature of 173 regulated genes during ID8 tumor growth (GSE126098) with 20 most differentially regulated genes extracted from TAM signature of ID8 tumor growth (n=4). **B** Analysis of mRNA expression (*Slamf8* and *Slamf9*) of macrophages isolated due to their attaching capacity from peritoneal fluid from *Rbpj*[iΔEC] compared to their corresponding control after three weeks of ID8 tumor growth (n≥3; mean±SD; two-tailed, unpaired Mann-Whitney U-test). **C** Ingenuity pathways analysis (IPA) for upstream regulator in recruited macrophages from *Rbpj*[iΔEC] and control mice (n=4).

Recruitment of monocyte-derived macrophages was significantly increased in tumor-bearing mice in the gain-of-function model compared to control (**Fig. 2.17.D**). Therefore, I decided to also evaluate the activation of newly recruited macrophages from ecN1ICD mice compared to controls. I performed GSEA to analyze if the gene set of TAM signature is enriched in newly recruited monocyte-derived macrophages from ecN1ICD mice compared to control. The analysis showed no enrichment in any of the groups, which indicates that there are no differences in the immunosuppressive phenotype between newly recruited macrophages of ecN1ICD mice compared to control (**Fig. 2.22.A**). To further emphasize the role of endothelial Notch signaling on the development of the immunosuppressive phenotype of newly recruited macrophages, I also analyzed the enrichment of the TAM signature between recruited macrophages isolated from ecN1ICD and $Rbpj^{i\Delta EC}$. I observed a highly significant enrichment of the TAM signature in TAMs of ecN1ICD mice compared to $Rbpj^{i\Delta EC}$ (**Fig. 2.22.B**). Even more remarkable, the immunosuppressive TAM signature showed an enrichment in isolated leukocytes from human colorectal cancer patient classified as endothelial Notch activation (*HEY1*) high compared to lower Notch activation in the sorted ECs. Taking together, endothelial Notch signaling mediated-education by TCs is physiological and overactivation of N1ICD in the gain-of-function model increases only the recruitment of monocyte-derived macrophages but not their polarization.
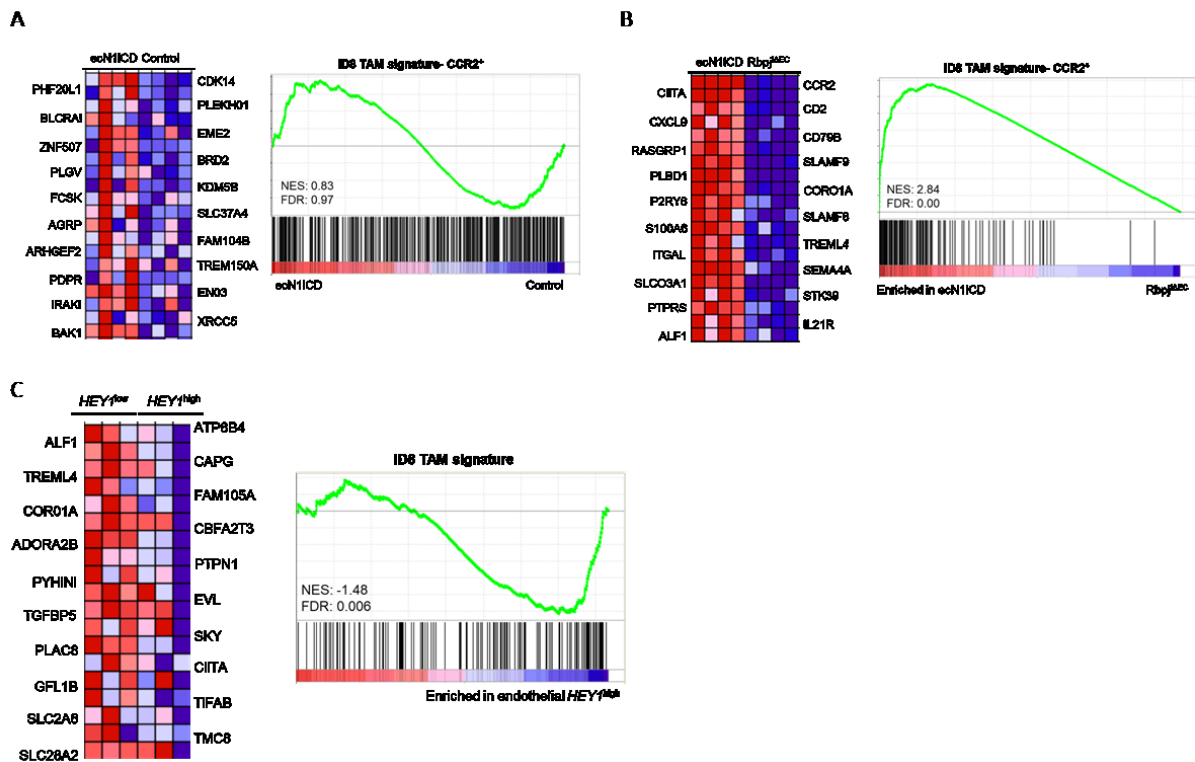
Figure 2.22: Analysis of tumor-associated macrophage signature in recruited macrophages of gain-of-function mice compared to control as well to loss-of-function mice and leukocytes from human colorectal cancer patients. Gene set enrichment analysis (GSEA) of recruited macrophages from ecN1ICD and control mice (**A**) as well as ecN1ICD and $Rbpj^{i\Delta EC}$ (**B**) compared with tumor-associated macrophage (TAM) signature of 173 regulated genes during ID8 tumor growth (GSE126098) with 20 most differentially regulated gene extracted from TAM signature of ID8 tumor growth (n=4). **C** GSEA of leukocytes from colorectal cancer patient data classified in endothelial Notch activation (HEY1) low and high compared to TAM signature with 20 most differentially regulated gene (Data kindly provided by Dr. Elisa Espinet, Divison of Stem Cells and Cancer (DKFZ); n=6).

2.4.4 Essential role of endothelial Notch on education of monocyte-derived macrophages through CD74

Newly recruited macrophages from mice that lack *Rbpj* in the endothelium showed a weaker expression level of the TAM signature including the downregulation of serval tumor-associated genes, for example CD74 (**Fig. 2.21.A**). Expression levels of CD74 correlate with poor prognosis in ovarian cancer patients (Cortes *et al.*, 2017) as well as expression of CD74 by TAM has an important role in shaping the immunosuppressive microenvironment (Cortes *et al.*, 2017). Indeed, I could also validate the downregulation of CD74 in TAMs isolated from *Rbpj*[iΔEC] mice compared to control by RT-qPCR (**Fig. 2.22.A**) and via flow cytometry analysis after four weeks of tumor growth (**Fig. 2.22.B**). Moreover, blocking CD74 on APC increased anti-tumor immunity and decreased their immunosuppressive phenotype (Figueiredo *et al.*, 2018). Therefore, I hypothesized that CD74 expression on macrophages could meditate their education in the TME. In order to support this idea, I analyzed publicly available data from Przybyl *et al.* (Przybyl *et al.*, 2016). In this publication, the IL4 responses in *CD74* knock-out (*CD74* KO) macrophages were analyzed. Since IL4 is the main driver of the TAM signature in EOC tumor progression (Goossens, *et al.*, 2019) and it is also a main upstream regulator in our model (**Fig. 2.21.B**), I decided to analyze the regulation of this signature in these datasets. By GSEA, I compared the IL4 stimulated-expression of the TAM signature gene set in control and *CD74* KO macrophages. I observed that the TAM signature is enriched in control compared to *CD74* KO macrophages, suggesting that CD74 is necessary for the TAM signature to be induced (**Fig. 2.23.A**). Using this same dataset, I generated a new gene signature with the 500 most enriched genes in control compared to *CD74* KO macrophages stimulated with IL4 (CD74-mediated signature). This represents a gene set induced by IL4 through CD74 expression. When comparing control and *Rbpj*[iΔEC] recruited macrophages from the ID8 model by GSEA I found that this CD74-mediated signature is significantly enriched in the control mice, indicating that the recruited macrophages from *Rbpj*[iΔEC] cannot induce their genes through CD74 (**Fig. 2.23.B**).

To validate these observations, I co-cultured primary human monocytes with HUVEC infected with N1ICD or constructs to knock-out *RBPJ* mediated by CRISPR-Cas9 and their corresponding controls together with or without conditioned medium (CM) from human ovarian cancer cells (SKOV-3). Analyzing the expression of CD74 on monocytes by flow cytometry, I observed no changes in any conditions without TCs CM. However, I could observe an effect of the co-culture in combination with the stimulation of the CM from SKOV-3 cells. CD74 expression on monocytes was inhibited in these conditions only when co-cultured with *RBPJ* KO ECs (**Fig. 2.23.F**). While, I observed an increased response towards SKOV-3 CM when monocytes were co-cultured with HUVECs overexpressing N1ICD (**Fig. 2.23.D**). In summary, endothelial Notch signaling educates the monocyte-derived macrophages through the regulation of CD74 on monocyte-derived macrophages.
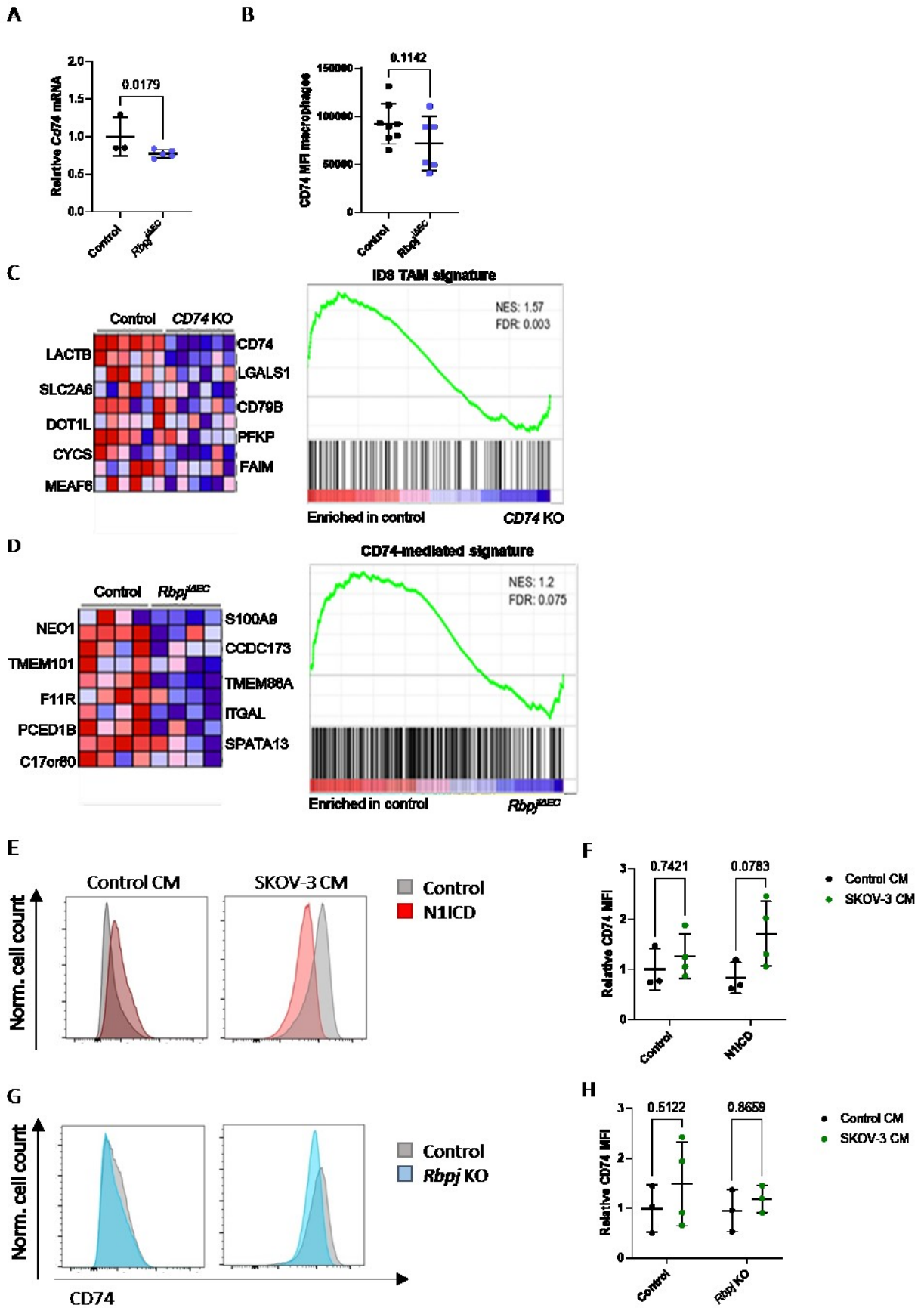
Figure 2.23: Role of CD74 for the development of immunosuppressive phenotype of tumor-associated macrophages. **A** mRNA expression of *Cd74* of isolated peritoneal macrophages due to their attaching capacity after three weeks of ID8 tumor growth from *Rbpj*[iΔEC] and control mice (n≥3; mean±SD; two-tailed, unpaired Mann-Whitney U-test). **B** Mean fluorescence intensity (MFI) of CD74 expression in macrophages (CD45^{+}, CD11b^{high}, F4/80^{+}) of tumor-bearing mice (four weeks) in *Rbpj*[iΔEC] and control mice (n≥6; mean±SD; two-tailed, unpaired Mann-Whitney U-test). **C** Gene set enrichment analysis (GSEA) of publicly available data of bone marrow-derived macrophages with and without *Cd74* knock-out (KO) compared with TAM signature of 173 regulated gene during ID8 tumor growth (GSE126098) with 20 most differentially regulated gene extracted from TAM signature of ID8 tumor growth (n=6; E-MTAB-3309). **D** GSEA of recruited macrophages from *Rbpj*[iΔEC] and control mice compared with CD74-mediated gene signature with 10 most differentially regulated gene extracted from TAM signature of ID8 tumor growth (n=4). **E** and **G** Representative histograms and quantification (**F** and **H**) of MFI of CD74 expression in primary human monocytes co-cultured with human primary endothelial cells overexpressing N1ICD and control (**F**) as well knock-out for *RBPJ* and stimulation with TCs (SKOV-3) conditioned medium (CM) (**H**) (n=4; mean±SD; two-way Anova multiple comparison).

To highlight the specific role of the tumor endothelium on the immune suppressive phenotype on the newly recruited macrophages, I repeated the same analysis on resident macrophages. Analysis of the ID8 TAM gene signature in CCR2^{-} macrophages (CD45^{+}, CD11b^{+}, F4/80^{+}, and CCR2^{-}) from tumor-bearing mice of *Rbpj*[iΔEC] and control mice showed that, the TAM signature is also enriched in the resident macrophages from control mice. Interestingly, the resulted list of differentially regulated genes does not include CD74 (**Fig. 2.24.A**). Therefore, I also performed GSEA using the CD74-mediated gene signature comparing CCR2^{-} macrophages from *Rbpj*[iΔEC] and control mice. I could not detect any enrichment of this gene set in any of the groups (**Fig 2.24.B**), confirming that only those newly recruited macrophages have CD74 inhibited. In summary, only monocytes which get recruited to the TME and pass the endothelium showed differences in their expression of the pro-tumorigenic marker CD74.
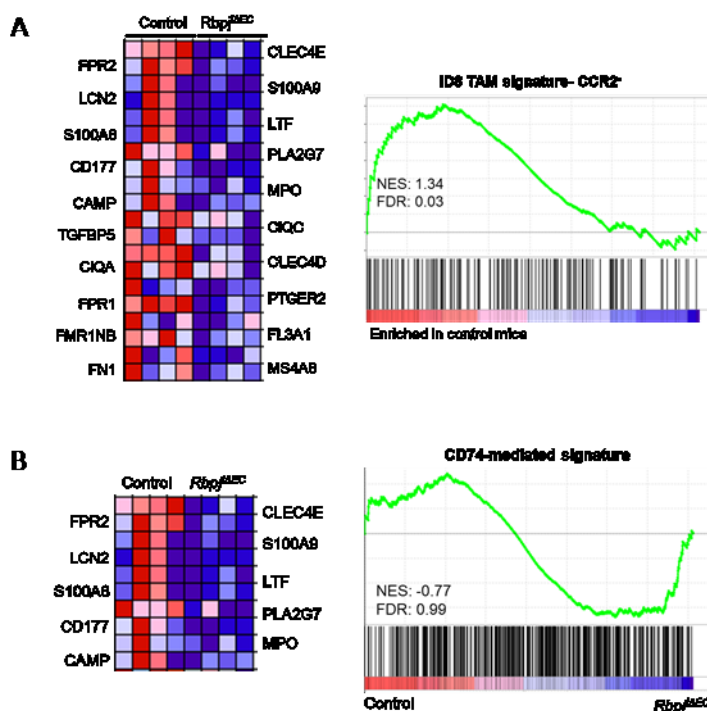
Figure 2.24: Analysis of tumor-associated macrophage signature and role of CD74 in resident macrophages. **A** Gene set enrichment analysis (GSEA) of resident macrophages (CD45^{+}, CD11b^{+}, F4/80^{+}, CCR2^{-}) from *Rbpj*[iΔEC] and control mice compared with tumor-associated macrophages (TAM) signature of 173 regulated gene during ID8 tumor growth (GSE126098) with 20 most differentially regulated gene extracted from TAM signature of ID8 tumor growth (n=6). **B** GSEA of resident macrophages from *Rbpj*[iΔEC] and control mice compared with CD74-mediated gene signature with 10 most differentially regulated gene extracted from TAM signature of ID8 tumor growth (n=4).

2.4.5 Loss of endothelial *Rbpj* has an impact on the immunosuppressive tumor microenvironment

In ovarian cancer patients, the TME is extremely immunosuppressive and the infiltration of TAMs have a major impact to this phenotype (Hensler *et al.*, 2020). Clinical studies show, that increased cytotoxic T cells in TME correlates with better outcome for patients in several different tumor types including ovarian cancer (An *et al.*, 2019; Vihervuori *et al.*, 2019), whereas cytotoxic T cells within the metastatic niche, the omentum does not increase overall survival of EOC patients (Wang *et al.*, 2018). Therefore, I functionally analyzed the impact of these transcriptomic changes that occur within monocyte-derived macrophages have on the TME. I isolated CD3$^+$ T cells of the peritoneal lavage from *Rbpj*$^{i\Delta EC}$ and control mice after six weeks of ID8 tumor growth and incubated them together with *in vitro* cultivated ID8 cells (**Fig 2.25.A**). I detected a significant increase of cytotoxic potential of T cells (LDH-cytotoxicity assay) isolated from *Rbpj*$^{i\Delta EC}$ mice compared to those isolated from their littermate controls in the peritoneal cavity (**Fig. 2.25.B**). Therefore, I also analyzed the T cell population after four weeks of tumor growth in *Rbpj*$^{i\Delta EC}$ mice compared to control. I could not observe any changes in the total T cell population neither in T helper cells (**Fig. 2.25.C and D**). However, I could observe a significant increase of cytotoxic T cells in peritoneal lavage from *Rbpj*$^{i\Delta EC}$ mice compared to control, indicating that not only T cell activity is changed but also their proportions (**Fig. 2.25.D**). Taking together, tumor endothelium is able to educate the phenotype of newly recruited monocyte-derived macrophages with a consequence on the T cell killing potential as well as their proportion in cytotoxic versus helper T cells within the peritoneal cavity.
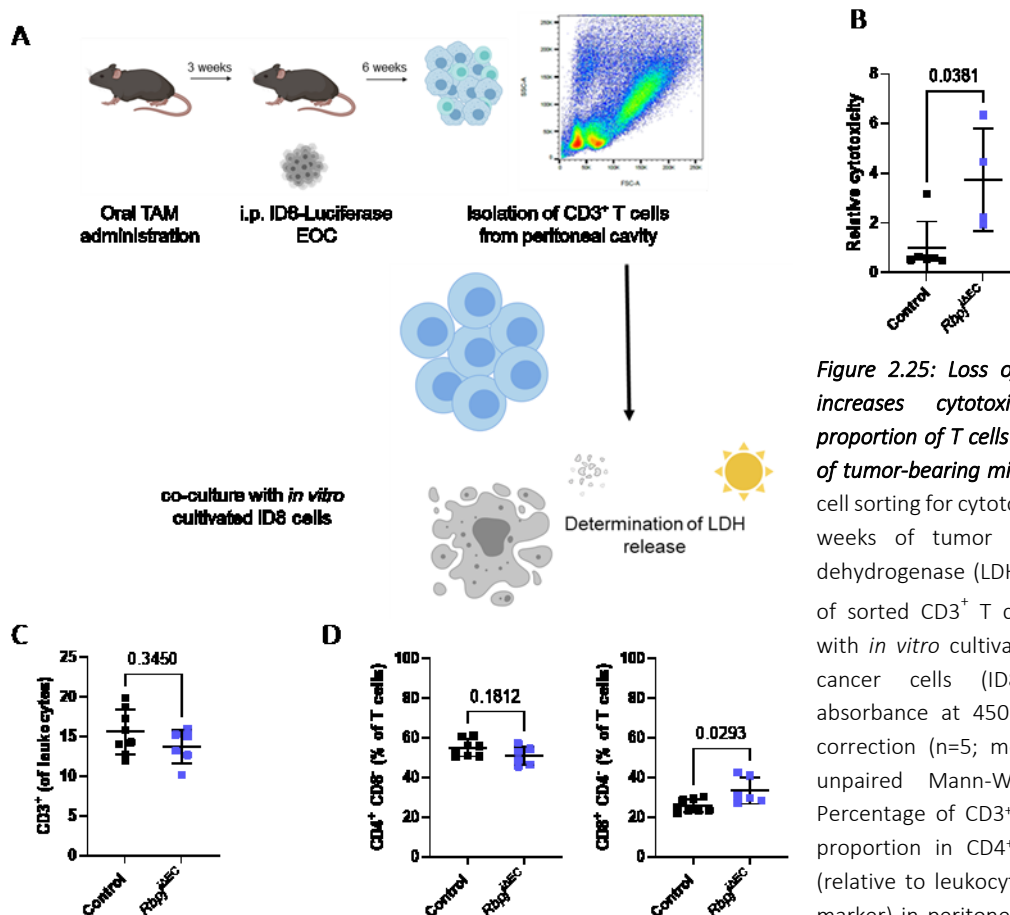
Figure 2.25: Loss of endothelial Notch increases cytotoxic potential and proportion of T cells in peritoneal lavage of tumor-bearing mice. **A** Workflow of T cell sorting for cytotoxicity assay after six weeks of tumor growth. **B** Lactate dehydrogenase (LDH)-cytotoxicity assay of sorted CD3$^+$ T cells and incubation with *in vitro* cultivated murine ovarian cancer cells (ID8) measured by absorbance at 450nm including blank correction (n=5; mean±SD; two-tailed, unpaired Mann-Whitney u-test). **C** Percentage of CD3$^+$ cells and (**D**) their proportion in CD4$^+$ and CD8$^+$ T cells (relative to leukocytes CD45$^+$ live/dead marker) in peritoneal lavage of *Rbpj*$^{i\Delta EC}$ and control mice (n≥6; mean±SD; two-tailed, unpaired Mann-Whitney U-test).

In addition, I also analyzed the contribution of the T cells on the decreased tumor burden in the omentum and I analyzed the infiltration of CD8$^+$ cells into tumor areas of the omentum. The analysis the omentum after four weeks of tumor growth, showed a trend of increased in infiltrating cytotoxic T cells in the tumor nodules of the omentum, even though this increase was not significant (**Fig 2.26.B**). Obtained results suggest, that endothelial Notch-depended education of monocyte-derived macrophages has an impact on their immunosuppressive phenotype with a consequence on cytotoxic T cells.
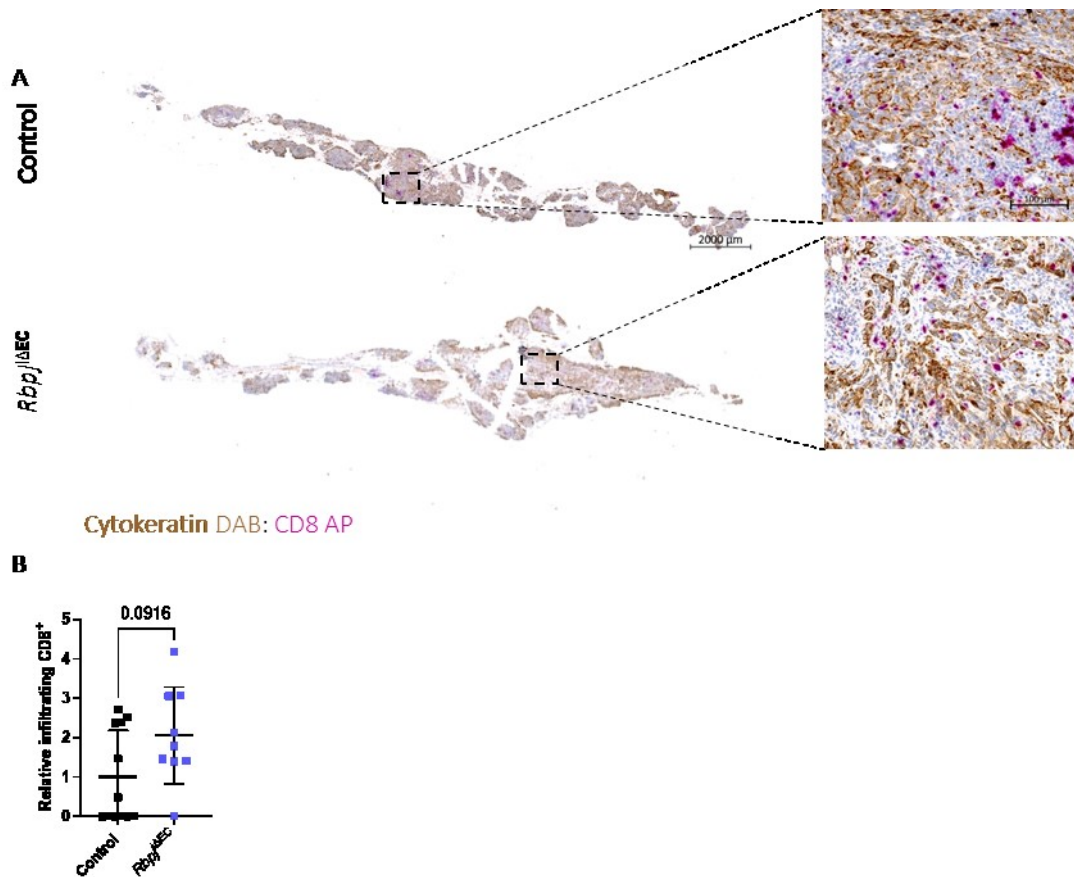
Figure 2.26: Loss of endothelial Notch increases cytotoxic T cells in metastatic niche of epithelial ovarian cancer. **A** Representative images of the whole omentum and increased magnification stained for tumor infiltrating cytotoxic T cells (CD8$^+$) in tumor areas (cytokeratin) of the omentum from control and *Rbpj*$^{i\Delta EC}$ four weeks after tumor injection and quantification (**B**) (n≥9; mean±SD; two-tailed, unpaired Mann-Whitney U-test).

2.5 Analysis of endothelial Notch-dependent regulation of myeloid cell recruitment in homeostasis and acute inflammation

2.5.1 Role of endothelial Notch signaling on myeloid cell composition in the peritoneal cavity under homeostatic condition

In order to investigate whether the changes described so far are solely due to altered Notch signaling in the endothelium or whether these require the additional presence of a tumor, I analyzed immune cell populations within the peritoneal cavity of the corresponding non-tumor-bearing mice. Therefore, recombination was performed in adult female mice of ecN1ICD as well as $Rbpj^{i\Delta EC}$ mice and after three weeks of tamoxifen administration the myeloid cell populations within the peritoneal cavity were analyzed using flow cytometry. I analyzed the different myeloid cell populations; neutrophils and macrophages and I could not observe any differences between ecN1ICD as well as $Rbpj^{i\Delta EC}$ compared to their littermate controls (**Fig. 2.27.A and B**). In addition, further analysis of the peritoneal macrophage populations did not show any differences in resident (**Fig. 2.27.A and B**) neither in LPM, no SPM populations between the different groups (**Fig 2.27.C**). In summary, the composition of monocyte-derived macrophages is not changed before tumor inoculation in both models of altered endothelial Notch signaling.
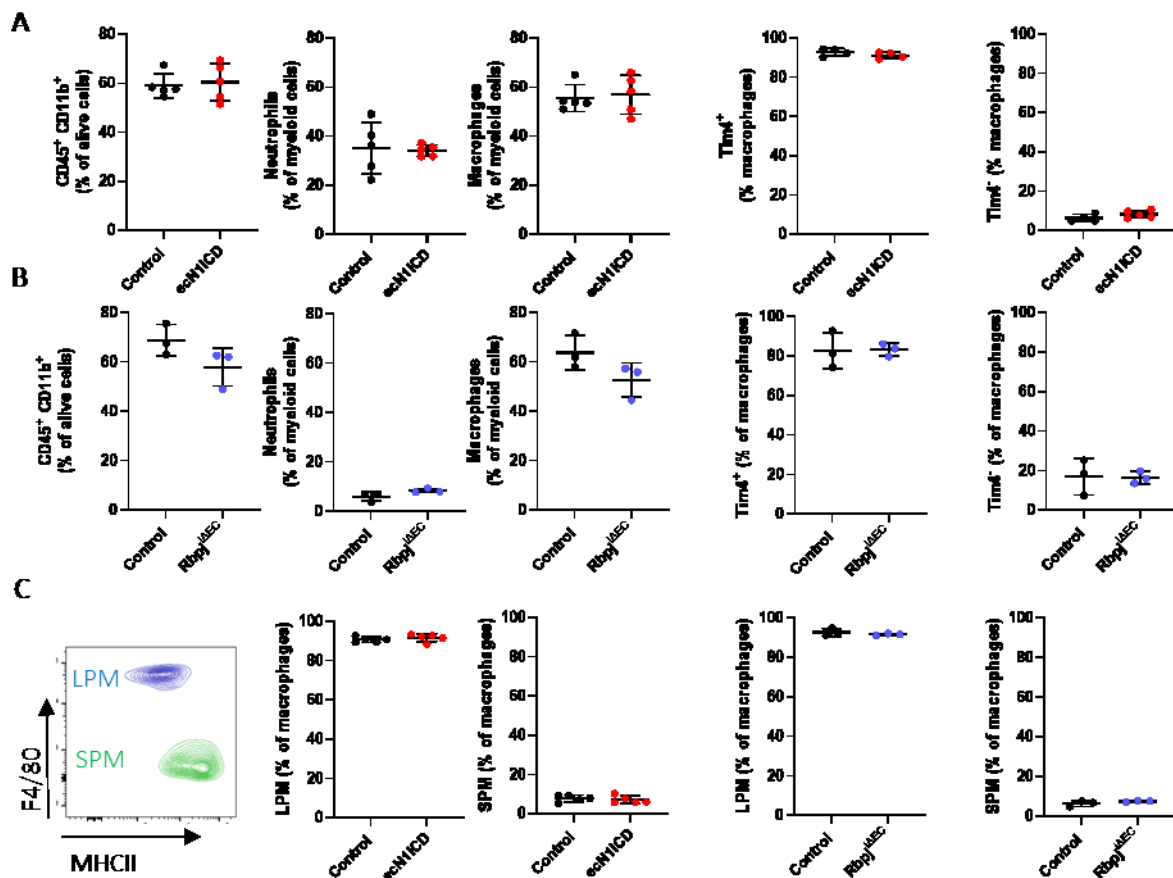
Figure 2.27: Analysis of myeloid cells in peritoneal lavage without tumor of ecN1ICD and Rbpj$^{i\Delta EC}$ mice compared to control. **A** Analysis of myeloid cells (CD45+, CD11b^{high}), neutrophils (CD45+, CD11b^{high}, Ly6G+), macrophages (CD45+, CD11b^{high}, F4/80+), resident macrophages (Tim4+) and recruited macrophages (Tim4-) relative to single cells in ecN1ICD mice compared to control (n=5; mean±SD). **B** Analysis of myeloid cells, neutrophils, macrophages, resident macrophages, and recruited macrophages, relative to single cells in $Rbpj^{i\Delta EC}$ mice compared to control (n=3; mean±SD). **C** Analysis of monocyte-derived macrophages in large peritoneal macrophages (LPM; F4/80^{high}, MHCII^{low}) and small PM (SPM; F4/80^{low}, MHCII^{high}) relative to macrophages in ecN1ICD mice (n=5; mean±SD) as well as $Rbpj^{i\Delta EC}$ (n=3; mean±SD) compared to control.

2.5.2 Role of endothelial Notch signaling on myeloid cell recruitment in the peritoneal cavity in acute inflammation

To further clarify if the endothelial Notch-depended recruitment of monocyte-derived macrophages into the peritoneal cavity is limited to a tumor-induced stimuli, I analyzed the infiltration of myeloid cells in an experimental peritonitis model. In the model of experimental peritonitis, mice received thioglycolate i.p. to mimic bacterial peritonitis, 3 weeks after recombination (**Fig 2.28.A**). Thioglycolate induces a neutrophil and monocyte infiltration in the first place, followed by differentiation of monocytes into macrophages (Gautier, *et al.*, 2013). I analyzed the different myeloid cell populations; neutrophils, monocytes as well macrophages and their responding monocyte-derived macrophage population after 72 and 24 hours in the peritoneal cavity and blood using flow cytometry.

Firstly, to address the question, if macrophage recruitment during peritoneal inflammation is affected due to loss of endothelial Notch signaling, I analyzed the peritoneal cavity after 72 hours after thioglycolate injection. Macrophages, differentiated from monocytes to phagocytose pathogens and are the second wave of immune response towards an inflammation in the peritoneal cavity (Gautier *et al.*, 2013). Analyzing the macrophage populations, I could not observe any changes in myeloid cells and macrophages, neither resident nor recruited, among the different groups; ecN1ICD and *Rbpj*[iΔEC] compared to their corresponding controls (**Fig 2.28.B** and **C**).
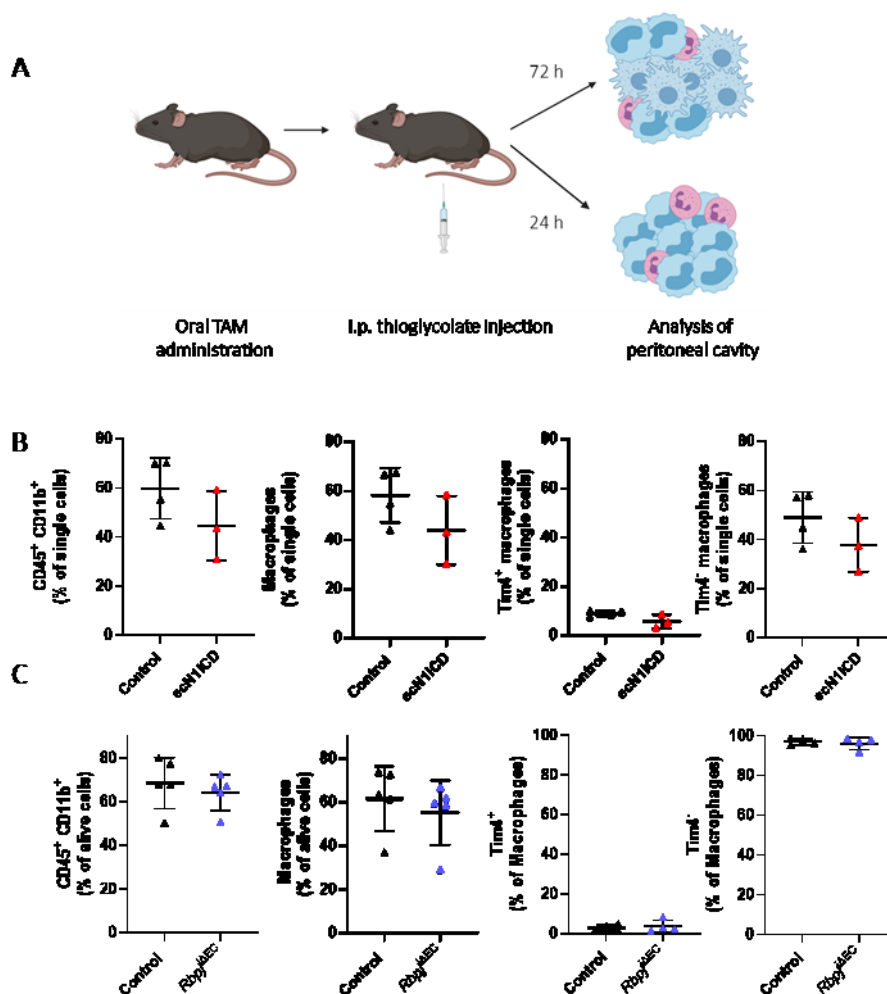
Figure 2.28: Analysis of macrophage infiltration in peritoneal lavage from ecN1ICD and Rbpj^{iΔEC} mice compared to controls after 72 hours of thioglycolate injection. **A** Workflow of peritoneal experimental peritonitis, mice received thioglycolate intraperitoneal (i.p.) to mimic bacterial peritonitis, three weeks after tamoxifen application to induce gene recombination. Myeloid cell compartment was analyzed 72 and 24 hours (h) after thioglycolate injection. **B** Analysis of myeloid cells (CD45$^+$, CD11b^{high}), macrophages (CD45$^+$, CD11b^{high}, F4/80$^+$), resident macrophages (Tim4$^+$) and recruited macrophages (Tim4$^-$) relative to single cells in ecN1ICD mice compared to control (n=3; mean±SD) after 72 h of thioglycolate injection. **C** Analysis of myeloid cells, macrophages, resident macrophages, and recruited macrophages, relative to single cells in *Rbpj*^{iΔEC} mice compared to control after 72 h of thioglycolate injection (n=5; mean±SD).

During tumor progression of EOC, monocyte-derived macrophages infiltration, in particular the IntPM and SPM populations, into the TME is regulated by endothelial Notch (**Fig. 2.17.C** and **D**). Therefore, I also analyzed the different populations of monocyte-derived macrophages in the model of experimental peritonitis model in ecN1ICD as well as *Rbpj*^{iΔEC} mice compared to their corresponding controls. I could not detect any differences in any of the macrophage populations in the different mouse model of endothelial Notch signaling 72 hours after thioglycolate injection. Therefore, the data suggest that the infiltration of monocyte-derived macrophages is a tumor-dependent phenotype during EOC tumor progression.
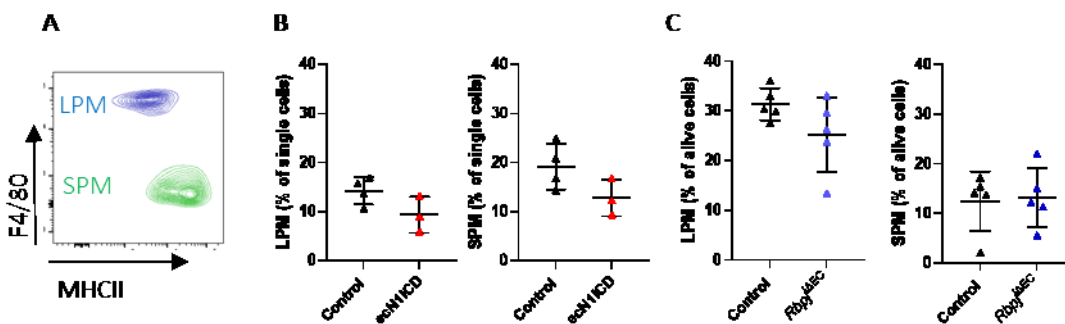
Figure 2.29: Analysis of monocyte-derived macrophage populations in peritoneal lavage from ecN1ICD and Rbpj^{iΔEC} mice compared to control after 72 hours of thioglycolate injection. **A** Gating of monocyte-derived macrophages by F4/80 and MHCII expression. Analysis of monocyte-derived macrophages relative to signle cells in ecN1ICD mice (**B**) (n=3; mean±SD) as well as *Rbpj*^{iΔEC} relative to alive cells (**C**) (n=5; mean±SD) compared to their corresponding control.

To further investigate the role of endothelial Notch1 in the infiltration of monocyte-derived macrophages in the model of bacterial peritonitis, I also analyzed the myeloid cell infiltration in the blood after 72 hours after thiogycolate injection. As already overserved in the peritoneal fluid, I also could not detect any significant changes in myeloid cells, neutrophils and monocytes in the blood of ecN1ICD and *Rbpj*^{iΔEC} compared to their corresponding controls. The analysis of the myeloid cell compartment within the peritoneal cavity and blood in the two different mouse models of endothelial Notch signaling indicates that modulating the activation of Notch in the endothelium is not sufficient to regulate macrophage recruitment in a model of acute inflammation, like the model of bacterial peritonitis.
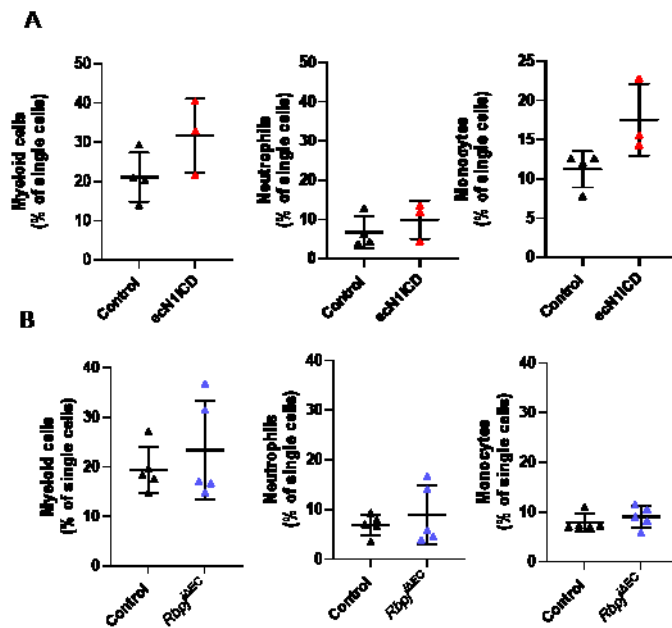
Figure 2.30: Analysis of monocyte populations in blood from ecN1ICD and Rbpj$^{i\Delta EC}$ mice compared to control after 72 hours of thioglycolate injection. A Characterisation of myeloid cells (CD45$^+$ CD11b$^+$), neutrophils (CD45$^+$ CD11b$^+$ FSC and SSC (Gating strategy Appendix **Fig. 5.3**) and monocytes (CD45$^+$ CD11b$^+$ FSC and SSC) relative to single cells in ecN1ICD mice (**B**) (n=3; mean±SD) as well as Rbpj$^{i\Delta EC}$ (neutrophils (CD45$^+$ CD11b$^+$ Ly6G$^+$), monocytes (CD45$^+$ CD11b$^+$ Ly6C$^+$)) (n=5; mean±SD) compared to their corresponding control.

As already mentioned, the immune response towards an inflammation leads to neutrophil and monocyte recruitment in the first place (Gautier *et al.*, 2013) and endothelial Notch signaling is able to regulate the infiltration of monocyte-derived macrophage in a tumor context (2.4.1 Endothelial Notch signaling regulates monocyte-derived macrophage recruitment in epithelial ovarian cancer). Consequently, I also analyzed the infiltration of neutrophils and monocytes after 24 hours in *Rbpj*$^{i\Delta EC}$ mice compared to littermate controls. Endothelial Notch loss-of-function mice showed no changes in the recruitment of neutrophils and monocytes within the peritoneal cavity 24 hours after thioglycolate administration (**Fig. 2.23.A and B**). Resident macrophages resolve the inflammation and are replaced by monocyte-derived macrophages afterwards (Gautier *et al.*, 2013). Consequently, I also analyzed the resident peritoneal macrophage population (Tim4$^+$), non-long-term macrophages (**Fig. 2.31.B**) as well the LPM and SPM population (**Fig 2.23.C**) in all different groups and could not detect any changes compared to littermate controls. In summary, loss of endothelial Notch signaling is also not sufficient to regulate early responses towards acute inflammation within the peritoneal cavity.
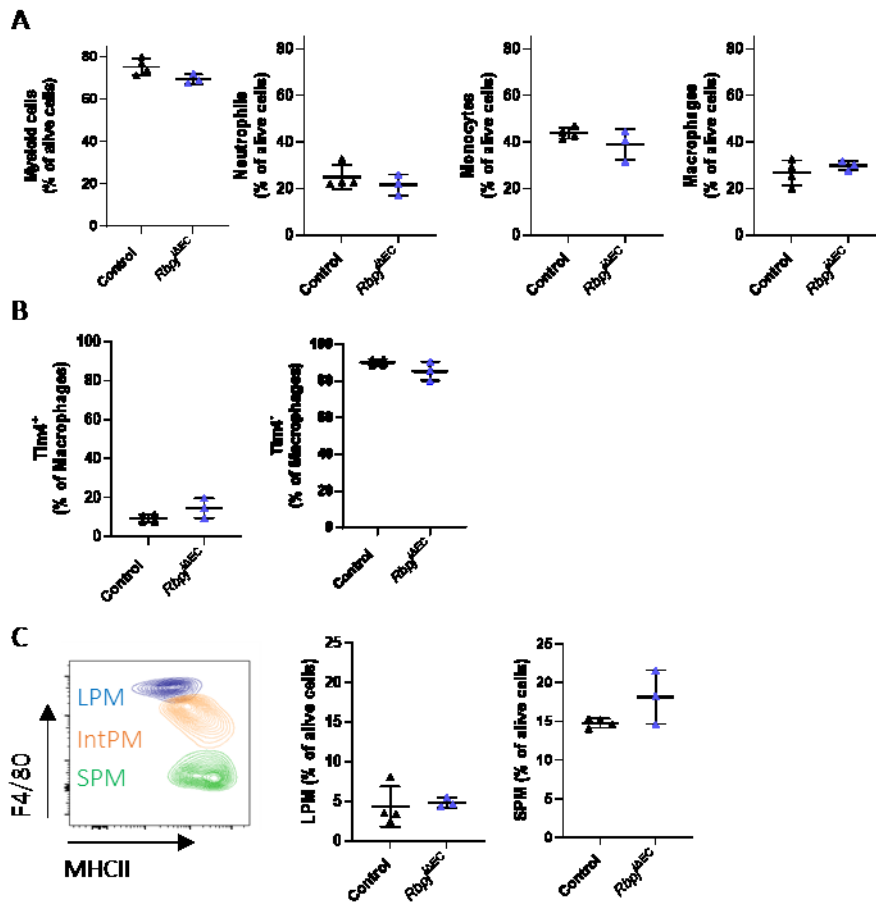
Figure 2.31: Analysis of myeloid cell populations in peritoneal cavity from Rbpj[iΔEC] mice compared to control after 24 hours of thioglycolate injection. **A** Analysis of myeloid cells (CD45^{+}, CD11b^{high}), neutrophils (CD45^{+}, CD11b^{high}, Ly6G^{+}), monocytes (CD45^{+}, CD11b^{high}, Ly6C^{+}) and macrophages (CD45^{+}, CD11b^{high}, F4/80^{+}) as well as resident macrophages (Tim4^{+}) and recruited macrophages (Tim4^{-}) (**B**) relative to alive cells in *Rbpj*[iΔEC] mice compared to control (n≥3; mean±SD). **C** Analysis of monocyte-derived macrophages in large peritoneal macrophages, LPM (F4/80[high], MHCII[low]) and small PM, SPM (F4/80[low], MHCII[high]) relative to alive cells in *Rbpj*[iΔEC] (n≥3; mean±SD) compared to control.

The blood is the major compartment for neutrophils, which patrol the blood stream and get recruited towards inflammatory responses (Kolaczkowska & Kubes, 2013). For that reason, I also analyzed the myeloid cell composition in the blood after 24 hours of thioglycolate injection. I could observe a decrease in myeloid cells and neutrophils, although not statistically significant, whereas monocytes were not affected in the blood of *Rbpj*[iΔEC] mice compared to control. These obtained results indicate, that loss of endothelial Notch affect the infiltration of neutrophils towards an inflammatory microenvironment. However, further studies need be performed to investigate if this reduction in neutrophil population in the blood is due to the inhibition endothelial Notch in the bone marrow niche effecting immune cell progenitors.
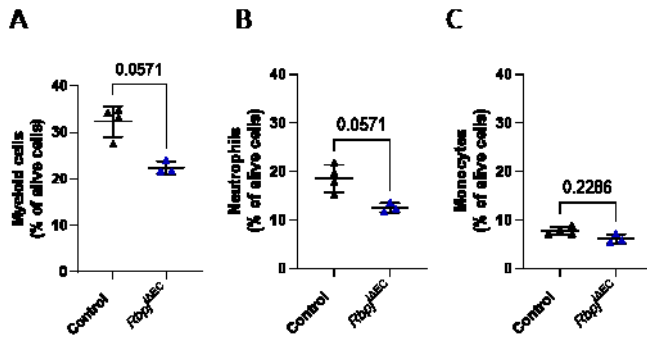
Figure 2.32: Analysis of monocyte populations in blood from Rbpj^{iΔEC} mice compared to control after 24 hours of thioglycolate injection. **A** Characterisation of myeloid cells (CD45$^+$ CD11b$^+$), (**B**) neutrophils (CD45$^+$ CD11b$^+$ Ly6G$^+$) and (**C**) monocytes (CD45$^+$ CD11b$^+$ Ly6G$^-$ FSC and SSC) relative to alive cells (Live/dead marker) in *Rbpj*^{iΔEC} mice compared to control (n≥3; mean±SD).

During tumor growth of EOC newly recruited macrophages from *Rbpj*^{iΔEC} mice showed an impaired immunosuppressive phenotype due to their decreased expression of the HA receptor CD44. As a result, I also analyzed the classical inflammatory and anti-inflammatory macrophage marker as well the expression of CD44 on macrophages in the peritoneal fluid after 24 hours of thioglycolate injection. Although, I could not detect changes in the expression of classical macrophages markers, *iNos* and *Arg1* (**Fig. 2.33.A**), I observed a significant reduction of *Cd44* (**Fig. 2.33.B**) and reduced expression of the cytokine *Il1b* (**Fig. 2.33.C**) on macrophages isolated from *Rbpj*^{iΔEC} mice compared to controls. The study from Noble *et al*. showed that stimulation of BMDM with HA increases IL1β production and blocking of HA receptor CD44 by monoclonal antibodies were able to inhibit these effects (Noble, Lake, Henson, & Riches, 1993). Therefore, it is reasonable to assume, that these downregulation of the cytokine IL1β is due to the regulation of CD44 expression by endothelial Notch signaling. Altogether, the data suggest that even though I could not observe any changes in the myeloid cell population within the peritoneal fluid in a model of acute inflammation, the macrophages isolated from *Rbpj*^{iΔEC} mice showed differences in the modulation of CD44 even though the role of HA in this model is not clear.
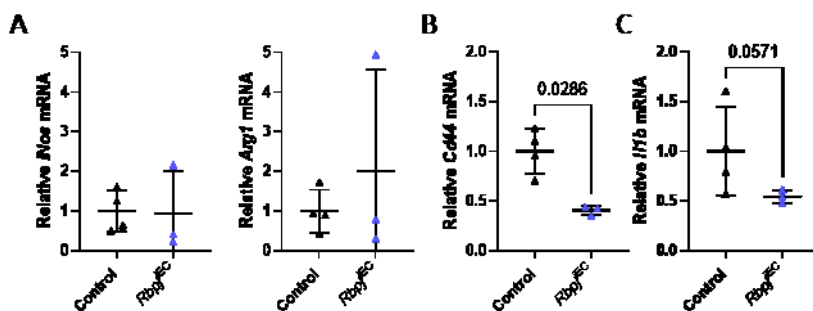
Figure 2.33: Loss of endothelial Notch decrease hyaluronic acid receptor CD44 on macrophages. Analysis of mRNA expression of macrophages isolated from peritoneal fluid from *Rbpj*^{iΔEC} compared to their corresponding control. Peritoneal macrophages were isolate due to their attaching capazity after 24 hours thioglycolate injection. **A** Analysis of classical inflammatory (*iNos*) and anti-inflammatory (*Arg1*) markers of macrophage activation, hyaluronic receptor *Cd44* (**B**) and the cytokine *Il1b* (**C**) via RT-qPCR (n≥3; mean±SD; two-tailed, unpaired Mann-Whitney U-test)

3 Discussion

3.1 Loss of endothelial Notch reduces myeloid cell infiltration in tumor microenvironment

The present PhD thesis highlights the crucial role of endothelial Notch1 signaling on the recruitment and activation of myeloid cells and therefore how ECs shape the TME. ECs are nowadays considered to be an important compartment in the tumor stroma due to their role in regulating the phenotype of the TME by secretion of angiocrine factors (Alsina-Sanchis, Mülfarth, & Fischer 2021; Augustin & Koh, 2017; Pasquier *et al.*, 2020). Angiocrine factors regulate organ homeostasis as well as the TME and prime pre-metastatic niches (Alsina-Sanchis, Mülfarth, & Fischer 2021; Rafii *et al.*, 2016; Singhal & Augustin, 2020). Our group has already demonstrated, that human primary tumors frequently have activated Notch1 in the tumor endothelium, which also correlates with immune cell recruitment into the TME and facilitates metastasis (Wieland *et al.*, 2017). Especially, myeloid cells are implicated in the immunosuppressive phenotype of most tumors (Schupp *et al.*, 2019). Samples from ovarian cancer patients showed that, the amount of cleaved Notch could be associated with an increased myeloid cells infiltration in the tumor tissue (**Fig. 2.1**). Further, *in vivo* mouse studies on the role of endothelial Notch signaling on the immune cell compartment within the TME showed a significant decrease in myeloid cell recruitment in the endothelial Notch loss-of-function model (**Fig. 2.3.B**). TAMs are the most abundant immune cell population within most TME (Bingle *et al.*, 2002; Lewis & Pollard, 2006). Tumor infiltrating macrophages get educated by the TCs to promote tumor progression, for example by attenuation of the anti-tumor response, remodeling of ECM and inducing angiogenesis (Yousefi, 2020). In line with this, deletion of *Rbpj* in the endothelium significantly decreased the infiltration of newly recruited macrophages into the TME (**Fig. 2.3.C**). Similar decreased immune cell infiltration was observed in an atherosclerosis model of apolipoprotein E (ApoE) KO mice when RBPJ was deleted in the endothelium (Nus *et al.*, 2016). In addition, activation of N1ICD in liver sinusoidal ECs leads to an increased infiltration of neutrophils during a hepatic ischemia (Zhang *et al.*, 2020). These observations of endothelial Notch-dependent infiltration of immune cells are limited to chronic inflammation. However, there are also indications that ECs activated by TCs control immune cell infiltration into the TME (Alsina-Sanchis, Mülfarth, & Fischer 2021; Augustin & Koh, 2017; Pasquier *et al.*, 2020). For instance, secretion of the angiocrine factor Angiopoetin2 (Ang2) leads to an autocrine activation of STAT3 signaling in the endothelium of distant metastatic sites and further to the secretion of CCL2 and the expression of ICAM (Srivastava *et al.*, 2014). The cytokine CCL2 is necessary to induce extravasation of CCR2$^+$ monocytes into the inflamed tissue or TME from the blood stream (Ostuni *et al.*, 2015; Serbina & Pamer, 2006), whereas integrins, like ICAM1 and VCAM1 play a role in the adhesion and transmigration of immune cells into the TME. Furthermore, also VCAM1 is reported to be highly expressed on tumor ECs in a Notch1-dependent manner (Nus *et al.*, 2016; Verginelli *et al.*, 2015; Wieland *et al.*, 2017). It was reported that TC secreted factors induce VCAM1 and Vascular adhesion protein-1 (VAP-1) expression on ECs in distant metastatic sites, which in turn leads to an increased myeloid cell recruitment and priming of the pre-metastatic niche by inducing an immunosuppressive microenvironment. Furthermore, blocking of VCAM1 or VAP1 reduces myeloid cell infiltration and metastasis (Ferjancic *et al.*, 2013). Therefore, these studies indicate the special importance of TCs and ECs interactions in shaping the TME by recruitment of immune cells and effecting TCs proliferation. Furthermore, there are increasing evidences that also ECs have an impact on the phenotype of recruited and infiltrating myeloid cells. In a mouse model of glioblastoma tumor ECs were shown to be the main source of IL6 in the TME. Moreover, EC-specific KO of *Il6* showed to improve the survival by reducing the infiltration of pro-tumorigenic, alternatively activated TAMs (Wang *et al.*, 2018). Furthermore, studies on VEGF blocking antibodies to reduce tumor angiogenesis resulted in an increased infiltration of cytotoxic T cells as well as effects on the activation of tumor-infiltrating macrophages (Allen *et al.*, 2017). Taking together, TC-induced activation of the endothelium, for

example by the activation of Notch1, is able to recruit myeloid cells into the TME. In addition, TCs also instruct ECs to pre-condition those infiltrating immune cells, which will impact the phenotype of the microenvironment.

The decreased immune cell infiltration into the TME of mice lacking *Rbpj* in the endothelium can unlikely be explained by either an impaired tumor vasculature or a decreased tumor growth (**Fig. 2.2.B** and **Fig. 2.2.E**). The s.c. tumor model in loss-of-function mice led to a significantly increased vessel density (**Fig. 2.2.E**). Depletion of *Rbpj* in adult endothelium increased vessel density in the heart, as well blocking of endothelial Notch signaling in the tumor vasculature by DLL4 blocking increased vessel density in long-term treatment (Jabs *et al.*, 2018; Ridgway *et al.*, 2006). Furthermore, blocking DLL4/Notch signaling in tumor models showed to impair the blood flow indicating an inefficient differentiation of the tumor vessel (Ridgway *et al.*, 2006). However, our model of *Rbpj* depletion in adult endothelium did not show any impairment of ECs maturation due to an increased vessel coverage of the tumor vasculature (**Fig. 2.2.G**). Also the study of Nus *et al.* demonstrated that the endothelial cell barrier function is not impaired in an atherosclerosis mouse model lacking *Rbpj* in the endothelium (Nus *et al.*, 2016). In summary, activation of EC Notch by TC leads to an increased infiltration of myeloid cells in human ovarian cancer patient samples and loss of endothelial Notch in s.c. tumor mouse model regulates the infiltration of TAMs into the TME of primary tumor without affecting the maturation of tumor blood vessels.

3.2   CXCL2 as novel canonical Notch target gene in endothelial cells

To address the question of how ECs regulate immune cells recruitment, I analyzed the angiocrine secretion of chemokines. Chemokines tightly regulate the recruitment and infiltration of immune cells into inflamed tissue or TME (Kohli *et al.*, 2021). Activation of Notch1 interacts with NF-κB signaling in ECs and is described to induce an inflammatory phenotype of the endothelium, mediating immune cell recruitment (Mack *et al.*, 2017; Poulsen *et al.*, 2018). Therefore, I confirmed several chemokines and cytokines to be induced upon Notch1 activation in ECs (**Fig. 2.4**). Moreover, determining canonical Notch target genes using CRISPR-Cas9 mediated KO showed a RBPJ-dependent regulation of CCL1, CXCL2, CXCL12 and IL33 in human ECs (**Fig. 2.6**). We already showed that activation of N1ICD in ECs lead to senescence phenotype (Wieland *et al.*, 2017). Moreover, IL33 is a target gene of quiescent ECs regulated by Notch (Sundlisaeter *et al.*, 2012). In line with this, the results suggested that IL33 is regulated via RBPJ-mediated canonical Notch1 pathway in ECs. Expression of CXCL2 by a canonical RBPJ-Notch1 pathway was validated with whole tissue lysates from endothelial Notch loss-of-function as well as gain-of-function mice *ex vivo* and by *in vitro* studies on human primary ECs (**Fig. 2.4.G, Fig. 2.5.C** and **Fig 2.6.A** to **Fig. 2.6.C**). Additional, *in silico* analysis of the CXCL2 promotor region showed RBPJ binding sites, in line with previous results (**Fig. 2.6.B**). In contrast, the functional homologs of CXCL2 were not regulated by canonical Notch signaling in ECs (**Fig. 2.6.D**). Activation of endothelial Notch by shear stress also showed to induce pro-inflammatory cytokines, including CXCL2 (Mack *et al.*, 2017). Interestingly, not all cytokines which are induced by Notch activation also showed a reduced or abolished induction in *RBPJ* KO human ECs, like *CCL2* (**Fig. 2.6.F**). As already mentioned, Notch1 activation can lead to a complex formation of N1ICD and NF-κB-p65 to induce non-canonical target genes including CCL2 (Mack *et al.*, 2017; Nus *et al.*, 2016; Poulsen *et al.*, 2018). Moreover, stimulation of human ECs with TNFα is able to induce the expression of Notch target genes like JAG1, HEY1 and VCAM1 in a NF-κB-mediated Notch activation (Nus *et al.*, 2016). Therefore, the data suggest a non-canonical induction of Notch target genes by interaction with other signal transduction pathways, like NF-κB. However, studying canonical Notch signaling mediated by RBPJ in human primary ECs unravel novel Notch target genes, especially CXCL2.

3.3   Activation of endothelial Notch by tumor cells mimic lymphatic endothelial cells

To further investigate, if overexpression of Notch1 in ECs not only increases cytokine expression but also if it could impact on the phenotype of ECs, I analyzed the tumor endothelium of endothelial Notch gain-of-function model. Overexpression of N1ICD in tumor ECs showed a significant increase of PROX1, a classical LEC marker, whereas other markers for LECs were not changed (**Fig. 2.7**). Furthermore, *in vitro* analysis showed that overactivation of N1ICD in LEC increased expression of cytokines as well as survival marker (**Fig. 2.9.A** and **Fig. 2.9.D**). Moreover, primary vein EC increase the expression of LEC markers and *VEGFc* after N1ICD overactivation (**Fig. 2.8**). Consistently, the knock-out of *RBPJ* in LEC showed the opposite effect (**Fig. 2.9.C** and **Fig. 2.9.D**). These observations are leading to two different possible scenarios: blood ECs mimic LECs and/or LECs start to increase their proliferation upon overexpression of N1ICD. LEC develop from vein vessels due to the activation of the transcription factor PROX1 and binding of VEGFc to its receptor VEGFR3 during early development (Karkkainen *et al.*, 2004; Y. Yang *et al.*, 2012). Moreover, the differentiation of LECs is not limited to vein ECs but also ECs from mesentery, skin and heart (Klotz *et al.*, 2015; Mahadevan *et al.*, 2014; Martinez-Corral *et al.*, 2015; Stanczuk *et al.*, 2015). Additionally, VE-Cadherin (the driver of Cre recombinase our mouse model) is a broad ECs specific marker, which is not only expressed by blood ECs but also weakly by LEC (Hagerling *et al.*, 2018). Therefore, it is reasonable to speculate that recombination does not only occur in blood ECs but also in LEC leading to increased lymph-angiogenesis. During tumor progression, LECs play a major role in the lymph metastasis promoted by tumor-associated LEC (Karpanen *et al.*, 2001; Mandriota *et al.*, 2001; Skobe, Hamberg, *et al.*, 2001; Skobe, Hawighorst, *et al.*, 2001; Stacker *et al.*, 2001). Studies on tumor-associated lymph-angiogenesis claim that angiogenesis of LECs occur due to proliferation of pre-existing LECs (Leu, Berk, Lymboussaki, Alitalo, & Jain, 2000). TC secretion of VEGF correlates with increased metastasis in cancer patients (Karpanen *et al.*, 2001; Mandriota *et al.*, 2001; Maula *et al.*, 2003; Stacker *et al.*, 2001), but it does not seem to be sufficient to induce *de novo* lymph-angiogenesis *in vitro* (Cao *et al.*, 2006). However, determination of LECs within the TME is only sufficient, if all histological LEC markers, like VEGFR3, PROX1, LYVE1 and Podoplanin are expressed by EC (CD31$^+$) (Ji, 2006). On the other hand, high specification of ECs to their tissue of origin also involves a re-modeling of established vasculature to organ changes like tumor growth. Similar to what occurs to ECs from arteries within the vascular bed of the placenta, which undergo remarkable changes during pregnancy. Moreover, those ECs start to express LECs markers (PROX1, LYVE1 and VEGFR3) and mimic lymphatic vessels to adapt to the new challenges of the environment (Pawlak *et al.*, 2019). Therefore, I conclude that activation of endothelial Notch within the TME induces an EC-mimicry of LEC to amplify tumor signals and induce an immunosuppressive TME. However, further studies, on for example linage tracing of tumor ECs, are needed to exclude the hypothesis of increased tumor lymph-angiogenesis.

3.4   Loss of endothelial *Rbpj* reduces tumor burden of epithelial ovarian cancer

The role of endothelial Notch signaling on the vasculature of the pre-metastatic niche before and during metastatic EOC in the omentum showed no changes prior tumor inoculation due to the deletion of *Rbpj* in omental ECs (**Fig. 2.11** and **Fig. 2.12**). The endothelium in the omentum of loss-of-function mice showed an increased vessel density after tumor inoculation (**Fig. 2.12.B**), which goes in line with the increased vessel density in the s.c. tumor model (**Fig. 2.2.E**). However, the endothelium of the omentum did not show any differences in vessel coverage (**Fig. 2.12.E**). Therefore observations suggest, that the effect of increased vessel coverage is limited to *de novo* angiogenesis induced by primary tumor growth. On the other hand, tumor growth in the omentum of gain-of-function mice did not show any changes in vessel density but increased endothelial VCAM1 expression, a known Notch1 target gene (Nus *et al.*, 2016; Verginelli *et al.*, 2015; Wieland *et al.*, 2017) upon tumor progression (**Fig. 2.11.C**). Taking together,

observed changes within the metastatic niche of EOC showed that tumor progression led to the expected activation of endothelial Notch1.

Recent publications already showed that endothelial specific depletion of *Rbpj* led to decreased primary tumor growth and reduced metastasis in lung and liver after ten days of primary tumor resection due to decreased population of endovascular progenitors (Donovan *et al.*, 2019). In line, in my work, the analysis of the metastatic niche of EOC showed a significant decreased tumor burden if *Rbpj* is lacking in the endothelium (**Fig. 2.13**), as well as reduced immune and myeloid cell population in the omentum (**Fig. 2.14**). As already mentioned, ovarian cancer cells preferentially metastasize to the peritoneal visceral fat pad, the omentum. The epithelial layer of the ovaries and the omentum mesothelial layer are developed from the same origin. Leading to the suggestion, that metastasis of EOC in the omental tissue provides more advantages for the TCs to invade the visceral fat pad, which is also in line with Paget´s "seed and soil" theory (Yousefi, 2020). Lastly, the adipocytes within the omentum also facilitate seeding of TCs by promoting tumor growth (Nieman *et al.*, 2011). Even more evident is that, ovarian cancer cells do not colonize other intra-peritoneal fat tissues due to the lack of milky spots (Clark *et al.*, 2013). Omental macrophages within the milky spots are critical mediators of tumor progression, which promote invasiveness of EOC cells (Etzerodt *et al.*, 2020). Depletion of tissue-resident omental macrophages prevent tumor progression and peritoneal spread of TCs (Krishnan *et al.*, 2020). Additionally, the early step of colonization of the omentum is independent of lymphocytes. This was demonstrated in studies of immunosuppressive mice, highlighting the role of macrophages on tumor progression in EOC (Clark *et al.*, 2013). However, in my studies further characterization did not show any differences in pro-tumorigenic CD163$^+$ omental macrophages (**Fig. 2.15**) neither changes of cytotoxic T cells in the different models of endothelial Notch signaling (**Fig. 2.26**). The preferential colonization of the omentum during EOC progression is not yet fully understood. Studies on the interaction of ovarian cancer cells and omental macrophages also described the importance of chemokine secretion of tissue-resident macrophages for successful colonization of TCs (Krishnan *et al.*, 2020). Therefore, not only the infiltration of macrophages in tumor areas but also their polarization and activation are important for the utmost crosstalk of ovarian cancer cells to promote tumor progression. Further characterization of omental myeloid cells needs to be performed to identify the (macrophage) subset regulated by endothelial Notch signaling mediating the tumor burden in the metastatic niche.

During metastatic EOC growth, TCs not only settle in the omentum but they also start to spread into the peritoneal cavity at the same time. Investigation of the tumor burden within the peritoneum showed no differences in the endothelial Notch gain-of-function model, whereas the tumor burden was significantly reduced in loss-of-function mice compared to control (**Fig. 2.16**). Metastasis is a complex process from detaching of TCs and migration from the primary tumor to settle in the metastatic niche. Ovarian cancer metastasis is characterized to a transcoelomic, transperitoneal metastasis due to a lack of physiological boarders as well to a less extend hematogenous metastasis (Yousefi, 2020). The resulting peritoneal carcinomatosis is characterized by TCs passively floating in the peritoneal fluid (van Baal *et al.*, 2018). Additionally, during colonizing of the omentum TCs interact with the stromal cell, which lead to the transcriptional changes allowing the TCs also to spread into the peritoneum. In the microenvironment within the omentum, TCs interact with adipocytes, fibroblast, mesothelial cells, ECs and immune cells which lead to transcriptional changes adapting TCs to spread in the peritoneal cavity. The crosstalk with omental macrophages increases the invasiveness and CSC-like phenotype of TC (Etzerodt *et al.*, 2020). Therefore, the decrease in tumor-infiltrating myeloid cells within the metastatic niche could also explain the decreased peritoneal spread in mouse lacking *Rbpj* in the endothelium. In summary, depletion of endothelial *Rbpj* impaired the tumor growth in EOC resulting in a reduced tumor burden in the metastatic niche as well as peritoneal carcinomatosis. It is possible to speculate that this

impaired tumor burden is mediated by a decreased myeloid infiltration into the metastatic niche in endothelial Notch loss-of-function mice without affecting the omental vascular functions.

3.5   Loss of endothelial Notch signaling reduces infiltration and primes monocyte-derived macrophages in epithelial ovarian cancer

3.5.1   Endothelial Notch regulates infiltration of monocyte-derived macrophages into the tumor microenvironment of epithelial ovarian cancer

As already mentioned, TAM infiltration and polarization in the TME is of striking importance for tumor progression, especially in EOC (Bingle *et al.*, 2002; Lewis & Pollard, 2006). Under homeostatic conditions, the most abundant peritoneal immune cells are B- and T lymphocytes as well as resident macrophages, within a constant volume of peritoneal fluid. During EOC progression, the production and exchange of peritoneal fluid is dysregulated, resulting in an increased peritoneal fluid volume, also called ascites. Several studies, indicate that these effects are induced by a TC-mediated inflammation, which recruits immune cells into the TME to further promote tumor growth (van Baal *et al.*, 2018). Moreover in EOC, Goossens *et al.* demonstrated that monocyte-derived TAMs replace the resident macrophages in the peritoneal cavity with tumor progression and therefore promote tumor growth by creating an immunosuppressive microenvironment (Goossens, *et al.*, 2019). Analysis of the myeloid cell population in the endothelial Notch gain-of-function model showed a significant increase of monocyte-derived macrophages in the model of metastatic EOC (**Fig. 2.17.C**). While the inhibition of Notch signaling in the endothelium by depletion of *Rbpj* leads to a significant decrease of infiltrating TAMs in two different tumor models, s.c. LLC (**Fig. 2.3.C**) and metastatic EOC (**Fig. 2.17.D**). As already discussed, several studies on the regulation of immune cell recruitment by ECs already described that endothelial Notch signaling is able to modulate the infiltration of immune cells towards a chronic inflammation. In particularly, the study from Nus *et al.* also demonstrated that depletion of endothelial *Rbpj* in ApoE KO mice showed a reduction of integrin's involved in immune cell movement like VCAM1 and ICAM1, whereas the endothelial barrier function was not affected, resulting in a reduced infiltration of leucocytes into the atherosclerotic plaques (Nus *et al.*, 2016). However, depletion of *Rbpj* in the endothelium did not show to effect on integrin expression (VCAM1) in the omentum in our model (**Fig. 2.12.C**). This indicates that secreted angiocrine factors play a role in the regulation of myeloid cell infiltration by endothelial Notch.

Studying the migration of myeloid cells into the TME *in vitro* by mimicking a physiological setting showed a significantly reduced infiltration of myeloid cells when *RBPJ* is lacking within the ECs barrier (**Fig. 2.19.C**). Additionally, knock down of the RBPJ-mediated angiocrine factor *CXCL2* showed a trend to decrease the myeloid cell recruitment into the TME (**Fig. 2.19.D**). Remarkably, in a study ovarian cancer patients had increased serum levels of CXCL1 and CXCL2, which correlated with myeloid cell infiltration and decreased overall survival (Katoh *et al.*, 2013). CXCL2, as well as functional homologs (CXCL1, CXCL5 and CXCL8), are recognized by CXCR2 on different cell types. Furthermore, blocking of CXCR2 decreased MDSC infiltration and inhibited tumor progression in several cancer types (Taki *et al.*, 2018). As well, IL8, the human homolog of CXCL2, is a pro-inflammatory cytokine that has been linked to increased proliferation and invasiveness of ovarian cancer (Zhang *et al.*, 2017). I could show that this CXCL2-mediated monocyte recruitment in ovarian cancer could be partially regulated by endothelial Notch signaling (**Fig. 2.6.C** and **Fig. 2.19.D**). Taking together, endothelial Notch regulates the myeloid cell infiltration into the TME of solid as well as metastatic tumor growth model in an angiogenesis independent manner. In more detail, preliminary results indicate that loss of endothelial Notch decrease the infiltration of monocyte-derived macrophages into the TME by regulating the expression of CXCL2.

Analysis of the myeloid cell compartment in the blood of tumor-bearing mice showed an increase of neutrophils in the gain-of-function model and a decrease of monocytes in the loss-of-function model (**Fig. 2.18**), whereas the neutrophils population within the TME of gain-of-function mice were not affected (**Fig. 2.17.A**). HPC give rise to both, common myeloid as well lymphocyte progenitors. The differentiation and self-renewal capacity of HPC need to be well-adjusted for the generation of blood cells (Seita & Weissman, 2010). HPC have a self-renewal capacity and display the stem cell for leukocytes within the blood stream (Seita & Weissman, 2010). Overexpression of endothelial Notch signaling within the bone marrow niche impacts stress responses on HPC (Vanderbeck & Maillard, 2019). EC-Notch signaling plays a profound role in the bone marrow niche by regulating HPC maintenance, promoting megakaryocyte/erythroid cell development and regulates myelopoiesis (Klinakis *et al*., 2011). Therefore, the expression of Notch ligands, like JAG1 by the ECs is of critical importance (Poulos *et al*., 2013). In detail, depletion of the Notch ligand JAG1 on ECs leads to an inhibition of HSC expansion (Poulos *et al*., 2013). However, the contribution of endothelial Notch signaling on the differentiation of HPC into circulating blood cells towards a tumor-induced stimulus is not part of this thesis and needs further investigation.

3.5.2 Loss of endothelial Notch educates monocyte-derived macrophages in epithelial ovarian cancer

Infiltrating myeloid cells in the TME show an immunosuppressive phenotype mediated by their cholesterol depletion in the model of metastatic EOC. Ovarian cancer cells secrete high molecular weight HA to induce the cholesterol efflux in TAMs, which leads to a hypersensitivity towards IL4, promoting immune responses and tumor progression (Goossens, *et al*., 2019). HA gets recognized by HA receptors, like LYVE1 and CD44 on the macrophages, which expression on myeloid cells correlates with metastasis and increased ascites (Jeon *et al*., 2008; Martincuks *et al*., 2020). Using several unbiased approaches (GSEA, IPA and GO-term analysis), I observed a downregulation of the cholesterol pathways in newly recruited TAMs isolated from *Rbpj*^{iΔEC} compared to control mice (**Fig. 2.20.B** to **Fig.2.20.D**), suggesting that also their immunosuppressive role could be affected by endothelial Notch signaling. Moreover, downregulation of the HA receptor, CD44 was observed in monocyte co-culture with ECs lacking *Rbpj* as well BMDM stimulated with CM from murine *Rbpj* KO ECs (**Fig. 2.20.E**). Additionally MMP9, a downstream target of CD44, was downregulated in stimulated BMDM (**Fig. 2.20.E** and **Fig.2.20.F**). Studies on patient-derived xenografts (PDX) models of ovarian cancer in *Mmp9* KO mice showed that, the expression of MMP9 by stromal cells is directly associated with invasiveness and aggressiveness of metastatic ovarian cancer cells (Huang *et al*., 2002). Moreover, loss of MMP9 showed to reduce the tumor growth, vessel density and macrophage recruitment. Analysis of the resulting tumors revealed that TAMs are the main source of MMP9 within the TME (Huang *et al*., 2002). Analysis of the interaction of TAMs and ovarian cancer cells in co-culture experiments showed that proliferation of TCs was increased and, moreover, using siRNA for *Mmp9* in both cell types showed, that MMP9 is secreted by TAMs to cleave heparin-bound epidermal growth factor promoting TC proliferation (Carroll *et al*., 2016). Therefore, I conclude that a multi-cell-interaction of ECs, TCs and TAMs controls the proliferation of ovarian cancer cells, possibly regulated by endothelial Notch signaling.

Furthermore, in our mouse model for metastatic EOC, endothelial-specific *Rbpj* depletion not only reduced monocyte-derived macrophage infiltration but also their phenotype. TAMs within the TME of *Rbpj*^{iΔEC} mice cannot deploy their expected TAM signature (**Fig. 2.21.A**) mediated by a downregulation of CD74 (**Fig. 2.21.B**). Analysis of the immunosuppressive phenotype in newly recruited TAMs from mice overexpressing N1ICD in the endothelium, in comparison to control or TAM isolated from mice lacking

Discussion

Rbpj in the endothelium confirmed previous results (**Fig. 2.22**). This means that activation of endothelial Notch signaling is not only important for the recruitment of TAMs but also for their education into tumor-promoting cells. As mentioned before, the TAM signature of monocyte-derived macrophages during all stages of tumor growth include a hypersensitivity towards the upstream regulator IL4. In line with this, the response towards the top upstream regulator, IL4, was inhibited in newly recruited monocyte-derived macrophages isolated from endothelial Notch loss-of-function mice compared to control (**Fig. 2.21.B**). Additionally, CD74 was one of the main downregulated genes in TAMs within the *Rbpj*[iΔEC] tumors and expression levels of CD74 correlate with poor prognosis in ovarian cancer patients (Cortes *et al.*, 2017). In a mouse model for metastatic melanoma, the blockade of CD74, on APC, inhibited the immunosuppressive effects of tumor-associated monocytes, which in turn reactivated anti-tumorigenic immune responses (Figueiredo *et al.*, 2018). In addition, we also observed that CD74 expression by monocyte-derived macrophages is necessary to develop the immunosuppressive TAM signature (**Fig. 2.23.A** and **Fig. 2.23.B**) and does not show any differential expression in resident macrophages (**Fig. 2.24.B**). CD74 can build a receptor complex with CXCR2 to induce signal transduction (Bernhagen et al., 2007). Additionally, Beswick *et al.* showed that binding of IL8 to CXCR1/2 increases CD74 expression in gastric epithelial cells (Beswick & Reyes, 2009). Since the murine homolog of IL8 is CXCL2 it is reasonable to speculate that CXCL2 expression by ECs, through canonical Notch activation, regulates CD74 expression in monocytes. This will eventually influence the behavior of monocyte-derived macrophages affecting TC-mediated education. Preliminary studies on this hypothesis, showed that co-culture of monocytes with human ECs with modulation of Notch1 signaling by either overexpression of N1ICD or depletion of *RBPJ* in HUVEC is able to prime monocyte-derived macrophages by regulating CD74 expression (**Fig. 2.23.C**). However, modulating endothelial Notch signaling alone did not lead to changes of CD74 expression on human monocytes (**Fig. 2.23.C**), whereas the incubation with TC CM in the co-culture experiment showed to impact on the CD74 expression on monocytes (**Fig 2.23.D**). Therefore, the data suggests that endothelial Notch impacts on the immunosuppressive phenotype of monocytes by priming the response of TAMs towards TC-induced stimuli. However, how endothelial Notch signaling affects the cholesterol metabolism through the regulation of CD44 and the induction of the immunosuppressive phenotype (and CD74) need further investigation. Moreover, studies need to be performed to unravel if CXCL2 could play a role in these processes.

Finally, I could validate the decreased immunosuppressive phenotype of TAMs in mice lacking endothelial *Rbpj* with an increased cytotoxic potential of sorted T cells in an *ex vivo* LDH-cytotoxicity assay. T cells isolated from *Rbpj*[iΔEC] tumor-bearing mice were more cytotoxic than those isolated from their littermate controls (**Fig. 2.25.B**). On top of that, also the proportion of T cells within the peritoneal cavity of tumor-bearing mice was changed in *Rbpj*[iΔEC] compared to control mice. The increase of CD8^{+} cytotoxic T cells is in line with the increased cytotoxic potential as well as decreased tumor burden in mice lacking endothelial *Rbpj* (**Fig. 2.25.D**). Increased cytotoxic T cells in TME correlates with better outcome for patients in several different tumor types including ovarian cancer (Wang *et al.*, 2018; Yildirim *et al.*, 2017). Cytotoxic T cells are able to kill TCs by granules perforin and granzyme B delivery after priming by antigen presentation from APC (Durgeau *et al.*, 2018). The immunosuppressive phenotype of TAMs are associated with activation of pro-tumorigenic T cell and impaired effector T cell function (Franklin & Li, 2016). Therefore, the decreased immunosuppressive phenotype of TAMs from mice lacking *Rbpj* in the endothelium could impact on the increased population of cytotoxic T cells and increased cytotoxic potential. However, the direct effect of the decreased immunosuppressive phenotype of monocyte-derived macrophages isolated from *Rbpj*[iΔEC] tumor-bearing mice on T cells needs further investigation for example in co-culture experiments in combination with more detailed

functional T cells assays (Enzyme Linked Immuno Spot Assay, ELIspot) measuring the (IFNγ) response and activation of T cells. Taking together, TC-induced activation of endothelial Notch signaling regulates the tumor burden as well as the infiltration and phenotype of monocyte-derived macrophages in EOC. In more detail, loss of endothelial Notch decreased HA receptor on macrophages affecting the education of TAMs (cholesterol pathway and TAM signature) and crosstalk with TCs resulting in a decreased immunosuppressive phenotype and reduced tumor burden.

3.6   Priming of monocyte-derived macrophages by endothelial Notch signaling during acute inflammation

As already mentioned, chronic inflammation can induce cancer especially in ovarian cancer (Balkwill & Montavini, 2001; Clendenen *et al.*, 2011). Infiltration of TAMs play a major role in the tumor progression (Bingle *et al.*, 2002; Lewis & Pollard, 2006). Therefore, studying the mechanism of macrophage recruitment into the microenvironment could improve the basic knowledge and therefore, cancer therapies. I investigated the infiltration of myeloid cells and macrophages into the peritoneum also in a tumor-independent model of acute peritonitis as well prior tumor inoculation. Investigation of the myeloid cell compartment previously to the tumor inoculation showed no effect in both models of endothelial Notch signaling within the peritoneum of the mice (**Fig. 2.27**). Furthermore, in the model of acute inflammation, peritonitis did not show any differences within the peritoneal cavity or blood neither in macrophage (72 hours) nor myeloid cell (24 hours) recruitment by endothelial Notch signaling (**Fig**. **2.28** to **Fig. 2.32**). Therefore data indicate that the observed effect of endothelial Notch-dependent myeloid cell recruitment could be restricted to the tumor context, which can be considered as a chronic inflammation. Moreover, studies on thioglycolate induced peritonitis claim that immune response towards this agent is not relevant to study macrophage infiltration on inflammatory diseases because the immune response generated towards this heterogeneous irritant is unknown. Studying the recruitment of macrophages towards thioglycolate showed that those macrophages were larger, more vacuolated and showed increased phagocytic potential compared to an Antigen (Ag)-mediated immune response. In particular, the thioglycolate-mediated immune response differs a lot from an acquired one (Cook *et al.*, 2003). Moreover, recruited macrophages by (broth) thioglycolate were not activated nor able to kill pathogens (Leijh *et al.*, 1984). Activation of endothelial Notch signaling leads to the secretion of pro-inflammatory cytokines (Mack *et al.*, 2017) but until now there is no evidence that acute inflammation of the microenvironment activates Notch in the endothelium. Investigations on endothelial Notch signaling regulating the immune cell infiltration are only studied in chronic inflammation like atherosclerosis (Nus *et al.*, 2016) and hepatic ischemia of the liver (Zhang *et al.*, 2020). Therefore discussed studies propose, that the obtained results from this thesis due to the activation of endothelial Notch and resulting regulation of myeloid cell recruitment into the microenvironment is a tumor-dependent effect or needs chronic inflammation. I could not observe any differences in myeloid cell infiltration neither activation of myeloid cells into the peritoneum during acute inflammation. However, I could detect a regulation of HA receptor CD44 as well IL1β due to loss of endothelial Notch signaling (**Fig. 2.33**). As already discussed, CD44 is the receptor for HA but it is also important for the induction and regulation of macrophage polarization (Schenk *et al.*, 2014). Moreover, blocking of HA receptor, CD44 decreases the production of IL1β in BMDM (Bousoik, Qadri, & Elsaid, 2020; Noble *et al.*, 1993). Also knock down of *CD44* in BMDM decreased NF-κB signaling which results in decreased downstream targets, like TNF-α and IL1β (Qadri, Almadani, Jay, & Elsaid, 2018). Additionally, in the atherosclerotic mouse model of *ApoE* KO, blocking of CXCR2 showed to reduce reactive oxygen species (ROS) and IL1β production in peritoneal macrophages, concluding that CXCR2 interaction with the ligands regulates oxidative stress and inflammatory responses (Sun *et al.*, 2021). The pro-inflammatory

cytokine pro-IL1β gets cleaved and activated by caspase-1 resulted by an inflammasome activation. Moreover, it leads to an activation of APC followed by an activation of T helper cells, Th1 and Th17 within the microenvironment to resolve the inflammation (Ben-Sasson, Wang, Cohen, & Paul, 2013; Hutton, Ooi, Holdsworth, & Kitching, 2016; Mailer *et al.*, 2015). However, in case of a chronic inflammation sustained IL1β production also leads to an induction of autoimmune disease (Abbate, Canada, Van Tassell, Wise, & Dinarello, 2014; Dumusc & So, 2015; Pilli, Zou, Tea, Dale, & Brilot, 2017) or cancer (Bent, Moll, Grabbe, & Bros, 2018).

Data indicate so far, that regulation of myeloid cell recruitment by endothelial Notch signaling is a tumor-dependent effect. However, loss of endothelial Notch is able to also prime monocyte-derived macrophages by regulating HA receptor expression in different microenvironments, tumor as well as inflammation even though the role of HA within inflamed tissue is not clear. Altogether, endothelial Notch1 signaling prime monocyte-derived macrophages and therefore, impact on the activation which depends on the microenvironment, TME or infection.

3.7   Model and Outlook

The present PhD thesis investigated the role of endothelial Notch signaling on myeloid cell recruitment and education. Analysis of tissue microarray samples from ovarian cancer patients, which showed that patient samples with increased cleaved Notch expression also had an increased myeloid cell infiltration. *In vivo* modeling of metastatic EOC as well primary tumor growth further unraveled the essential role of endothelial Notch signaling on the recruitment and education of myeloid cells into the TME. TCs are able to induce Notch signaling in the endothelium (Wieland *et al.*, 2017), which further leads to an upregulation of tumor-dependent angiocrine factors as well as mimicry of LEC. Moreover, I could validate novel canonical Notch target genes, especially CXCL2. Loss of endothelial Notch signaling showed an impaired education of TAM. In EOC, TAMs get educated by TCs though the secretion of HA leading to a cholesterol efflux with tumor promoting function (Goossens, *et al.*, 2019). Depletion of endothelial *Rbpj* reduces the expression of HA receptors (CD44) on monocyte-derived macrophages with an impact on the phenotype of the TME due to the regulation of CD74. Effects resulted in an increased infiltration of effector T cells and decreased tumor burden when endothelial Notch was inhibited. In conclusion, endothelial Notch activation by TCs is necessary for the immunosuppressive role of TAMs within the TME.

Further studies need to be performed to address the question how HA receptors are regulated by endothelial Notch signaling and if the angiocrine factor CXCL2 could impact in the cholesterol as well the immunosuppressive phenotype of monocyte-derived macrophages.
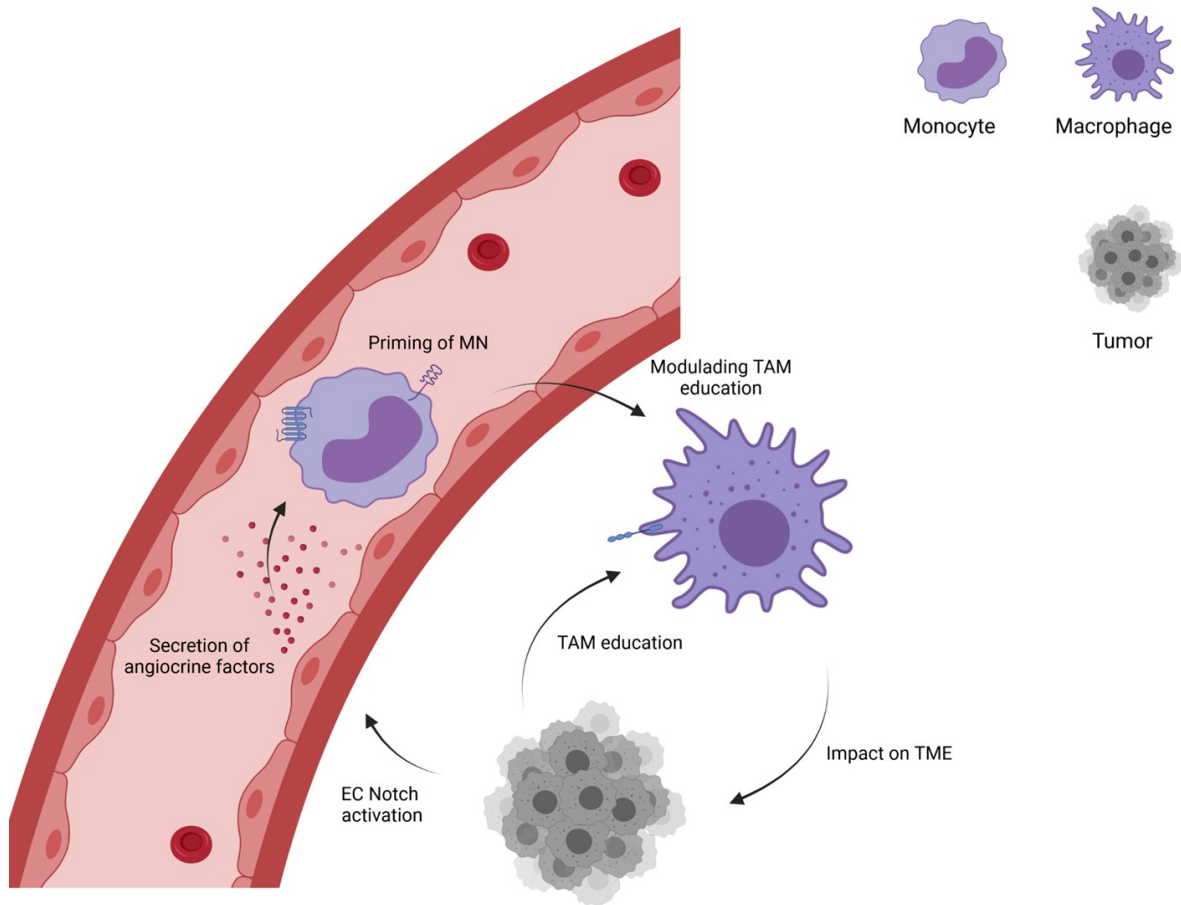
Figure 3.1: Model of endothelial Notch1-dependent recruitment and education of monocyte-derived macrophages into the tumor microenvironment. Tumor cells activate Notch1 on the tumor endothelium. Activation of endothelial Notch signaling leads to a secretion of angiocrine factors, especially CXCL2, which leads to an increased infiltration of monocyte-derived macrophages into the tumor microenvironment. Loss of endothelial Notch signaling also showed to inhibit TC-induced education of tumor-associated macrophages (TAMs) by priming of monocytes (MN) leading to a downregulation of hyaluronan receptor, CD44 as well as CD74 on TAMs.

4 Material and Methods

4.1 Material

4.1.1 Laboratory Equipment

Table 4.1 List of laboratory equipment including device and manufacture.

Device	Manufacture
Analytical balance Kern ABJ	Kern&Sohn
Balance PBS/PBJ	Kern&Sohn
Biosafety Cabinet Safe 2020	Thermo Fischer Scientific
Bottles	Schott
Cell Observer flourescence micropscope	Carl Zeiss
Centrifuge	Thermo Scientific
Centrifuge (5418 and 5418R)	Eppendorf
ChemiDoc Image System	Bio-Rad
Confocal microscope LSM700	Carl Zeiss
Cryostat-microtome CM1950	Leica Microsystem
CLARIOStar Reader	BMG LabTech
EasySep Magnet	Stemcell Technologies
Electrophoresis Power Supply EV231	Consort
Erlenmyer flask	Fisherbrand
Flow cytomerter Canto II	BD Biosciences
Flow cytometer LSR	BD Biosciences
Flow cytometer sorter Aria I	BD Biosciences
Freezer (-20 °C)	Liebherr
Freezer (-80 °C)	Thermo Fischer Scientific
Gel documentation	Intas Science Imaging
Gel electrophoresis equipement	StarLab
Hamilton Syringe	Hamilton
Incubator for bacteria culture	Infors HT
Incubator cell culture HERAcell 150i	Thermo Fischer Scientific
Magnetic stirrer	Heidolph Instrumens
Microscope EPLIPSE TS100	Nikon
Microtome Mocro HM355S	Thermo Fishcer Scientific
Milli-Q water	Merck Millipore
Nanodrop1000	Thermo Fischer Scientific
Neubauer cell counting chamber	Brand
PCR cycle pepstar 2x gradient	Peqlab Biotechnology
pH Meter	Roth
Plate reader	BMG Labtech
Protein electrophoresis Mini-PROTEAN	Bio-Rad
Refigerator (4 °C)	Liebherr
StepOnePlus Real-Time PCR System	Applied Biosystems
Tube roller	StarLab
Ultra-centrifuge	Thermo Fischer Scientific

Vortex mixer	StarLab
Water bath	GFL
Western Blot system	PeqLab Biotechnology

4.1.2   Software

Table 4.2: List of analysis software including developer.

Software	Developer
ApE v2.047	M. Wayne Davis
Flowing Software 2.5.1	Perttu Terho
Gene set enrichment analysis (GSEA)	(Mootha *et al.*, 2003; Subramanian *et al.*, 2005)
ImageJ	Wayne Rasband (NIH)
ImageLab 3.0	BioRad
Ingenuity Pathway Analysis (IPA)	Qiagen
MARS Software	BMG Labtech
Microsoft Office 2013-2016	Microsoft Corp.
Prizm	Graphpad
Zen 2012 (black and blue edition)	Carl Zeiss

4.1.3   Consumables

Table 4.3: List of consumables including material and manufacture.

Material	Manufacture
Cell culture dish (100mm and 350mm)	Corning
Cell culture flask (T75 and T175)	Sigma-Aldrich
Cell culture plate (6-, 12-, 24, 96-well)	Greiner Bio-One
Cell scraper	Sarstedt
Cell strainer (40, 70, 100 µm)	Corning
Conical tubes (15 and 50 mL)	Sarstedt
Cryo embedding molds	Thermo Fischer Scientific
Cyto tubes	Vials Nunc
Dako Pen	Dako
Embedding cassettes	Carl Roth
FACS tubes	BD Falcon
Insulin syringe	B. Braun Melsungen
Laboratory paraffin film, Parafilm M	Pechiney Packaging
Microscope coverglasses	Thermo Fischer Scientific
Microscope slide Superfrost Plus	Thermo Fischer Scientific
Nitrocellulose membrane	GE Healthcare
Pasteur pipettes	WU Mainz
PCR disposable plates	Biozym
PCR disposable tubes	Biozym
PCR seal sheets clear	Biozym
Pipette tips	StarLab

Pipetts	Corning
Reaction tubes	Eppendorf
Rotilabo-embedding cassettes	Carl Roth
Rotilabo Filter	Carl Roth
Safe seal tip	Biozym
Spektra-plate	Perkin-Elmer
Stericum BP	Merck Millipore
Transwell inserts (24 well)	Greiner Bio-One

4.1.4   Kits and Reagents

Table 4.4: List of kit and reagents including chemicals and manufacture.

Chemical	Manufacture
AceGlow chemiluminescence substrate	Peqlab Biotechnology
ACK	Sigma-Aldrich
Biocoll density solution (1.007g/mL)	VWR
BD Com Beads	BD Bioscience
Bovine serum albumin (BSA)	Serva
Bradford Ultra	BioRad
Cell lysis buffer (10x)	Cell Signaling Technology
CellTrace™ CFSE	ThermoFischer
Desoxynuceleotide	Eurofins MWG operon
DMEM Glutamax	Thermo Fischer Scientific
DNA ladder mix	Fermentas
Dual-Luciferase Reporter Assay	Promega
Dynabeads ProteinG	Thermo Fischer Scientific
Dynabeads sheep anti rat IgG	Thero Fischer Scientific
ELC Western blot Detection Kit	Thermo Fischer Scientific
ELISA human MIP-2 (CXCL2)	Abcam
Fetal Calf Serum (FCS), heat inactivated	Biochrom
Fibronectin	R&D Systems
Flurescence mounting medium	Dako
Gelatine, type B	Sigma-Aldrich
HIER T-EDTA Buffer pH 9,0 (10x)	Zytomed Systems
High Capacity cDNA RT Kit	Thermo Fischer Scientific
InnuPrep RNA Mini Kit	Analytic Jena
L-Glutamine	Sigma-Aldrich
Luria Bertani Agar (LB)	Sigma-Aldrich
Luria Bertani medium (LB Broth)	Sigma-Aldrich
PageRuler-Plus prestained (Protein ladder)	Fermentas
PBS (1 and 10x)	Life Technologies
Penicillin/Streptomycin	Life Technologies
Plasmid Maxi Kit	Qiagen
Power SYBR Green PCR Kit	Qiagen

Rotiphorese gel 30	Carl Roth
Skim milk powder	Gerbu
Streptavidin-HPR	Thermo Fischer Scientific
Tissue Tek O.C.T.	Sakura

4.1.5   Chemicals

Table 4.5: List of chemicals including manufacture.

Chemical	Manufacture
1,2-propanediol	Sigma-Aldrich
1,4-dithiothreithol (DTT)	Sigma-Aldrich
2-mercaptoethanol	Carl Roth
2-propanol	Sigma-Aldrich
3-(4,5-Dimethylthiazol-2-yl)-2,5-Diphenyletrazolium Bromide) (MTT)	Thermo Fischer Scientific
Acetic acid	Carl Roth
Adenosine triphosphate (ATP)	Carl Roth
Agarose	Carl Roth
Ammoniumpersulfate (APS)	Carl Roth
Ampicillin sodium salt	Carl Roth
Blasticidin-S-Hydrochlorid	Carl Roth
Bromphenol blue	Serva
Calcium acetate hydrate	Sigma-Aldrich
Calcium chloride	Sigma-Aldrich
Calcium chlorid	Sigma-Aldrich
Citric acid	Sigma-Aldrich
Coomassie Brilliant Blue G-250	Serva
DAPI	Carl Roth
DAPT	Merk
Dimethyl sulfoxide (DMSO)	Sigma-Aldrich
EDTA disodium salt	Merk
EGTA	Sigma-Aldrich
Ethanol	Sigma-Aldrich
Ethylene glycol	Sigma-Aldrich
Formamide	Sigma-Aldrich
Glycerol	Carl Roth
Glycine	Carl Roth
Hydrochloric acid (HCl, 37%)	Sigma-Aldrich
Igepal CA-630	Sigma-Aldrich
Isoflurane	Abbott
Kanamycin sulfate	Carl Roth
Macrophage colonie stimulating factor (M-CSF)	PreproTech
Magnesium chloride	Sigma-Aldrich
Magnesium sulfate heptahydrate	Sigma-Aldrich

Menganese chloride	Sigma-Aldrich
Methanol	Sigma-Aldrich
Methyl cellulose	Sigma-Aldrich
Monopotassium phosphate	Sigma-Aldrich
NHS-SS-Biotin	Thermo Fischer
Nonidet P40	AppliChem
Ortho-phenylediamine	Sigma-Aldrich
Paraformaldehyde	Sigma-Aldrich
Phenylmethylsulfonylflourid (PMSF)	Sigma-Aldrich
Polyethyleneimine (PEI)	Polysciences
Ponceau S-Solution	AppliChem
Potassium chloride	Merck
Primaquine diphosphate	Sigma-Aldrich
Puromycin dihydrochloride	Sigma-Aldrich
Sodium acetate	Sigma-Aldrich
Sodium chloride	PAA laboratories
Sodium chloride dehydrate	Sigma-Aldrich
Sodium deoxycholate	Sigma-Aldrich
Sodium dodecylsulfat (SDS	Sigma-Aldrich
Sodium fluride	Sigma-Aldrich
Sodium hydroxide	Carl Roth
Sodum orthovanade	Sigma-Aldrich
Spectinomycine dihyrochloride pentahydrate	AppliChem
Sulfuric acid	Merck
Tetramethylethylenediamine (TMED)	Sigma-Aldrich
Tris	Carl Roth
Triton X-100	Sigma-Aldrich
Trypan blue	Sigma-Aldrich
Tween-20	Sigma-Aldrich
Xylene	Sigma-Aldrich
Xylene cyanol	Sigma-Aldrich

4.1.6 Bacteria and Enzymes

Table 4.6: List of Bacteria and enzymes including manufacture.

Chemical	Manufacture
Collagenase type 2	Worthington
Dispase II	Sigma-Aldrich
Escherichia Coli Stabl 3	Thermo Fischer Scientific
GoTaq G2 Flexi DNA Polymerase	Promega

4.1.7 Antibodies

4.1.7.1 Western blotting primary Antibodies

Table 4.7: List of primary western blot antibodies.

Epitope	Host	Dilution	Manufacturer	Cat.-No.
β-Actin (h/m)	Mouse	1/2500	Sigma-Aldrich	A5441
IL33	Mouse	1/100	Abcam	ab54385
Rbpj (h/m)	Rabbit	1/1000	Cell signaling	5313P

4.1.7.2 Western blotting secondary Antibodies

Table 4.8: List of secondary western blot antibodies.

Reactivity	Host	Dilution	Manufacturer	Cat.-No.
Mouse-HRP	Rabbit	1/2500	Dako	P0260
Rabbit-HRP	Goat	1/2500	Dako	P0448

4.1.7.3 Flow cytometer Antibodies

Table 4.9: List of murine flow cytometer antibodies and reagents.

Epitope	Host	Fluorochrom	Dilution	Manufacturer	Cat.-No.
CD11b	Rat	APC	1/300	BioLegend	553312
	Rat	BUV805	1/500	BioLegend	741934
CD19	Rat	Pe-Cy7	1/100	BioLegend	115519
CD3	Rat	PerCP	1/100	BioLegend	560468
CD31	Rat	BV510	1/200	BD Biosciences	563089
CD4	Rat	Pe-Cy7	1/100	BioLegend	552775
CD45	Rat	BV750	1/500	BioLegend	103157
	Rat	FITC	1/500	BD Bioscience	553079
CD74	Rat	APC	1/200	BioLegend	151005
CD8	Rat	APC-Cy7	1/100	BioLegend	557654
CCR2	Rat	FITC	1/100	BioLegend	150608
Live/Dead	-	BUV395	1/1000	LIFE Technologies	L34961
Ly6C	Rat	V450	1/200	BD Bioscience	560594
Ly6G	Rat	APC-Cy7	1/200	BD Bioscience	560600
F4/80	Rat	PerCP-Cy7	1/200	BioLegend	123128
	Rat	AlexaFlour700	1/200	BioLegend	123129

MHCII	Rat	BV510	1/100	BioLegend	742893
Tim4	Rat	PE	1/500	LIFE Technologies	12-5866-82

Table 4.10: List of human flow cytometer antibodies.

Epitope	Host	Fluorochrom	Dilution	Manufacturer	Cat.-No.
CD14	Rat	APC-Cy7	1/100	BioLegend	367111
CD74	Rat	APC	1/100	BioLegend	326811

4.1.7.4 Immunohistochemistry Antibodies

Table 4.11: List of immunohistochemistry (murine) antibodies.

Epitope	Host	Dilution	pH	Manufacturer	Cat.-No.
aSMA	Mouse	1/200	9	Sigma-Aldrich	A5228
CD8	Rabbit	1/200	9	Abcam	ab217344
CD11b	Mouse	1/200	6	Abcam	ab133357
CD31	Mouse	1/50	9	Abcam	ab9498
	Rabbit	1/50	9	Abcam	ab28364
CD163	Rabbit	1/500	6	Abcam	ab182422
Lectin	N.A.	1/200	6	Invitrogen	132450
Pan-cytokeratin	Mouse	undiluted	9	Zytomed	ZUC001-125
PROX1	rabbit	1/500	9	Abcam	ab199359
VCAM1	Rabbit	1/100	9	Abcam	ab134047
VEGFR3	Rabbit	1/100	6	Abcam	ab27278

4.1.7.5 Cell Isolation Antibodies

Table 4.12: List of antibodies for cell isolation.

Epitope	Host	Manufacturer	Cat.-No.
CD14	human	Miltenyi Biotec	130-050-201

4.1.8 Cell culture

Table 4.13: List of cell culture cells and growth media. N.A. not applicable

Cell type	Growth media	Manufacturer	Cat.-No.
Bone marrow derived-macrophages (BMDM)	DMEM (4,5 g/L glucose) + 10% FCS+ 1% Pen/Strep+ 10ng/mL M-CSF	Gibco	N.A.
HEK293 A and T	DMEM (4,5 g/L glucose) + 10% FCS+ 1% Pen/Strep	Gibco	N.A.
Human Dermal Lymphatic Endothelial Cells (HDLEC-c)	Growth media MV-2 with Supplements	Promocell	C-22022

Human Umbilical Vein Endothelial Cells (HUVEC)	Endothelial cell basal Medium (Endopan3) with Supplements and 1% Pen/Strep	PAN-Biotech	N.A.
ID8-Luc ovarian surface epithelial cell line	DMEM (4,5 g/L glucose) + 10% FCS+ 1% Pen/Strep	Gibco	Prof. Frances Balkwill, Barts Cancer Institute, London, UK
Murine Lewis Lung Carcinoma RFP labbled (LLC-RFP)	DMEM (4,5 g/L glucose) + 10% FCS + 1% Pen/Strep	Gibco	N.A.
Murine Cardiac Endothelial cell line (MCEC)	DMEM (4,5 g/L glucose) + 5% FCS +1% HEPES + 1% Pen/Strep	Gibco	N.A.
Trypsin	Trypsin-EDTA 0,005%	Life Technologie	-

4.1.9 Buffers and solutions

Table 4.14: 10x phosphate-buffered saline (PBS) buffer components.

PBS (10x)	
1,37 M	NaCl
26,8 mM	KCl
100 mM	$NaHPO_4*2\ H_2O$
20 mM	KH_2PO_4
Add 1 L ddH_2O	

Table 4.15: 1x Tris-buffered saline (TBS) buffer components.

TBS (1x)	
20 mM	Tris
150 mM	NaCl
Adjust pH to 8,0	

Table 4.16: Tris-acetate-EDTA (TAE) buffer components.

TAE buffer (50x)	
2 M	Tris
1 M	Acetic acid
50 mM	EDTA (pH 8,0)
Add to 1L with ddH_2O	
Adjust pH to 7,8	

Table 4.17: Flow cytometer staining buffer

Staining buffer for flow cytometry	
48 mL	PBS
2 mL	FCS

Table 4.18: Electrophoresis running buffer components.

Electrophoresis Running buffer (10x)	
1,92 M	Glycine
250 mM	Tris
1 %	SDS
Add 1L ddH$_2$O	

Table 4.19: Electrophoresis transfer buffer components.

Electrophoresis transfer buffer (10x)	
1,42 M	Glycine
250 mM	Tris
Add 1L ddH$_2$O	

Table 4.20: Electrophoresis running gel (10%).

Electrophoresis: Running gel (10%)	
4,0 mL	H$_2$O
3,3 mL	Rotiphese Gel 30
2,5 mL	Tris buffer 1.5M, pH 8,8
100 µL	SDS (10%)
100 µL	APS (10%)
4 µL	TMED

Table 4.21: Electrophoresis stacking gel (4%).

Electrophoresis: Stacking gel (4%)	
3,4 mL	H$_2$O
0,83 mL	Rotiphese Gel 30
0,63 mL	Tris buffer 1.0M, pH 6,8
50 µL	SDS (10%)
50 µL	APS (10%
5 µL	TMED

Table 4.22: Lämmlie buffer (4x).

Lämmlie buffer (4x)	
200 mM	Tris (pH 6,8)
5%	β-mercaptoenthanol
8%	SDS
40%	Glycerol
0,4%	Bromphenol blue

Table 4.23: Mouse tail/ear punch lysis buffer (50x).

Mouse tail/ear punch lysis buffer (50x)	
1,25 M	NaOH
10 mM	EDTA

Table 4.24: Mouse neutralization buffer (50x).

Mouse tail/ear punch neutralization buffer (50x)	
2 M	Tris-HCl (pH 5)

4.1.10 Mouse strains

Table 4.25: List of mouse strains and abbreviation.

Abbreviation	Name
Control	Cre-
N1ICD	STOCK-Gt(ROSA)26Sortm1(Notch1); Tg(Cdh5-cre/ERT2)1Rha:, C57Bl/6 mice
Rbpj^{iEC}	Rbpjk floxed x VE-Cadherin; CreERT2/4(tb4652), C57Bl/6 mice
Wild type (WT)	C57BL/6

4.1.11 RT-qPCR Primer

Table 4.26: List of human RT-qPCR primers with sequence.

Target	Forward Sequence (5´ to 3´)	Reverse Sequence (5´ to 3´)
HES1	TCAACACGACACCGGATAAA	CCGCGAGCTATCTTTCTTCA
HES5	TAGTCCTGGTGCAGGCTCTT	CGGGATCGAGCTGAGAATAG
HEY1	GAGAAGGCTGGTACCCAGTG	CGAAATCCCAAACTCCGATA
HEY2	CTTGTGCCAACTGCTTTTGA	GCACTCTCGGAATCCTATGC
HPRT	TGTTGTAGGATATGCCCTTGACT	CTAAGCAGARGGCCACAGAAC
CCL1	CATTTGCGGAGCAAGAGATT	TGCCTCAGCATTTTTCTGTG
CCL21	CCCAGCTATCCTGTTCTTGC	TCAGTCCTCTTGCAGCCTTT
CXCL1	GCGCCCAAACCGAAGTCATA	ATGGGGGATGCAGGATTGAG
CXCL2	GGCAGAAAGCTTGTCTCAACCC	CTCCTTCAGGAACAGCCACCAA
CXCL5	AGCTGCGTTGCGTTTGTTTAC	TGGCGAACACTTGCAGATTAC
CXCL8	AAGAAACCACCGGAAGGAAC	AAATTTGGGGTGGAAAGGTT

77

CXCL12	ATTCTCAACACTCCAAACTGTGC	ACTTTAGCTTCGGGTCAATGC
IL33	GTGACGGTGTTGATGGTAAGAT	AGCTCCACAGAGTGTTCCTTG
LYVE1	AGGCTCTTTGCGTGCAGAA	GGTTCGCCTTTTTGCTCACAA
KLF2	CACCAAGAGTTCGCATCTGA	GGCTACATGTGCCGTTTCAT
LTb	GACGAAGGAACAGGCGTTTCT	GTAGCCGACGAGACAGTAGAG
PROX1	CCAGCTCCAATATGCTGAAGACCTA	CATCGTTGATGGCTTGACGTG
VEGFc	TTGCTGGGCTTCTTCTCTGT	TGCTCCTCCAGATCTTTGCT
VEGFR3	CATCATGCTGAACTGCTGGT	GAGAAGCTGCCCTCTTCTGA

Table 4.27: List of murine RT-qPCR primers with sequence.

Target	Forward Sequence (5′ to 3′)	Reverse Sequence (5′ to 3′)
Cph	ATGGTCAACCCCACCGTG	TTCTTGCTGTCTTTGGAACTTTGTC
Cd44	TCGATTTGAATGTAACCTGCCG	CAGTCCGGGAGATACTGTAGC
Cd74	AGTGCGACGAGAACGGTAAC	CGTTGGGGAACACACACCA
Il1β	TCCAGGATGAGGACATGAGCAC	GAACGTCACACACCAGCAGGTTA
Slamf8	TCTCCTTCCCGTTGTGGTTG	CCAGATAGCCTCACGCACTTG
Slamf9	CAAAACAACATTGCCATCGTGA	GCTAATATGCAGGGAGTAGCTG
Mmp9	TGGAGGATCTCTAGCTCAGC	CAGGAAGACGAAGGGGAAGA

4.1.12 Plasmids

Table 4.28: List of plasmid constructs.

Name	Construct	Vector	Resistance
pAD-N1-ICD	Notch1 ICD	pAD-CMV-V5	Ampicillin
pAD-GFP	GFP	pAD-CMV-V5	Ampicillin
pLenti-CRIPR Cas9 human *Rbpj* KO1	gRNA hRbpj KO1	pLenti-CRISPR Cas9 v2	Puromycine
pLenti-CRIPR Cas9 human *Rbpj* KO2	gRNA hRbpj KO2	pLenti-CRISPR Cas9 v2	Puromycine
pLenti-CRIPR Cas9 murine *Rbpj* KO	gRNA mRbpj KO	pLenti-CRISPR Cas9 v2	Puromycine
pLenti-CRISPR Cas9 Control	gRNA scrambled control	pLenti-CRISPR Cas9 v2	Puromycine
pLKO.1 Control	Sh Control	pLKO.1	Puromycine
pLKO.1 shRNA1 *CXCL2*	ShRNA1 CXCL2	pLKO.1	Puromycine
pLKO.1 shRNA2 *CXCL2*	ShRNA2 CXCL2	pLKO.1	Puromycine

4.2 Methods

4.2.1 Cell culture Methods

4.2.2 Cell culture maintenance

All cell culture experiments were performed in a laminar flow hood to work sterile. Cells were cultivated in their respected cell culture media including supplements (Tab. 4.1.8) and cultured in CO_2 incubator at 37°C and 95% relative humidity and 5% CO_2. Cell counting was conducted by using Neubauer chamber and tryptophan blue to identify viable cells. Suspension and detached cells were centrifuged for 5 min at 300 g. Cell culture were tested on a regularly base for mycoplasma contamination (se 4.2.3 Mycoplasma test).

Adherent cells were passaged regularly by washing the cells with PBS to remove culture medium and adding an appropriate amount of 0,05% Trypsin-EDTA and incubating for 5 min at 37°C. Enzymatic activity was stopped by adding media containing FCS. Detached cells were collected and pellet before resuspending in fresh media.

To cryopreserve cell culture aliquots of 1-2 10^6 cells/mL were frozen in FCS with cryoprotectant 10% DMSO and placed in Mr. Frosty at -80°C for 24h before transferring in to liquid nitrogen for long-term storage of cells.

4.2.3 Mycoplasma test

To test cell culture maintenance for mycoplasma contaminations, 500µL cell culture medium were collected. Supernatant was headed up to 95°C for 5min before performing the mycoplasma PCR.

Table 4.29: Mycoplasma test protocol.

Reagent	Volume per reaction [µL]
5x Buffer	5
dNTPs	0,5
$MgCl_2$	1,25
DMSO	0,75
Forward primer (GGGAGCAAACAGTAGATACCCT) 10mM	1
Reverse Primer (TCGACCATCTGTTACATCTGTTAACCTC) 10mM	1
Polymerase	0,25
ddH_2O	14
Sample	4
Total Volume	25

Table 4.30: PCR protocol for mycoplasma test.

Cycle	Step	Temperature [°C]	Time [sec]	
1	Initial denaturation	95	900	
2	Denaturation	95	60	38x
3	Annealing	60	20	
4	Extension	72	15	
5	Final Extension	60	30	

Amplification of mycoplasma products were detected on a 1% Agarose gel with Ethidium bromide. The separation was performed for 40min at 120V and visualized with a UV transilluminator.

4.2.4   Generation of conditioned medium

To generate conditioned medium (CM) from different tumor cell lines, 0,25*10^6 cells/mL were seeded in culture media with 4% FCS for 72 h. Supernatant was collected and sterile filtrated and stored at -20°C.

For the generation of ECs CM 2*10^6 cells were seeded in a 10cm dish and infected with 300 µl of Adenovirus for 24h. After the incubation time cells were washed with PBS and fresh Media was added for 24h. Supernatant was collected and sterile filtrated and stored at -20°C.

4.3   Isolation of monocytes cells from buffy coats

Human buffy coat were purchase from blood donation service DRK Mannheim. Peripheral blood nuclear cells (PBMC) were isolated by gradient centrifugation using Biocoll density solution. Human buffy coat was diluted 1:1 with PBS and added to the Biocoll density solution. This mixture was centrifuged at 1000g for 20min at RT without break. After centrifugation, the white intermediate phase containing leukocytes were collected and washed with PBS.

To perform a positive isolation of monocytes CD14 MACS Bead were used with the LS column. The isolation of CD14$^+$ Monocytes were performed following the enclosed protocol.

Experiments were performed right after isolation of CD14$^+$ monocytes.

4.4   Transwell assay

To check chemotaxis potential transwell assay was performed in 24-well plates.

Human ovarian cancer cells were seeded 100.000 cells/mL in 500 µL RPMI medium without FCS for 48h. For the ECs monolayer, inserts were coated for 2 h with 2 µg/mL fibronectin in PBS. 50.000 human ECs with *Rbpj* KO, shRNA for *CXCL2* and adenovirus infection of N1ICD and GFP as control were seeded on top of insert membrane for 48 h. To analyze monocyte transmigration 200.000 CD14$^+$ cells were stained with carboxyfluorescein succinimidyl ester (CSFE) and added into the human ECs monolayer insert. Transwell plate was incubated for 2h at 37°C and 5% CO_2. After incubation time, remaining cell suspension in upper well were aspirated and transwell was cleaned with cotton swab. The migrated cells at the membrane were fixed with 4 % PFA for 20 min at room temperature (RT). Imaging of transwell was performed with Cell Observer (Carl Zeiss) from DKFZ Core facility Light core facility. From each transwell 5 evenly spaced field picture were taken using 20x objective and analysis was performed with Image J software.

4.5   Generation of Viruses and transduction of cells

4.5.1   Amplification of Adenovirus

HEK239A cells were used to amplify adenoviral particles. HEK293A cells were cultured and expanded to 80% confluence in 10cm cell culture dishes. 1 mL of Adenovirus particles was added to amplify the virus particles. Cell culture of infected cells was performed until 80-90% of cells died. Subsequently, cells and supernatant was harvested and three freezing at -80°C and thawing at 37°C cycles were performed. Cells and supernatant were centrifuged to spin down the cell debris and virus containing supernatant was aliquoted at stored at -80°C.

4.5.2   Adenovirus transduction of cell culture

For Adenovirus transduction ECs cells were seeded in appropriate format. To generate conditioned Medium (CM) $2*10^6$ cells were seeded in a 10cm dish. For induction experiments $0.25*10^6$ cells were seeded per well into a 6-well plate. Cells were tranduced with appropriate volume of adenoviral solution as indicated into the growth medium. After 24h incubation of the Adenovirus the medium was changed and CM and cells were collected after 24h incubation.

4.5.3   Amplification of lentivirus

To generate stable knock-out cells of *Rbpj* using CRISPR-Cas9 cells and knock-down of *CXCL2* were transduced with lentivirus. The lentivirus was generate with HEK293T cells and were transfected three different plasmids: psPAX2 (encoding structural proteins and enzymes), pMD2.G (encoding the capsid glycoprotein *vesicular stomatitis virus G*) and plasmid containing genes of interested. HEK293T cells were cultured in DMEM with 10% FCS in 15cm dishes until 90% confluence. The plasmid transfection of the cells were performed using polyethyleneimine (PEI). 1 mg/mL PEI was mixed with 2,5 mL IMEM per cell culture plate. For the DNA solution 21 µg psPAX2, 14 µg pMD2.G and 21 µg of the pLentiCRISPR-Cas9 v2 was added in 2,5 mL IMEM per cell culture plate. In the next step the PEI and DNA solution was mixed and incubated for 30 min at RT. In the meanwhile, the growth media from HEK293T cells were replaced by 10 mL IMEM with 15% FCS. After the incubation time, the 5 mL transfection solution were added dropwise to the cells and incubated for 12h at 37°C. The next day, the medium was changed to DMEM with 10% FCS and after 24 h and 48 h the culture medium containing the lentiviral particels were collected and fresh media was added. The collected media was sterile filtrated through 0,22 µm filter and centrifuged at 250.000 rpm for 2 h at 4°C. The supernatant was aspirated and the pellet was dried for 10 min at RT. The pellet of lentiviral particles was dissolved in 70 µL PBS for 30 min, aliquoted and stored at -80°C.

4.5.4   Lentivirus transduction of cell culture

For lentiviral transduction ECs were seeded in a 6-well plate with $0.25*10^6$ cells per well. The cells were infected with 5 µL lentiviral particles solution per well and incubated overnight. After incubation time cells were washed and replaced by selection medium containing the appropriate antibiotics for cell selection.

4.6   Molecular biology and biochemistry methods

4.6.1   Transformation of *E.coli*

Insertion of a plasmid into competent E.Coli (Stabl3/ XL10-Gold) was performed via transformation. Competent bacteria vial of 50 µL were thawed on ice. Afterwards 2 µL of DNA plasmid was added and incubated for 30 min on ice. For the plasmid uptake a heat shock of 45 sec at 42°C followed by a 2 min incubation on ice were performed. 250 µL of medium was added to the bacteria vial and cells were incubated for 1 h at 37°C. After the incubation time, bacteria were plated in different dilutions on LB agar plates containing appropriate antibiotics. LB plates with bacteria were incubated over night at 37°C. The next day, colonies were picked and LB medium with antibiotics was inoculated to amplify transformed bacteria. E. coli glycerol stocks containing the expression vector were conserved at -80°C in 50% glycerol.

4.6.2   Plasmid purification

For the plasmid amplification bacteria containing the expression vector of interested were cultured in LB media with appropriate antibiotics for 18 h at 37°C and 200 rpm. The plasmid were isolated and purified using the Maxi Kit (Qiagen) and following the enclosed protocol of the Kit. In brief, bacteria

were centrifuged and lysed. Followed by a neutralization step and DNA binding to a silica membrane. After washing several washing steps, DNA was eluted with ddH$_2$O and plasmid concentration was determinate using the spectrophotometer Nanodrop at 260nm. DNA was stored at -20°C.

4.6.3   Genotyping of mouse lines

To isolate the genomic DNA from the tail/ear punches or Lung pieces, tissue was lysed with 80 µL lysis buffer for 45 min (for ear punches) to 1 h (for lung tissue) at 95°C. Afterwards the solution was cooled down and 80 µL neutralization buffer was added. Lysed tissue was stored at -20 °C.

To determine the genotype of the mice polymerase chain reaction (PCR) of the gene of interested was performed using specific primers (Tab. 4.32). GoTaq DNA polymerase (Promega) was used for the PCR as described in the protocol (Tab. 4.34 to 4.36) using the PCR master mix (Tab. 4.33).

Table 4.31: Primer of mouse tissue genotyping.

Target	Forward Sequence (5´ to 3´)	Reverse Sequence (5´ to 3´)
VE-Cad-Cre	GCC TGC ATT ACC GGT CGA TGC AAC GA	GTG GCA GAT GGC GCG GCA ACA CCA TT
ROSA(N1-ICD)-transgene	TAAGCCTGCCCAGAAGACTC	GAAAGACCGCGAAGAGTTTG
ROSA(N1ICD)-recombination	CAAACTCTTCGCGGTCTTTC	GGCTCTCTCCGCTTCTTCTT
Rbpj flox-transgene	GTGGAACTTGCTATGTGCTTTG	CTGCCATATTGCTGAATGAAAA
Rbpj flox-recombination	GTGGAACTTGCTATGTGCTTTG	CACATTCCCATTATGATACTGAGTG

Table 4.32: PCR master mix of mouse tissue genotyping.

Reagenz	1x master mix [µL]
5x Puffer	5,00
dNTPs (2,5 mM)	0,50
Primer forward (10µm)	1,25
Primer reverse (10µm)	1,25
MgCl$_2$	1,50
Taq	0,10
ddH20	14,40
Sum	24,00

Table 4.33: PCR protocol of CRE transgene

Cycle	Step	Temperature [°C]	Time [sec]	
1	Initial denaturation	94	300	
2	Denaturation	94	30	35x
3	Annealing	70	45	
4	Extension	72	60	
5	Final Extension	72	420	

Table 4.34: PCR protocol of (ROSA)-N1ICD transgene

Cycle	Step	Temperature [°C]	Time [sec]	
1	Initial denaturation	94	300	
2	Denaturation	94	30	35x
3	Annealing	54	60	
4	Extension	72	60	
5	Final Extension	72	420	

Table 4.35: PCR protocol of Rbpj transgene

Cycle	Step	Temperature [°C]	Time [sec]	
1	Initial denaturation	94	300	
2	Denaturation	94	30	38x
3	Annealing	60	30	
4	Extension	72	60	
5	Final Extension	72	420	

Amplification products were analyzed with 1,5 % agarose gel using agarose gel electrophoresis for 1 h at 120 V and DNA was visualized with ethidium bromide using UV-light at 254 nm.

4.6.4 RNA isolation

RNA isolation from cell culture was performed using the InnuPrep Mini Kit (Analytik Jena) according manufactures protocol.

RNA isolation form tissue was performed using PicoPure RNA Isolation Kit (Acturus, Life Technology). 1mL Trizol was added to the tissue and homogenized for 1min and a frequency of 30/sec. After disruption of the tissue 200 µL chloroform was added and mixed by inverting several times followed by a centrifugation step for 15 min 12.000g at 4°C. Further RNA isolation step were performed using the manufactures protocol.

For small RNA amount of fluorescence activated cell sorted cell (FACS) or primary monocytes RNA isolation was performed using the PicoPure Kit following the enclosed manufacture protocol.

RNA concentration was measured with NanoDrop Spectrometer (Thermo Fischer Scientific) at wavelenge 270nm. Samples were stored at -80°C.

4.6.5 cDNA Synthesis

Reverse transcription of isolated RNA into complementary DNA was performed using High Capacity cDNA Reverse Transcription Kit (Thermo Fisher Scientific) according manufactures protocol.

Table 4.36: cDNA protocol.

Reagent	Volume per reaction [μL]
10x Buffer	2
10x Oligo	2
100nM dNTPs	0,8
20x Reverse Transcriptase	1
RNA Sample	14,2
Total Volume	20

Table 4.37: PCR protocol for cDNA synthesis.

Time [min]	Temperature [℃]
10	25
120	37
5	85

4.6.6 Real time-quantitative PCR

Quantitative real-time PCR (RT-qPCR) was performed with SYBR Green PCR mix (Applied Biosystems) mixing with specific primers and cDNA template. Per reaction 5 μL SYBR Green mix, 1 μL Primer mix (10mM) and 4 μL cDNA sample was mixed per well in a 96-well format. Samples were run in duplicates on a QuantStudio3 Real-time PCR system (Applied Biosystems). Resulting fold changes were calculated using the $2^{\Delta\Delta CT}$ method and mRNA expression was normalized to housekeeping gene.

Table 4.38: RT-qPCR protocol.

Cycle	Step	Temperature [℃]	Time [min]	
1	Initiation step	50	2	
2	Denaturation	95	10	40x
3	Annealing	95	15	
4	Extension	60	1	

4.6.7 Microarray analysis

For microarray analysis, RNA of sorted cells was submitted to the genomics and proteomics core facility of the DKFZ, Heidelberg. After successful quality control samples were run on the Affymetrix Gene Chip mouse Genome 430 2.0 Array from Thermo Fisher was used according to the manufacturer's instructions. First statistical analysis was performed and provided by the microarray unit by Dr. Melanie Bewerunge-Hudler. Using this analysis date were analyzed using IPA, GO term and GSEA analysis.

For Ingenuity Pathway Analysis (IPA) analysis (Qiagen) data of fold-changes were uploaded and differentially regulated and upstream regulator analysis was performed. Gene Ontology (GO) term analysis and pathways analysis were obtained from public external databases (EnrichR) and analyzed as -2log fold changes. Raw data were used for Gene Set Enrichment Analysis (GSEA). GSEA analyze if a defined lists of genes exhibit a statistically significant bias in their distribution (false discovery rate (FDR)) within a ranked gene list using the software GSEA (Subramanian *et al*., 2005) resulting to an enrichment in one of the compared groups (normalized enrichment score (NES)).

4.6.8 Protein isolation

For protein isolation from cell culture experiments cells were washed with PBS to remove remaining cell culture medium. Cell lysis was performed adding 60µL 1x Cell lysis buffer (Cell signaling) containing 20 µL/mL Phenylmethylsulfonylfluorid (PMSF) to 6-well plate. After 5 min incubation on ice cells were collected and centrifuged at 14.000 g for 4°C and 15 min. Supernatant containing the proteins was transferred into a fresh collection tube. Protein concentration was determinate with Bradford assay in a 96-well format. 10 µL Standard curve and protein samples were mixed with 200µL Bradford reagent followed by the measurement of optical density (OD) at 595nm using plate reader (BMG Labtech). Protein concentration was calculated with MARS software using linear regression. For denaturation of the protein the samples were mix with 4x Lämmlie buffer and boiled for 5 min at 95°C. Protein samples were stored at -20°C until usage.

4.6.9 Western blot

For sodium dodecyl sulfate polyacrylamide gel electrophoresis, Natriumdodecylsulfat-Polyacrylamidgelelektrophorese (SDS-PAGE) the Polyacrylamid gels were prepared (Tab. 4.21) for protein separation and samples and marker were loaded in Mini-PROTEAN Tetra Cell (BioRad) running chamber at 80 to 120 V using Running-Buffer (Tab. 4.19).

The separated protein samples were transferred to a PVDF membrane (Merck) by electroblotting in Tank Electroblotter WEBTM (PeqLab) chamber at 80 mA at 4°C overnight. Before using the PVDF membrane were activated with methanol to bind the proteins. After blotting, the membrane was washed and blocked with 5% BSA in TBS-T buffer (Tab. 4.16) for at least 1 h at RT on shaker. PVDF membrane was washed three times with TBS-T buffer each washing step for 5 min at RT on shaker. After washing of membrane antibody solution were added. The primary antibodies were incubated over night at 4°C in 5% BSA TBS-T solution followed by a washing step and 1 h incubation of secondary antibody solution in 5% milk TBS-T buffer. Developing of the signal was performed using AceGlowTM Chemiluninescence Substrate (VWR Life Science) for 3 min and developed with ChemiDoc Image system (Bio-Rad).

4.6.10 Enzyme-linked immunosorbent assay

Protein expression of CXCL2 (MIP-2) was quantified using an Enzyme-linked immunosorbent assay (ELISA; Abcam). Cell culture supernatant was collected after 24 hours and ELISA was performed following manufacture protocol.

4.6.11 Flow cytometer staining

Surface and intracellular expression of protein were analyzed by flow cytometer.

Extracellular flow cytometer staining of cells was performed in flow cytometer buffer (Tab. 4.18) for 20 min on ice and kept in the dark. In the meanwhile, compensation beads of used antibodies were prepared. For an intracellular staining cells were fixed for 30 min and intracellular staining was performed while permeabilisation for 30 min (Fix and Stain KIT, Invitrogen). After staining cells were washed with PBS and stored on ice until acquisition using BD FACSCanto TM II or BD LSR (BD Biosciences) form DKFZ core facility Flow cytometer. Experiments were analyzed using FlowJo Software.

For isolation of cells by flow cytometer activated cell sorting $3*10^6$ cells were stained and gated cell population collected in pre-coated tubes.

4.6.12 Tissue microarray analysis

Tissue microarray (TMA) stained for cleaved Notch and CD33 in human ovarian cancer patients were provided from Gewebebank des *Nationale Centrum für Tumorerkrankungen* (NCT), Heidelberg and analyzed the whole tissue scans using Axioscan microscope from DKFZ Core facility Light core facility.

4.7   Animal experiments

Mice were kept under specific pathogen-free barrier conditions at 21 ± 2°C, 60% humidity and 12-hour light-dark rhythm in the animal facility of the DKFZ. All animal experiments were performed following the guidelines of FELASA, the government for animal experiments in Karlsruhe with the reference numbers DFKZ-244; 35-9185.81/G67-15; 35-9185.81/G206-17.

4.7.1   Organ extraction

4.7.1.1   Isolation of Bone marrow derived-macrophages

Animals were sacrificed by cervical dislocation to isolate cell from the legs. The hind legs were cleaned from excess muscles and tissue with scissors and scalpel. Femur and tibia were separated from knee joint and flushed with PBS using a 25-G needle and 5 mL syringe. Each side of the bone marrow were flushed several time with PBS and collected cells were centrifuged. Bone marrow cells were resuspended in media and cells were seeded on 10 cm petri dish (Corning). To differentiate these cells into macrophages 10ng/mL M-CSF1 (PreproTech) were added to the media for 7 days of differentiation.

4.7.2   Effects of Endothelial Notch signaling on immune cell recruitment into metastatic ovarian cancer

4.7.2.1   Gene recombination

Recombination of transgenic mouse lines was performed by oral administration of tamoxifen (Sigma). Female mice between 8 and 12 weeks received once 100 µL tamoxifen (1mg/mL in peanut oil) and experiment were performed three weeks after gene recombination. Successful recombination was confirmed via PCR (see 4.6.3 Genotyping of mouse lines) using lung tissue.

4.7.2.2   Tumor cell injection

ID8-luc cells were cultured as described in 4.2.2 Cell culture maintenance. For i.p. tumor cell injection washed with PBS, resuspended into desired cell concentrations ($5*10^6$ cells/animal) in ice-cold PBS and stored on ice until implantation. Cell suspension was injected into the peritoneum of the animals. Tumor growth was monitored weighting and checking the animals until termination criteria were reached.

4.7.2.3   Collection of peritoneal fluid

Animals were sacrificed by cervical dislocation before collection of cell from peritoneal cavity. To collect the cells in peritoneal cavity 5 mL ice cooled PBS were injected into the peritoneum of female mice. After injection of PBS the mice were massaged to detach cells from peritoneal organs. Skin of the mice were cut to collect the PBS cell solution from peritoneal cavity. Volume and weight of cell suspension was noted down and stored on ice until processing.

For analysis of ID8-luc tumor growth cell suspension was centrifuged and supernatant was collected and stored at -80°C. The cell pellet was resuspended in 1 mL PBS and 100 µL were used to determine the luciferase activity amount. The 100 µL cell sususpension were centrifuged and the cell pellet was resuspend in 100 µL lysis buffer (Promega) and 20 µL of lysed cells were pipetted into white 96-well plate in triplicates. 50 µL of LAR substrate (Promega) was added to the lysed cell suspension and luminescence signal was determined using the plate reader (BMG Labtech).

For analysis of immune cell recruitment into the peritoneal cavity the collected cell suspension of peritoneal was centrifuged and red blood cells in the cell pellet were lysed with 1 mL ACK (Thermo Fisher Scientifics). After red blood cell lysis and washing of cell suspension was counted using Neubauer Counting chamber $1*10^6$ cells were used for FACS staining (4.6.11 Flow cytometer staining).

4.7.2.4 Collection of Blood

Blood was collected from *Vena facialis* and collected in heparin tubes for FACS staining and in serum tubes to isolate serum form the animals.

For later FACS analysis, blood was resuspendend in 1 mL ACK and washed with 3 mL PBS. ACK and washing was performed until the pellet was clean. After red blood cell lysis and washing of cell were used for FACS staining (4.6.11 Flow cytometer staining).

4.7.2.5 Conservation of tissue

For PFA fixed tissues, omentum was collected and directly placed in 4% PFA solution and stored at 4°C overnight. The next day, PFA solution was washed out using tap water for 1 h and replaced and stored in 70% EtOH at 4°C.The tissue was dehydrated using the TissueTek VIP6 Vacuum Infiltration Tissue Processor (Sakura) according manufactures protocol. In brief, dehydration was performed in several series if incubation steps in 70% EtOH, 80% EtOH, 95% EtOH, 99% EtOH, Xylenes and Paraffin (65°C) each step for 2 min. Afterwards, tissue was embedded in paraffin blocks using Hiso Star machine (Thermo Fisher Scientics) at 4°C. Paraffin blockes were stored at 4°C and cutted in 4 µm thick sections using microtome (Thermo Fisher Scientifics) and transferred onto microscope slides.

Immunohistological staining was performed with properly dried tissue sections.

4.7.2.6 Immunohistological staining

For Diaminobenzidin (DAB) staining tissue sections were deparaffinization using HIER citrate buffer with appropriate pH (ph6 or 9; Zytomed) and steamed. Tissue sections were cooked for 25 min. After boiling slides were cooled and rinsed with water for 20 min followed by a washing with TBS buffer and permeabilisation using 0.025% Triton X-100 TBS for 5 min. Before staining with primary antibodies, tissue sections were blocked using animal free blocking solution for 1 h at RT. Staining of primary antibodies were performed in blocking solution and indicated dilutions overnight at 4 °C. Next days, slides were washed three times using permeabilisation buffer followed by a washing and incubation with 0.3% H_2O_2 in TBS for 10 min. Secondary HRP-conjugated antibodies were diluted (1/200) in antibody diluent (Cell Signaling) and incubated for 1 h at RT. Tissue sections were washed three times and treated with Diaminobenzidin (DAB; DAKO) for 10 to 15 min, washed with water and dipped into hematoxylin solution. Stained tissue slides were dehydrated and mounted before analyzing using microscopy. From each tissue several evenly spaced field picture were taken using 20x objective and analysis was performed with Image J software.

For immunohistochemistry tissue slides were treated as described before, the second day of staining secondary fluorescent-labeled antibodies were incubated for 1h at RT. After secondary antibody incubation slides were washed with TBS-triton buffer and incubated with DAPI (1/5.000) in PBS for 5 min for fluorescence staining. For AP staining, slides were incubated with Alkaline Phosphatase (AP) polymere and treated with AP red KIT (Zytomed) and AP substrate (AP Red Chromogen, Zytomed) for 30min. Tissue sections were again washed with PBS and mounted in fluorescence mounting media (DAKO). From each tissue several evenly spaced field picture were taken using 20x objective and analysis was performed with Image J software.

4.7.2.7   Whole mount staining of omentum

To analyze the tumor burden of freshly isolated omentum was performed following the protocol from Y. Jiang *et al.,* 2018 (Jiang *et al.*, 2018). For imaging tissue was mounted with mounting media and analyzed using LSM710 from DKFZ Core facility Light core facility. From each tissue several evenly spaced field picture were taken using 20x objective and analysis was performed with Image J software.

4.7.2.8   Cytotoxicity assay

One day before T cell sorting, murine metastatic EOC cells (7.500 ID8 cells in 100uL DMEM medium) were seeded in a 96-well plate. After six weeks of tumor growth T cells (CD3$^+$) were sorted using FACS and 10.000 CD3$^+$ cells were added to each well in technical triplicates including untreated control and Blank. After overnight incubation, cytotoxicity was measured using lactate dehydrogenase (LDH) assay of cell supernatant from TC and T cell co-culture. LDH levels were determinate using LDH-Cytotoxicity Assay Kit (Ab65393, Abcam) following the manufacturer's protocol.

4.7.3   Effects of Endothelial Notch signaling on immune cell recruitment in subcutaneous tumor model

4.7.3.1   Gene recombination

Recombination of transgenic mouse lines was performed by oral administration of tamoxifen (Sigma). Female mice between 8 and 12 weeks received once 100 µL tamoxifen (1mg/mL in peanut oil) and experiment were performed one weeks after gene recombination. Successful recombination was confirmed via PCR (see 4.6.3 Genotyping of mouse lines) using lung tissue.

4.7.3.2   Tumor cell injection

LLC cells were cultured as described in 4.4.2 Cell culture maintenance. For subcutaneous tumor experiments LLC cells washed with PBS, resuspended into desired cell concentrations in ice-cold PBS and stored on ice until implantation. After shaving on skin, $0.5*10^6$ cells resuspendend in PBS was injected into the right flank of the animals. Tumor volume was monitored by measuring the largest (d) and smallest (w) tumor diameter with a caliper every 2-3 days. Tumor volume was calculated as follows:

$$V\ [mm^3] = d\ [mm] * \frac{w[mm]^2}{2}$$

Tumor growth was monitored until termination criteria; largest diameter >15 mm, tumor ulceration, signs of severe illness such as apathy, respiratory distress, or weight loss over 20% were reached.

4.7.3.3   Digestion of tumor tissue

Subcutaneous tumors were weighted and cut into pieces for FACS analysis, immunohistochemistry, RNA and protein isolation. For FACS analysis of the tumor tissue was digested using 1 mg/mL Collagenase II in PBS. 5mL digestion solution was used per tumor piece and incubated for 1 to 2 h at 37°C. After digestion tumor tissue was filtered through 70um filters and flushed with 5mL PBS with 10% FCS to inactivate the enzyme. Cell suspension was centrifuges and washed with PBS before counting. After red blood cell lysis and washing of cell suspension was counted using Neubauer Counting chamber and 0,5 or $1*10^6$ cells were used for FACS staining (4.6.11 Flow cytometer staining).

4.8 Bioinformatic methods

4.8.1 *In silco* analysis of promotor region

Analysis of murine (NM_009140; chr5+:90902580-90903927) and human (NM_002089; chr4-:74100502-74099123) CXCL2 promotor region for RBPJ binding site (Lake, Tsai, Choi, Won, & Fan, 2014) (5´-GTGGGAA-3´) were performed using the ApE Software (ApE v2.047, M. Wayne Davis) and presented as scheme.

4.8.2 Gene set enrichment analysis

Gene set enrichment analysis (GSEA) was performed on microarray results to determinate enrichment of gene sets in the different groups. Public availed gene list were used to compare between treated groups as indicated in the figure legends.

4.8.3 Ingenuity Pathway Analysis

Ingenuity Pathway Analysis (IPA) was used to determinate differentially regulated pathways and upstream regulator using microarray results.

4.9 Statistical analysis

Statistical analysis were performed using GraphPad Prism (GraphPad Software, Inc.; La Jolla, CA, USA) and discussed with Dr. A. Kopp-Schneider, Biostatics department, DKFZ. Comparison analysis were performed unpaired or paired, one-tail or two-tailed using students T-test or Mann-Whitney U-test, multiple comparison was performed using two-way Anova and indicated in the figure legend. Data are presented as mean± standard deviation (SD) in both direction and indicated statistical analysis. Scheme and graphical abstracts are created with BioRender.com.
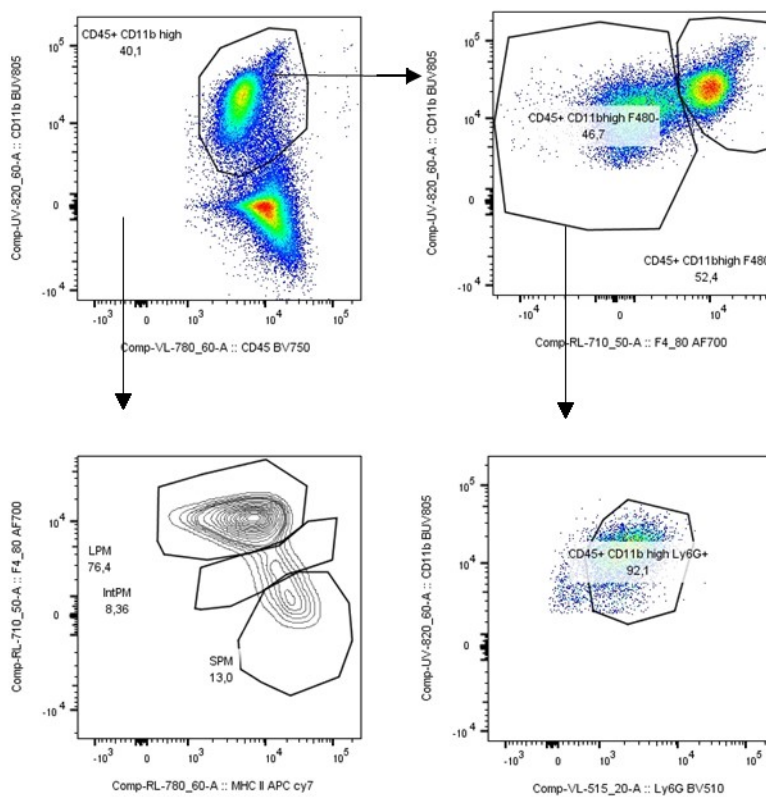
5   Appendix
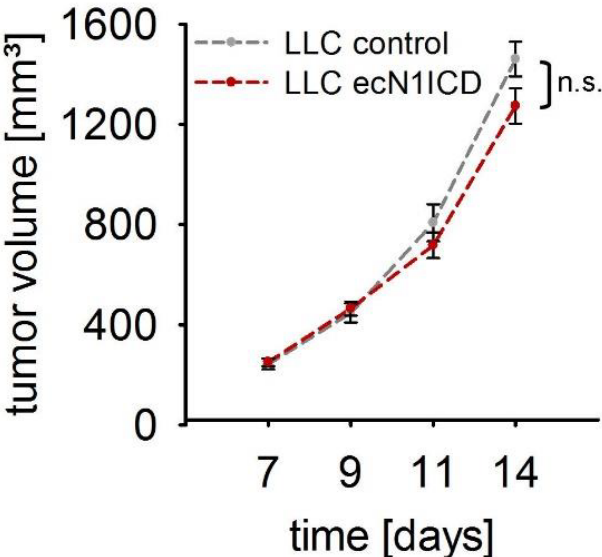
Figure 5.1: Increased tumor growth of subcutaneous LLC tumors in ecN1ICD compared to control. Modulation of endothelial Notch signaling affect tumor growth in a subcutaneous model of LLC tumor. Tumor cells were injected one weeks after recombination and tumor growth was monitored for 14 days. Kindly provided by E. Wieland
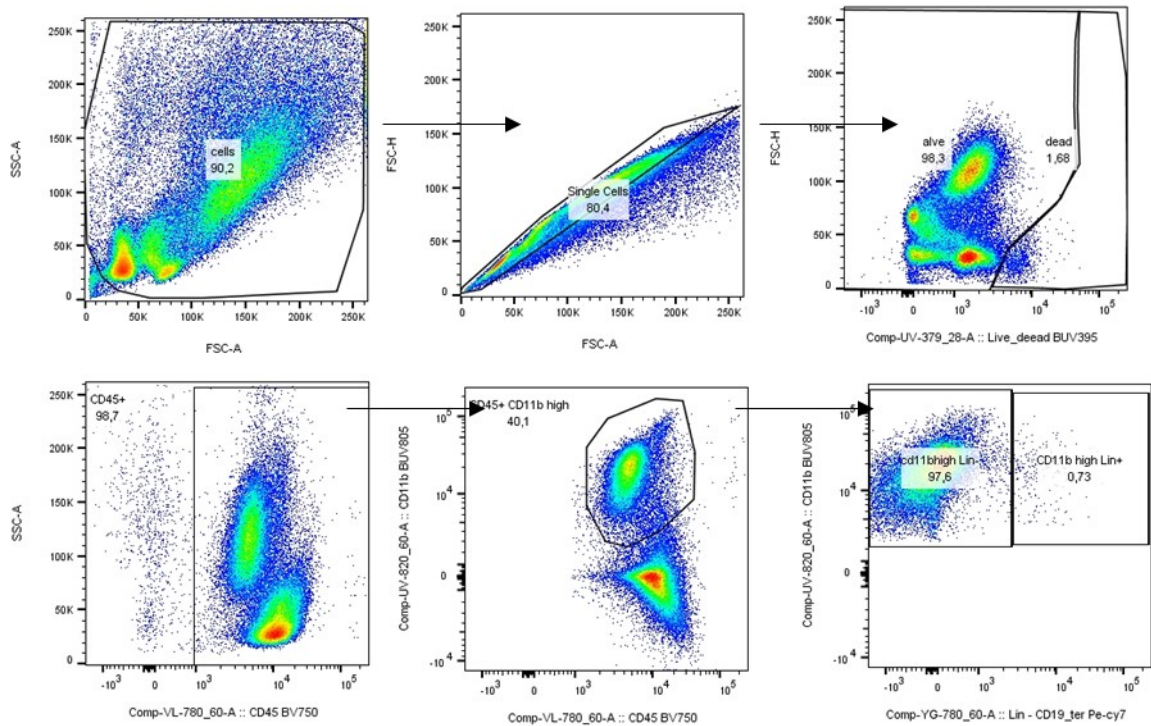
Figure 5.2: Gating strategy for myeloid cell form peritoneal lavage. Flow cytometer analysis of peritoneal lavage. **A** Gating strategy for myeloid cells by FSC and SSC for alive CD45$^+$ CD11b^{high} expression with determination of Lin$^-$ (CD19, Ter119) population. **B** Gating strategy from myeloid cell into neutrophils (Ly6G), macrophages (F4/80) and monocyte-derived macrophages (F4/80 and MHCII).
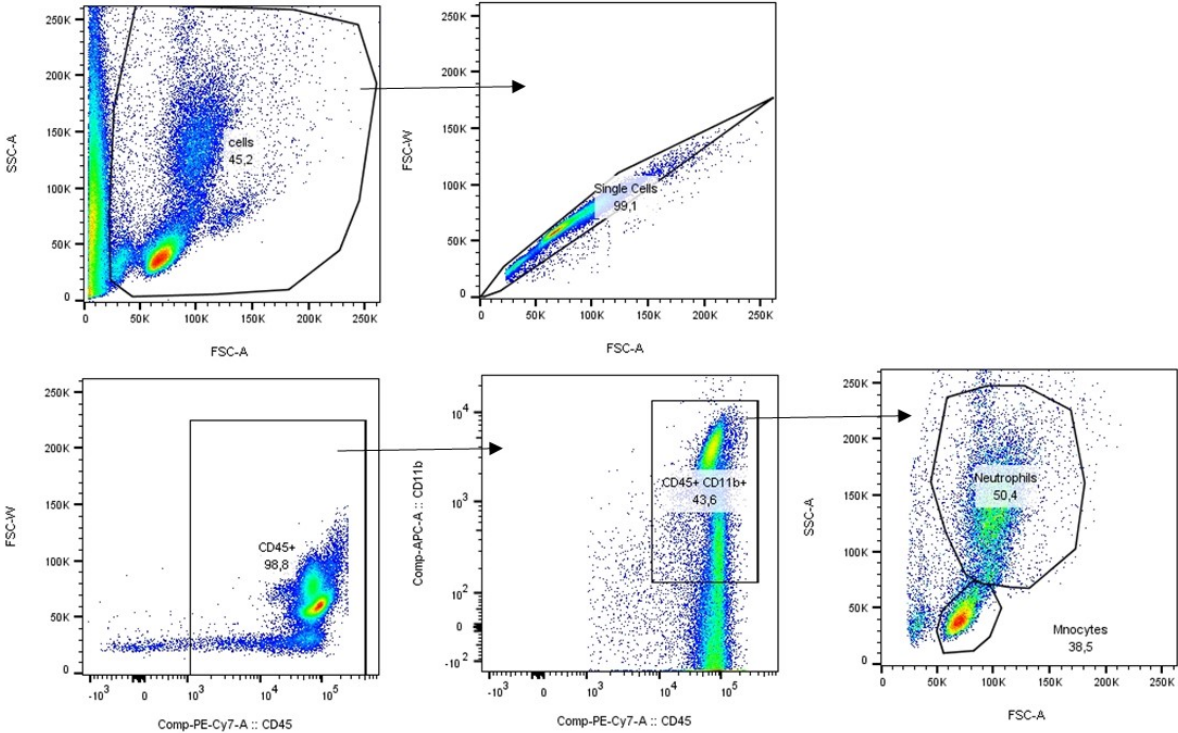
Figure 5.3: Gating strategy for myeloid cell form blood. Flow cytometry gating for granulocytes (neutrophils) and monocytes in SSC and FSC scatter plot.

6 References

Abbate, A., Canada, J. M., Van Tassell, B. W., Wise, C. M., & Dinarello, C. A. (2014). Interleukin-1 blockade in rheumatoid arthritis and heart failure: a missed opportunity? *Int J Cardiol, 171*(3), e125-126. doi:10.1016/j.ijcard.2013.12.078

Ai, L., Mu, S., Wang, Y., Wang, H., Cai, L., Li, W., & Hu, Y. (2018). Prognostic role of myeloid-derived suppressor cells in cancers: a systematic review and meta-analysis. *BMC Cancer, 18*(1), 1220. doi:10.1186/s12885-018-5086-y

Akhtar, M., Haider, A., Rashid, S., & Al-Nabet, A. (2019). Paget's "Seed and Soil" Theory of Cancer Metastasis: An Idea Whose Time has Come. *Adv Anat Pathol, 26*(1), 69-74. doi:10.1097/PAP.0000000000000219

Al-Soudi, A., Kaaij, M. H., & Tas, S. W. (2017). Endothelial cells: From innocent bystanders to active participants in immune responses. *Autoimmun Rev, 16*(9), 951-962. doi:10.1016/j.autrev.2017.07.008

Alfaro, C., Teijeira, A., Onate, C., Perez, G., Sanmamed, M. F., Andueza, M. P., . . . Melero, I. (2016). Tumor-Produced Interleukin-8 Attracts Human Myeloid-Derived Suppressor Cells and Elicits Extrusion of Neutrophil Extracellular Traps (NETs). *Clin Cancer Res, 22*(15), 3924-3936. doi:10.1158/1078-0432.CCR-15-2463

Allen, E., Jabouille, A., Rivera, L. B., Lodewijckx, I., Missiaen, R., Steri, V., . . . Bergers, G. (2017). Combined antiangiogenic and anti-PD-L1 therapy stimulates tumor immunity through HEV formation. *Sci Transl Med, 9*(385). doi:10.1126/scitranslmed.aak9679

Alsheikh, A. J., Dasinger, J. H., Abais-Battad, J. M., Fehrenbach, D. J., Yang, C., Cowley, A. W., Jr., & Mattson, D. L. (2020). CCL2 mediates early renal leukocyte infiltration during salt-sensitive hypertension. *Am J Physiol Renal Physiol, 318*(4), F982-F993. doi:10.1152/ajprenal.00521.2019

Alsina-Sanchis, E., Mülfarth, R., & Fischer, A. (2021). Control of Tumor Progression by Angiocrine Factors. *Cancers (Basel), 13*(11). doi:10.3390/cancers13112610

An, N., Wang, H., Jia, W., Jing, W., Liu, C., Zhu, H., & Yu, J. (2019). The prognostic role of circulating CD8(+) T cell proliferation in patients with untreated extensive stage small cell lung cancer. *J Transl Med, 17*(1), 402. doi:10.1186/s12967-019-02160-7

Augustin, H. G., & Koh, G. Y. (2017). Organotypic vasculature: From descriptive heterogeneity to functional pathophysiology. *Science, 357*(6353). doi:10.1126/science.aal2379

Baci, D., Bosi, A., Gallazzi, M., Rizzi, M., Noonan, D. M., Poggi, A., . . . Mortara, L. (2020). The Ovarian Cancer Tumor Immune Microenvironment (TIME) as Target for Therapy: A Focus on Innate Immunity Cells as Therapeutic Effectors. *Int J Mol Sci, 21*(9). doi:10.3390/ijms21093125

Baek, S. H., Lee, H. W., Gangadaran, P., Oh, J. M., Zhu, L., Rajendran, R. L., . . . Ahn, B. C. (2020). Role of M2-like macrophages in the progression of ovarian cancer. *Exp Cell Res, 395*(2), 112211. doi:10.1016/j.yexcr.2020.112211

Bagley, R. G. (2016). Commentary on Folkman: "Tumor Angiogenesis Factor". *Cancer Res, 76*(7), 1673-1674. doi:10.1158/0008-5472.CAN-16-0675

Beck, L. A., Thaci, D., Hamilton, J. D., Graham, N. M., Bieber, T., Rocklin, R., . . . Radin, A. R. (2014). Dupilumab treatment in adults with moderate-to-severe atopic dermatitis. *N Engl J Med, 371*(2), 130-139. doi:10.1056/NEJMoa1314768

Ben-Sasson, S. Z., Wang, K., Cohen, J., & Paul, W. E. (2013). IL-1beta strikingly enhances antigen-driven CD4 and CD8 T-cell responses. *Cold Spring Harb Symp Quant Biol, 78*, 117-124. doi:10.1101/sqb.2013.78.021246

Bent, R., Moll, L., Grabbe, S., & Bros, M. (2018). Interleukin-1 Beta-A Friend or Foe in Malignancies? *Int J Mol Sci, 19*(8). doi:10.3390/ijms19082155

Bernhagen, J., Krohn, R., Lue, H., Gregory, J. L., Zernecke, A., Koenen, R. R., . . . Weber, C. (2007). MIF is a noncognate ligand of CXC chemokine receptors in inflammatory and atherogenic cell recruitment. *Nat Med, 13*(5), 587-596. doi:10.1038/nm1567

References

Beswick, E.J., & Montavini A., (2001). Inflammation and cancer: back to Virchow. *The Lancet*, *357*(9255), 539-545. doi: 10.1016/S0140-6736(00)04046-0

Beswick, E. J., & Reyes, V. E. (2009). CD74 in antigen presentation, inflammation, and cancers of the gastrointestinal tract. *World J Gastroenterol, 15*(23), 2855-2861. doi:10.3748/wjg.15.2855

Beyer, M., Mallmann, M. R., Xue, J., Staratschek-Jox, A., Vorholt, D., Krebs, W., . . . Schultze, J. L. (2012). High-resolution transcriptome of human macrophages. *PLoS One, 7*(9), e45466. doi:10.1371/journal.pone.0045466

Bingle, L., Brown, N. J., & Lewis, C. E. (2002). The role of tumour-associated macrophages in tumour progression: implications for new anticancer therapies. *J Pathol, 196*(3), 254-265. doi:10.1002/path.1027

Blattner, C., Fleming, V., Weber, R., Himmelhan, B., Altevogt, P., Gebhardt, C., . . . Umansky, V. (2018). CCR5(+) Myeloid-Derived Suppressor Cells Are Enriched and Activated in Melanoma Lesions. *Cancer Res, 78*(1), 157-167. doi:10.1158/0008-5472.CAN-17-0348

Bousoik, E., Qadri, M., & Elsaid, K. A. (2020). CD44 Receptor Mediates Urate Crystal Phagocytosis by Macrophages and Regulates Inflammation in A Murine Peritoneal Model of Acute Gout. *Sci Rep, 10*(1), 5748. doi:10.1038/s41598-020-62727-z

Bray, F., Ferlay, J., Soerjomataram, I., Siegel, R. L., Torre, L. A., & Jemal, A. (2018). Global cancer statistics 2018: GLOBOCAN estimates of incidence and mortality worldwide for 36 cancers in 185 countries. *CA Cancer J Clin, 68*(6), 394-424. doi:10.3322/caac.21492

Brou, C., Logeat, F., Gupta, N., Bessia, C., LeBail, O., Doedens, J. R., . . . Israel, A. (2000). A novel proteolytic cleavage involved in Notch signaling: the role of the disintegrin-metalloprotease TACE. *Mol Cell, 5*(2), 207-216. doi:10.1016/s1097-2765(00)80417-7

Bussolino L. N., M. A. a. F. B. (2017). VEGF-Mediated Signal Transduction in Tumor Angiogenesis. *Physiol. Pathol. Angiogenes. Signal. Mech. Target. Ther, 227*. doi: 10.5772/66764

Cao, J., Zhu, X., Zhao, X., Li, X. F., & Xu, R. (2016). Neutrophil-to-Lymphocyte Ratio Predicts PSA Response and Prognosis in Prostate Cancer: A Systematic Review and Meta-Analysis. *PLoS One, 11*(7), e0158770. doi:10.1371/journal.pone.0158770

Cao, R., Bjorndahl, M. A., Gallego, M. I., Chen, S., Religa, P., Hansen, A. J., & Cao, Y. (2006). Hepatocyte growth factor is a lymphangiogenic factor with an indirect mechanism of action. *Blood, 107*(9), 3531-3536. doi:10.1182/blood-2005-06-2538

Carroll, M. J., Kapur, A., Felder, M., Patankar, M. S., & Kreeger, P. K. (2016). M2 macrophages induce ovarian cancer cell proliferation via a heparin binding epidermal growth factor/matrix metalloproteinase 9 intercellular feedback loop. *Oncotarget, 7*(52), 86608-86620. doi:10.18632/oncotarget.13474

Chambers, A. F., MacDonald, I. C., Schmidt, E. E., Morris, V. L., & Groom, A. C. (2000). Clinical targets for anti-metastasis therapy. *Adv Cancer Res, 79*, 91-121. doi:10.1016/s0065-230x(00)79003-8

Chen, J., Hong, D., Zhai, Y., & Shen, P. (2015). Meta-analysis of associations between neutrophil-to-lymphocyte ratio and prognosis of gastric cancer. *World J Surg Oncol, 13*, 122. doi:10.1186/s12957-015-0530-9

Chen, X., Wang, Y., Nelson, D., Tian, S., Mulvey, E., Patel, B., . . . Rollins, B. J. (2016). CCL2/CCR2 Regulates the Tumor Microenvironment in HER-2/neu-Driven Mammary Carcinomas in Mice. *PLoS One, 11*(11), e0165595. doi:10.1371/journal.pone.0165595

Chillakuri, C. R., Sheppard, D., Lea, S. M., & Handford, P. A. (2012). Notch receptor-ligand binding and activation: insights from molecular studies. *Semin Cell Dev Biol, 23*(4), 421-428. doi:10.1016/j.semcdb.2012.01.009

Chiu, D. K., Tse, A. P., Xu, I. M., Di Cui, J., Lai, R. K., Li, L. L., . . . Wong, C. C. (2017). Hypoxia inducible factor HIF-1 promotes myeloid-derived suppressor cells accumulation through ENTPD2/CD39L1 in hepatocellular carcinoma. *Nat Commun, 8*(1), 517. doi:10.1038/s41467-017-00530-7

Clark, R., Krishnan, V., Schoof, M., Rodriguez, I., Theriault, B., Chekmareva, M., & Rinker-Schaeffer, C. (2013). Milky spots promote ovarian cancer metastatic colonization of peritoneal adipose in experimental models. *Am J Pathol, 183*(2), 576-591. doi:10.1016/j.ajpath.2013.04.023

Clendenen, T. V., Lundin, E., Zeleniuch-Jacquotte, A., Koenig, K. L., Berrino, F., Lukanova, A., . . . Arslan, A. A. (2011). Circulating inflammation markers and risk of epithelial ovarian cancer. *Cancer Epidemiol Biomarkers Prev, 20*(5), 799-810. doi:10.1158/1055-9965.EPI-10-1180

Colditz, G. A., Sellers, T. A., & Trapido, E. (2006). Epidemiology - identifying the causes and preventability of cancer? *Nat Rev Cancer, 6*(1), 75-83. doi:10.1038/nrc1784

Conteduca, V., Kopf, B., Burgio, S. L., Bianchi, E., Amadori, D., & De Giorgi, U. (2014). The emerging role of anti-angiogenic therapy in ovarian cancer (review). *Int J Oncol, 44*(5), 1417-1424. doi:10.3892/ijo.2014.2334

Cook, A. D., Braine, E. L., & Hamilton, J. A. (2003). The phenotype of inflammatory macrophages is stimulus dependent: implications for the nature of the inflammatory response. *J Immunol, 171*(9), 4816-4823. doi:10.4049/jimmunol.171.9.4816

Cortes, M., Sanchez-Moral, L., de Barrios, O., Fernandez-Acenero, M. J., Martinez-Campanario, M. C., Esteve-Codina, A., . . . Postigo, A. (2017). Tumor-associated macrophages (TAMs) depend on ZEB1 for their cancer-promoting roles. *EMBO J, 36*(22), 3336-3355. doi:10.15252/embj.201797345

Cotechini, T., Atallah, A., & Grossman, A. (2021). Tissue-Resident and Recruited Macrophages in Primary Tumor and Metastatic Microenvironments: Potential Targets in Cancer Therapy. *Cells, 10*(4). doi:10.3390/cells10040960

DeNardo, D. G., & Ruffell, B. (2019). Macrophages as regulators of tumour immunity and immunotherapy. *Nat Rev Immunol, 19*(6), 369-382. doi:10.1038/s41577-019-0127-6

Dong, H., Strome, S. E., Salomao, D. R., Tamura, H., Hirano, F., Flies, D. B., . . . Chen, L. (2002). Tumor-associated B7-H1 promotes T-cell apoptosis: a potential mechanism of immune evasion. *Nat Med, 8*(8), 793-800. doi:10.1038/nm730

Donovan, P., Patel, J., Dight, J., Wong, H. Y., Sim, S. L., Murigneux, V., . . . Khosrotehrani, K. (2019). Endovascular progenitors infiltrate melanomas and differentiate towards a variety of vascular beds promoting tumor metastasis. *Nat Commun, 10*(1), 18. doi:10.1038/s41467-018-07961-w

Duarte, A., Hirashima, M., Benedito, R., Trindade, A., Diniz, P., Bekman, E., . . . Rossant, J. (2004). Dosage-sensitive requirement for mouse Dll4 in artery development. *Genes Dev, 18*(20), 2474-2478. doi:10.1101/gad.1239004

Ducoli, L., Agrawal, S., Sibler, E., Kouno, T., Tacconi, C., Hon, C. C., . . . Detmar, M. (2021). LETR1 is a lymphatic endothelial-specific lncRNA governing cell proliferation and migration through KLF4 and SEMA3C. *Nat Commun, 12*(1), 925. doi:10.1038/s41467-021-21217-0

Dumusc, A., & So, A. (2015). Interleukin-1 as a therapeutic target in gout. *Curr Opin Rheumatol, 27*(2), 156-163. doi:10.1097/BOR.0000000000000143

Durgeau, A., Virk, Y., Corgnac, S., & Mami-Chouaib, F. (2018). Recent Advances in Targeting CD8 T-Cell Immunity for More Effective Cancer Immunotherapy. *Front Immunol, 9*, 14. doi:10.3389/fimmu.2018.00014

Dvorak, H. F. (1986). Tumors: wounds that do not heal. Similarities between tumor stroma generation and wound healing. *N Engl J Med, 315*(26), 1650-1659. doi:10.1056/NEJM198612253152606

Etzerodt, A., Moulin, M., Doktor, T. K., Delfini, M., Mossadegh-Keller, N., Bajenoff, M., . . . Lawrence, T. (2020). Tissue-resident macrophages in omentum promote metastatic spread of ovarian cancer. *J Exp Med, 217*(4). doi:10.1084/jem.20191869

Ferjancic, S., Gil-Bernabe, A. M., Hill, S. A., Allen, P. D., Richardson, P., Sparey, T., . . . Muschel, R. J. (2013). VCAM-1 and VAP-1 recruit myeloid cells that promote pulmonary metastasis in mice. *Blood, 121*(16), 3289-3297. doi:10.1182/blood-2012-08-449819

Figueiredo, C. R., Azevedo, R. A., Mousdell, S., Resende-Lara, P. T., Ireland, L., Santos, A., . . . Mielgo, A. (2018). Blockade of MIF-CD74 Signalling on Macrophages and Dendritic Cells Restores the Antitumour Immune Response Against Metastatic Melanoma. *Front Immunol, 9*, 1132. doi:10.3389/fimmu.2018.01132

Finn, R. S., Qin, S., Ikeda, M., Galle, P. R., Ducreux, M., Kim, T. Y., . . . Investigators, I. M. (2020). Atezolizumab plus Bevacizumab in Unresectable Hepatocellular Carcinoma. *N Engl J Med, 382*(20), 1894-1905. doi:10.1056/NEJMoa1915745

References

Fischer, A., Schumacher, N., Maier, M., Sendtner, M., & Gessler, M. (2004). The Notch target genes Hey1 and Hey2 are required for embryonic vascular development. *Genes Dev, 18*(8), 901-911. doi:10.1101/gad.291004

Franklin, R. A., & Li, M. O. (2016). Ontogeny of Tumor-associated Macrophages and Its Implication in Cancer Regulation. *Trends Cancer, 2*(1), 20-34. doi:10.1016/j.trecan.2015.11.004

Fridlender, Z. G., Sun, J., Kim, S., Kapoor, V., Cheng, G., Ling, L., . . . Albelda, S. M. (2009). Polarization of tumor-associated neutrophil phenotype by TGF-beta: "N1" versus "N2" TAN. *Cancer Cell, 16*(3), 183-194. doi:10.1016/j.ccr.2009.06.017

Fu, C., & Jiang, A. (2018). Dendritic Cells and CD8 T Cell Immunity in Tumor Microenvironment. *Front Immunol, 9*, 3059. doi:10.3389/fimmu.2018.03059

Gale, N. W., Dominguez, M. G., Noguera, I., Pan, L., Hughes, V., Valenzuela, D. M., . . . Yancopoulos, G. D. (2004). Haploinsufficiency of delta-like 4 ligand results in embryonic lethality due to major defects in arterial and vascular development. *Proc Natl Acad Sci U S A, 101*(45), 15949-15954. doi:10.1073/pnas.0407290101

Gautier, E. L., Ivanov, S., Lesnik, P., & Randolph, G. J. (2013a). Local apoptosis mediates clearance of macrophages from resolving inflammation in mice. *Blood, 122*(15), 2714-2722. doi:10.1182/blood-2013-01-478206

Gautier, E. L., Ivanov, S., Lesnik, P., & Randolph, G. J. (2013b). Local apoptosis mediates clearance of macrophages from resolving inflammation in mice. *Blood, 122*(15), 2714-2722. doi:10.1182/blood-2013-01-478206

Ghoochani, A., Schwarz, M. A., Yakubov, E., Engelhorn, T., Doerfler, A., Buchfelder, M., . . . Eyupoglu, I. Y. (2016). MIF-CD74 signaling impedes microglial M1 polarization and facilitates brain tumorigenesis. *Oncogene, 35*(48), 6246-6261. doi:10.1038/onc.2016.160

Ghosn, E. E., Cassado, A. A., Govoni, G. R., Fukuhara, T., Yang, Y., Monack, D. M., . . . Herzenberg, L. A. (2010). Two physically, functionally, and developmentally distinct peritoneal macrophage subsets. *Proc Natl Acad Sci U S A, 107*(6), 2568-2573. doi:10.1073/pnas.0915000107

Giakoustidis, A., Neofytou, K., Costa Neves, M., Giakoustidis, D., Louri, E., Cunningham, D., & Mudan, S. (2018). Identifying the role of neutrophil-to-lymphocyte ratio and platelets-to-lymphocyte ratio as prognostic markers in patients undergoing resection of pancreatic ductal adenocarcinoma. *Ann Hepatobiliary Pancreat Surg, 22*(3), 197-207. doi:10.14701/ahbps.2018.22.3.197

Gibeon, D., & Menzies-Gow, A. N. (2012). Targeting interleukins to treat severe asthma. *Expert Rev Respir Med, 6*(4), 423-439. doi:10.1586/ers.12.38

Goossens, P., Rodriguez-Vita, J., Etzerodt, A., Masse, M., Rastoin, O., Gouirand, V., . . . Lawrence, T. (2019). Membrane Cholesterol Efflux Drives Tumor-Associated Macrophage Reprogramming and Tumor Progression. *Cell Metabolism, 29*(6), 1376-+. doi:10.1016/j.cmet.2019.02.016

Gorbachev, A. V., & Fairchild, R. L. (2014). Regulation of chemokine expression in the tumor microenvironment. *Crit Rev Immunol, 34*(2), 103-120. doi:10.1615/critrevimmunol.2014010062

Gordon, W. R., Arnett, K. L., & Blacklow, S. C. (2008). The molecular logic of Notch signaling--a structural and biochemical perspective. *J Cell Sci, 121*(Pt 19), 3109-3119. doi:10.1242/jcs.035683

Groth, C., Hu, X., Weber, R., Fleming, V., Altevogt, P., Utikal, J., & Umansky, V. (2019). Immunosuppression mediated by myeloid-derived suppressor cells (MDSCs) during tumour progression. *Br J Cancer, 120*(1), 16-25. doi:10.1038/s41416-018-0333-1

Guo, F. F., & Cui, J. W. (2019). The Role of Tumor-Infiltrating B Cells in Tumor Immunity. *J Oncol, 2019*, 2592419. doi:10.1155/2019/2592419

Haber, T., Cornejo, Y. R., Aramburo, S., Flores, L., Cao, P., Liu, A., . . . Berlin, J. M. (2020). Specific targeting of ovarian tumor-associated macrophages by large, anionic nanoparticles. *Proc Natl Acad Sci U S A, 117*(33), 19737-19745. doi:10.1073/pnas.1917424117

Hagerling, R., Hoppe, E., Dierkes, C., Stehling, M., Makinen, T., Butz, S., . . . Kiefer, F. (2018). Distinct roles of VE-cadherin for development and maintenance of specific lymph vessel beds. *EMBO J, 37*(22). doi:10.15252/embj.201798271

Hanahan, D., & Coussens, L. M. (2012). Accessories to the crime: functions of cells recruited to the tumor microenvironment. *Cancer Cell, 21*(3), 309-322. doi:10.1016/j.ccr.2012.02.022

Hanahan, D., & Weinberg, R. A. (2011). Hallmarks of cancer: the next generation. *Cell, 144*(5), 646-674. doi:10.1016/j.cell.2011.02.013

Hensler, M., Kasikova, L., Fiser, K., Rakova, J., Skapa, P., Laco, J., . . . Fucikova, J. (2020). M2-like macrophages dictate clinically relevant immunosuppression in metastatic ovarian cancer. *J Immunother Cancer, 8*(2). doi:10.1136/jitc-2020-000979

Hermida, M. D. R., Malta, R., de, S. S. M., & Dos-Santos, W. L. C. (2017). Selecting the right gate to identify relevant cells for your assay: a study of thioglycollate-elicited peritoneal exudate cells in mice. *BMC Res Notes, 10*(1), 695. doi:10.1186/s13104-017-3019-5

Huang, S., Van Arsdall, M., Tedjarati, S., McCarty, M., Wu, W., Langley, R., & Fidler, I. J. (2002). Contributions of stromal metalloproteinase-9 to angiogenesis and growth of human ovarian carcinoma in mice. *J Natl Cancer Inst, 94*(15), 1134-1142. doi:10.1093/jnci/94.15.1134

Hutton, H. L., Ooi, J. D., Holdsworth, S. R., & Kitching, A. R. (2016). The NLRP3 inflammasome in kidney disease and autoimmunity. *Nephrology (Carlton), 21*(9), 736-744. doi:10.1111/nep.12785

Ishikawa, M., Nakayama, K., Nakamura, K., Yamashita, H., Ishibashi, T., Minamoto, T., . . . Kyo, S. (2020). High PD-1 expression level is associated with an unfavorable prognosis in patients with cervical adenocarcinoma. *Arch Gynecol Obstet, 302*(1), 209-218. doi:10.1007/s00404-020-05589-0

Iwai, Y., Ishida, M., Tanaka, Y., Okazaki, T., Honjo, T., & Minato, N. (2002). Involvement of PD-L1 on tumor cells in the escape from host immune system and tumor immunotherapy by PD-L1 blockade. *Proc Natl Acad Sci U S A, 99*(19), 12293-12297. doi:10.1073/pnas.192461099

Jabs, M., Rose, A. J., Lehmann, L. H., Taylor, J., Moll, I., Sijmonsma, T. P., . . . Fischer, A. (2018). Inhibition of Endothelial Notch Signaling Impairs Fatty Acid Transport and Leads to Metabolic and Vascular Remodeling of the Adult Heart. *Circulation, 137*(24), 2592-2608. doi:10.1161/CIRCULATIONAHA.117.029733

Jackson-Jones, L. H., Smith, P., Portman, J. R., Magalhaes, M. S., Mylonas, K. J., Vermeren, M. M., . . . Benezech, C. (2020). Stromal Cells Covering Omental Fat-Associated Lymphoid Clusters Trigger Formation of Neutrophil Aggregates to Capture Peritoneal Contaminants. *Immunity, 52*(4), 700-715 e706. doi:10.1016/j.immuni.2020.03.011

Jeon, B. H., Jang, C., Han, J., Kataru, R. P., Piao, L., Jung, K., . . . Koh, G. Y. (2008). Profound but dysfunctional lymphangiogenesis via vascular endothelial growth factor ligands from CD11b+ macrophages in advanced ovarian cancer. *Cancer Res, 68*(4), 1100-1109. doi:10.1158/0008-5472.CAN-07-2572

Ji, R. C. (2006). Lymphatic endothelial cells, tumor lymphangiogenesis and metastasis: New insights into intratumoral and peritumoral lymphatics. *Cancer Metastasis Rev, 25*(4), 677-694. doi:10.1007/s10555-006-9026-y

Jiang, Y., Yeung, J. L., Lee, J. H., An, J., Steadman, P. E., Kim, J. R., & Sung, H. K. (2018). Visualization of 3D White Adipose Tissue Structure Using Whole-mount Staining. *J Vis Exp*(141). doi:10.3791/58683

Karkkainen, M. J., Haiko, P., Sainio, K., Partanen, J., Taipale, J., Petrova, T. V., . . . Alitalo, K. (2004). Vascular endothelial growth factor C is required for sprouting of the first lymphatic vessels from embryonic veins. *Nat Immunol, 5*(1), 74-80. doi:10.1038/ni1013

Karpanen, T., Egeblad, M., Karkkainen, M. J., Kubo, H., Yla-Herttuala, S., Jaattela, M., & Alitalo, K. (2001). Vascular endothelial growth factor C promotes tumor lymphangiogenesis and intralymphatic tumor growth. *Cancer Res, 61*(5), 1786-1790.

Katoh, H., Wang, D., Daikoku, T., Sun, H., Dey, S. K., & Dubois, R. N. (2013). CXCR2-expressing myeloid-derived suppressor cells are essential to promote colitis-associated tumorigenesis. *Cancer Cell, 24*(5), 631-644. doi:10.1016/j.ccr.2013.10.009

Kennedy, R., & Celis, E. (2008). Multiple roles for CD4+ T cells in anti-tumor immune responses. *Immunol Rev, 222*, 129-144. doi:10.1111/j.1600-065X.2008.00616.x

Kim, R., Emi, M., & Tanabe, K. (2007). Cancer immunoediting from immune surveillance to immune escape. *Immunology, 121*(1), 1-14. doi:10.1111/j.1365-2567.2007.02587.x

References

Klichinsky, M., Ruella, M., Shestova, O., Lu, X. M., Best, A., Zeeman, M., . . . Gill, S. (2020). Human chimeric antigen receptor macrophages for cancer immunotherapy. *Nat Biotechnol, 38*(8), 947-953. doi:10.1038/s41587-020-0462-y

Klinakis, A., Lobry, C., Abdel-Wahab, O., Oh, P., Haeno, H., Buonamici, S., . . . Aifantis, I. (2011). A novel tumour-suppressor function for the Notch pathway in myeloid leukaemia. *Nature, 473*(7346), 230-233. doi:10.1038/nature09999

Klotz, L., Norman, S., Vieira, J. M., Masters, M., Rohling, M., Dube, K. N., . . . Riley, P. R. (2015). Cardiac lymphatics are heterogeneous in origin and respond to injury. *Nature, 522*(7554), 62-67. doi:10.1038/nature14483

Kohli, K., Pillarisetty, V. G., & Kim, T. S. (2021). Key chemokines direct migration of immune cells in solid tumors. *Cancer Gene Ther*. doi:10.1038/s41417-021-00303-x

Kolaczkowska, E., & Kubes, P. (2013). Neutrophil recruitment and function in health and inflammation. *Nat Rev Immunol, 13*(3), 159-175. doi:10.1038/nri3399

Koukourakis, G. V., & Sotiropoulou-Lontou, A. (2011). Targeted therapy with bevacizumab (Avastin) for metastatic colorectal cancer. *Clin Transl Oncol, 13*(10), 710-714. doi:10.1007/s12094-011-0720-z

Krebs, L. T., Shutter, J. R., Tanigaki, K., Honjo, T., Stark, K. L., & Gridley, T. (2004). Haploinsufficient lethality and formation of arteriovenous malformations in Notch pathway mutants. *Genes Dev, 18*(20), 2469-2473. doi:10.1101/gad.1239204

Krebs, L. T., Starling, C., Chervonsky, A. V., & Gridley, T. (2010). Notch1 activation in mice causes arteriovenous malformations phenocopied by ephrinB2 and EphB4 mutants. *Genesis, 48*(3), 146-150. doi:10.1002/dvg.20599

Krishnan, V., Tallapragada, S., Schaar, B., Kamat, K., Chanana, A. M., Zhang, Y., . . . Dorigo, O. (2020). Omental macrophages secrete chemokine ligands that promote ovarian cancer colonization of the omentum via CCR1. *Commun Biol, 3*(1), 524. doi:10.1038/s42003-020-01246-z

Kubota, K., Moriyama, M., Furukawa, S., Rafiul, H., Maruse, Y., Jinno, T., . . . Nakamura, S. (2017). CD163(+)CD204(+) tumor-associated macrophages contribute to T cell regulation via interleukin-10 and PD-L1 production in oral squamous cell carcinoma. *Sci Rep, 7*(1), 1755. doi:10.1038/s41598-017-01661-z

Lake, R. J., Tsai, P. F., Choi, I., Won, K. J., & Fan, H. Y. (2014). RBPJ, the major transcriptional effector of Notch signaling, remains associated with chromatin throughout mitosis, suggesting a role in mitotic bookmarking. *PLoS Genet, 10*(3), e1004204. doi:10.1371/journal.pgen.1004204

Lawrence, T., & Natoli, G. (2011). Transcriptional regulation of macrophage polarization: enabling diversity with identity. *Nat Rev Immunol, 11*(11), 750-761. doi:10.1038/nri3088

Lee, P. Y., Li, Y., Kumagai, Y., Xu, Y., Weinstein, J. S., Kellner, E. S., . . . Reeves, W. H. (2009). Type I interferon modulates monocyte recruitment and maturation in chronic inflammation. *Am J Pathol, 175*(5), 2023-2033. doi:10.2353/ajpath.2009.090328

Lee, W. L., & Wang, P. H. (2020). Immunology and ovarian cancers. *J Chin Med Assoc, 83*(5), 425-432. doi:10.1097/JCMA.0000000000000283

Leijh, P. C., van Zwet, T. L., ter Kuile, M. N., & van Furth, R. (1984). Effect of thioglycolate on phagocytic and microbicidal activities of peritoneal macrophages. *Infect Immun, 46*(2), 448-452. doi:10.1128/iai.46.2.448-452.1984

Leu, A. J., Berk, D. A., Lymboussaki, A., Alitalo, K., & Jain, R. K. (2000). Absence of functional lymphatics within a murine sarcoma: a molecular and functional evaluation. *Cancer Res, 60*(16), 4324-4327.

Lewis, C. E., & Pollard, J. W. (2006). Distinct role of macrophages in different tumor microenvironments. *Cancer Res, 66*(2), 605-612. doi:10.1158/0008-5472.CAN-05-4005

Li, Y., Liang, L., Dai, W., Cai, G., Xu, Y., Li, X., . . . Cai, S. (2016). Prognostic impact of programed cell death-1 (PD-1) and PD-ligand 1 (PD-L1) expression in cancer cells and tumor infiltrating lymphocytes in colorectal cancer. *Mol Cancer, 15*(1), 55. doi:10.1186/s12943-016-0539-x

Limbourg, F. P., Takeshita, K., Radtke, F., Bronson, R. T., Chin, M. T., & Liao, J. K. (2005). Essential role of endothelial Notch1 in angiogenesis. *Circulation, 111*(14), 1826-1832. doi:10.1161/01.CIR.0000160870.93058.DD

98

Logeat, F., Bessia, C., Brou, C., LeBail, O., Jarriault, S., Seidah, N. G., & Israel, A. (1998). The Notch1 receptor is cleaved constitutively by a furin-like convertase. *Proc Natl Acad Sci U S A, 95*(14), 8108-8112. doi:10.1073/pnas.95.14.8108

Lucas, E. D., & Tamburini, B. A. J. (2019). Lymph Node Lymphatic Endothelial Cell Expansion and Contraction and the Programming of the Immune Response. *Front Immunol, 10*, 36. doi:10.3389/fimmu.2019.00036

Mabuchi, S., & Sasano, T. (2021). Myeloid-Derived Suppressor Cells as Therapeutic Targets in Uterine Cervical and Endometrial Cancers. *Cells, 10*(5). doi:10.3390/cells10051073

Mack, J. J., & Iruela-Arispe, M. L. (2018). NOTCH regulation of the endothelial cell phenotype. *Curr Opin Hematol, 25*(3), 212-218. doi:10.1097/MOH.0000000000000425

Mack, J. J., Mosqueiro, T. S., Archer, B. J., Jones, W. M., Sunshine, H., Faas, G. C., . . . Iruela-Arispe, M. L. (2017). NOTCH1 is a mechanosensor in adult arteries. *Nat Commun, 8*(1), 1620. doi:10.1038/s41467-017-01741-8

Mahadevan, A., Welsh, I. C., Sivakumar, A., Gludish, D. W., Shilvock, A. R., Noden, D. M., . . . Kurpios, N. A. (2014). The left-right Pitx2 pathway drives organ-specific arterial and lymphatic development in the intestine. *Dev Cell, 31*(6), 690-706. doi:10.1016/j.devcel.2014.11.002

Mailer, R. K., Joly, A. L., Liu, S., Elias, S., Tegner, J., & Andersson, J. (2015). IL-1beta promotes Th17 differentiation by inducing alternative splicing of FOXP3. *Sci Rep, 5*, 14674. doi:10.1038/srep14674

Mandriota, S. J., Jussila, L., Jeltsch, M., Compagni, A., Baetens, D., Prevo, R., . . . Pepper, M. S. (2001). Vascular endothelial growth factor-C-mediated lymphangiogenesis promotes tumour metastasis. *EMBO J, 20*(4), 672-682. doi:10.1093/emboj/20.4.672

Mantovani, A., Allavena, P., Sica, A., & Balkwill, F. (2008). Cancer-related inflammation. *Nature, 454*(7203), 436-444. doi:10.1038/nature07205

Mantovani, A., Sozzani, S., Locati, M., Allavena, P., & Sica, A. (2002). Macrophage polarization: tumor-associated macrophages as a paradigm for polarized M2 mononuclear phagocytes. *Trends Immunol, 23*(11), 549-555. doi:10.1016/s1471-4906(02)02302-5

Marcelo, K. L., Goldie, L. C., & Hirschi, K. K. (2013). Regulation of endothelial cell differentiation and specification. *Circ Res, 112*(9), 1272-1287. doi:10.1161/CIRCRESAHA.113.300506

Martincuks, A., Li, P. C., Zhao, Q., Zhang, C., Li, Y. J., Yu, H., & Rodriguez-Rodriguez, L. (2020). CD44 in Ovarian Cancer Progression and Therapy Resistance-A Critical Role for STAT3. *Front Oncol, 10*, 589601. doi:10.3389/fonc.2020.589601

Martinez-Corral, I., Ulvmar, M. H., Stanczuk, L., Tatin, F., Kizhatil, K., John, S. W., . . . Makinen, T. (2015). Nonvenous origin of dermal lymphatic vasculature. *Circ Res, 116*(10), 1649-1654. doi:10.1161/CIRCRESAHA.116.306170

Massague, J., Batlle, E., & Gomis, R. R. (2017). Understanding the molecular mechanisms driving metastasis. *Mol Oncol, 11*(1), 3-4. doi:10.1002/1878-0261.12024

Masucci, M. T., Minopoli, M., & Carriero, M. V. (2019). Tumor Associated Neutrophils. Their Role in Tumorigenesis, Metastasis, Prognosis and Therapy. *Front Oncol, 9*, 1146. doi:10.3389/fonc.2019.01146

Maula, S. M., Luukkaa, M., Grenman, R., Jackson, D., Jalkanen, S., & Ristamaki, R. (2003). Intratumoral lymphatics are essential for the metastatic spread and prognosis in squamous cell carcinomas of the head and neck region. *Cancer Res, 63*(8), 1920-1926.

Mehta, A. K., Cheney, E. M., Hartl, C. A., Pantelidou, C., Oliwa, M., Castrillon, J. A., . . . Guerriero, J. L. (2021). Targeting immunosuppressive macrophages overcomes PARP inhibitor resistance in BRCA1-associated triple-negative breast cancer. *Nat Cancer, 2*(1), 66-82. doi:10.1038/s43018-020-00148-7

Meza Guzman, L. G., Keating, N., & Nicholson, S. E. (2020). Natural Killer Cells: Tumor Surveillance and Signaling. *Cancers (Basel), 12*(4). doi:10.3390/cancers12040952

Mootha, V. K., Lindgren, C. M., Eriksson, K. F., Subramanian, A., Sihag, S., Lehar, J., . . . Groop, L. C. (2003). PGC-1alpha-responsive genes involved in oxidative phosphorylation are coordinately downregulated in human diabetes. *Nat Genet, 34*(3), 267-273. doi:10.1038/ng1180

References

Mordenti, J., Thomsen, K., Licko, V., Chen, H., Meng, Y. G., & Ferrara, N. (1999). Efficacy and concentration-response of murine anti-VEGF monoclonal antibody in tumor-bearing mice and extrapolation to humans. *Toxicol Pathol, 27*(1), 14-21. doi:10.1177/019262339902700104

Murray, P. J., Allen, J. E., Biswas, S. K., Fisher, E. A., Gilroy, D. W., Goerdt, S., . . . Wynn, T. A. (2014). Macrophage activation and polarization: nomenclature and experimental guidelines. *Immunity, 41*(1), 14-20. doi:10.1016/j.immuni.2014.06.008

Nielsen, C. M., Cuervo, H., Ding, V. W., Kong, Y., Huang, E. J., & Wang, R. A. (2014). Deletion of Rbpj from postnatal endothelium leads to abnormal arteriovenous shunting in mice. *Development, 141*(19), 3782-3792. doi:10.1242/dev.108951

Nieman, K. M., Kenny, H. A., Penicka, C. V., Ladanyi, A., Buell-Gutbrod, R., Zillhardt, M. R., . . . Lengyel, E. (2011). Adipocytes promote ovarian cancer metastasis and provide energy for rapid tumor growth. *Nat Med, 17*(11), 1498-1503. doi:10.1038/nm.2492

Noble, P. W., Lake, F. R., Henson, P. M., & Riches, D. W. (1993). Hyaluronate activation of CD44 induces insulin-like growth factor-1 expression by a tumor necrosis factor-alpha-dependent mechanism in murine macrophages. *J Clin Invest, 91*(6), 2368-2377. doi:10.1172/JCI116469

Nourshargh, S., Hordijk, P. L., & Sixt, M. (2010). Breaching multiple barriers: leukocyte motility through venular walls and the interstitium. *Nat Rev Mol Cell Biol, 11*(5), 366-378. doi:10.1038/nrm2889

Nowak, M., & Klink, M. (2020). The Role of Tumor-Associated Macrophages in the Progression and Chemoresistance of Ovarian Cancer. *Cells, 9*(5). doi:10.3390/cells9051299

Nus, M., Martinez-Poveda, B., MacGrogan, D., Chevre, R., D'Amato, G., Sbroggio, M., . . . de la Pompa, J. L. (2016). Endothelial Jag1-RBPJ signalling promotes inflammatory leucocyte recruitment and atherosclerosis. *Cardiovasc Res, 112*(2), 568-580. doi:10.1093/cvr/cvw193

Obermajer, N., Muthuswamy, R., Odunsi, K., Edwards, R. P., & Kalinski, P. (2011). PGE(2)-induced CXCL12 production and CXCR4 expression controls the accumulation of human MDSCs in ovarian cancer environment. *Cancer Res, 71*(24), 7463-7470. doi:10.1158/0008-5472.CAN-11-2449

Okabe, Y., & Medzhitov, R. (2014). Tissue-specific signals control reversible program of localization and functional polarization of macrophages. *Cell, 157*(4), 832-844. doi:10.1016/j.cell.2014.04.016

Oliver, G., Kipnis, J., Randolph, G. J., & Harvey, N. L. (2020). The Lymphatic Vasculature in the 21(st) Century: Novel Functional Roles in Homeostasis and Disease. *Cell, 182*(2), 270-296. doi:10.1016/j.cell.2020.06.039

Orecchioni, M., Ghosheh, Y., Pramod, A. B., & Ley, K. (2019). Macrophage Polarization: Different Gene Signatures in M1(LPS+) vs. Classically and M2(LPS-) vs. Alternatively Activated Macrophages. *Front Immunol, 10*, 1084. doi:10.3389/fimmu.2019.01084

Ostuni, R., Kratochvill, F., Murray, P. J., & Natoli, G. (2015). Macrophages and cancer: from mechanisms to therapeutic implications. *Trends Immunol, 36*(4), 229-239. doi:10.1016/j.it.2015.02.004

Park, G. T., & Choi, K. C. (2016). Advanced new strategies for metastatic cancer treatment by therapeutic stem cells and oncolytic virotherapy. *Oncotarget, 7*(36), 58684-58695. doi:10.18632/oncotarget.11017

Pasquier, J., Ghiabi, P., Chouchane, L., Razzouk, K., Rafii, S., & Rafii, A. (2020). Angiocrine endothelium: from physiology to cancer. *J Transl Med, 18*(1), 52. doi:10.1186/s12967-020-02244-9

Pawlak, J. B., Balint, L., Lim, L., Ma, W., Davis, R. B., Benyo, Z., . . . Caron, K. M. (2019). Lymphatic mimicry in maternal endothelial cells promotes placental spiral artery remodeling. *J Clin Invest, 129*(11), 4912-4921. doi:10.1172/JCI120446

Peinado, H., Zhang, H., Matei, I. R., Costa-Silva, B., Hoshino, A., Rodrigues, G., . . . Lyden, D. (2017). Pre-metastatic niches: organ-specific homes for metastases. *Nat Rev Cancer, 17*(5), 302-317. doi:10.1038/nrc.2017.6

Pilli, D., Zou, A., Tea, F., Dale, R. C., & Brilot, F. (2017). Expanding Role of T Cells in Human Autoimmune Diseases of the Central Nervous System. *Front Immunol, 8*, 652. doi:10.3389/fimmu.2017.00652

Platell, C., Cooper, D., Papadimitriou, J. M., & Hall, J. C. (2000). The omentum. *World J Gastroenterol, 6*(2), 169-176. doi:10.3748/wjg.v6.i2.169

Pober, J. S., & Sessa, W. C. (2007). Evolving functions of endothelial cells in inflammation. *Nat Rev Immunol, 7*(10), 803-815. doi:10.1038/nri2171

Potente, M., & Makinen, T. (2017). Vascular heterogeneity and specialization in development and disease. *Nat Rev Mol Cell Biol, 18*(8), 477-494. doi:10.1038/nrm.2017.36

Poulos, M. G., Guo, P., Kofler, N. M., Pinho, S., Gutkin, M. C., Tikhonova, A., . . . Butler, J. M. (2013). Endothelial Jagged-1 is necessary for homeostatic and regenerative hematopoiesis. *Cell Rep, 4*(5), 1022-1034. doi:10.1016/j.celrep.2013.07.048

Poulsen, L. C., Edelmann, R. J., Kruger, S., Dieguez-Hurtado, R., Shah, A., Stav-Noraas, T. E., . . . Hol, J. (2018). Inhibition of Endothelial NOTCH1 Signaling Attenuates Inflammation by Reducing Cytokine-Mediated Histone Acetylation at Inflammatory Enhancers. *Arterioscler Thromb Vasc Biol, 38*(4), 854-869. doi:10.1161/ATVBAHA.117.310388

Przybyl, L., Haase, N., Golic, M., Rugor, J., Solano, M. E., Arck, P. C., . . . Herse, F. (2016). CD74-Downregulation of Placental Macrophage-Trophoblastic Interactions in Preeclampsia. *Circ Res, 119*(1), 55-68. doi:10.1161/CIRCRESAHA.116.308304

Qadri, M., Almadani, S., Jay, G. D., & Elsaid, K. A. (2018). Role of CD44 in Regulating TLR2 Activation of Human Macrophages and Downstream Expression of Proinflammatory Cytokines. *J Immunol, 200*(2), 758-767. doi:10.4049/jimmunol.1700713

Qian, B. Z., Li, J., Zhang, H., Kitamura, T., Zhang, J., Campion, L. R., . . . Pollard, J. W. (2011). CCL2 recruits inflammatory monocytes to facilitate breast-tumour metastasis. *Nature, 475*(7355), 222-225. doi:10.1038/nature10138

Quail, D. F., & Joyce, J. A. (2013). Microenvironmental regulation of tumor progression and metastasis. *Nat Med, 19*(11), 1423-1437. doi:10.1038/nm.3394

Quail, D. F., & Joyce, J. A. (2017). Molecular Pathways: Deciphering Mechanisms of Resistance to Macrophage-Targeted Therapies. *Clin Cancer Res, 23*(4), 876-884. doi:10.1158/1078-0432.CCR-16-0133

Rafii, S., Butler, J. M., & Ding, B. S. (2016). Angiocrine functions of organ-specific endothelial cells. *Nature, 529*(7586), 316-325. doi:10.1038/nature17040

Ren, G., Zhao, X., Wang, Y., Zhang, X., Chen, X., Xu, C., . . . Shi, Y. (2012). CCR2-dependent recruitment of macrophages by tumor-educated mesenchymal stromal cells promotes tumor development and is mimicked by TNFalpha. *Cell Stem Cell, 11*(6), 812-824. doi:10.1016/j.stem.2012.08.013

Ridgway, J., Zhang, G., Wu, Y., Stawicki, S., Liang, W. C., Chanthery, Y., . . . Yan, M. (2006). Inhibition of Dll4 signalling inhibits tumour growth by deregulating angiogenesis. *Nature, 444*(7122), 1083-1087. doi:10.1038/nature05313

Rini, B. I., Plimack, E. R., Stus, V., Gafanov, R., Hawkins, R., Nosov, D., . . . Investigators, K.-. (2019). Pembrolizumab plus Axitinib versus Sunitinib for Advanced Renal-Cell Carcinoma. *N Engl J Med, 380*(12), 1116-1127. doi:10.1056/NEJMoa1816714

Rodriguez, P. C., & Ruffell, B. (2021). Cavity macrophages stop anti-tumor T cells. *Cancer Cell, 39*(7), 900-902. doi:10.1016/j.ccell.2021.06.007

Rudzinska, M., & Czarnocka, B. (2020). The Impact of Transcription Factor Prospero Homeobox 1 on the Regulation of Thyroid Cancer Malignancy. *Int J Mol Sci, 21*(9). doi:10.3390/ijms21093220

Salas-Benito, D., Vercher, E., Conde, E., Glez-Vaz, J., Tamayo, I., & Hervas-Stubbs, S. (2020). Inflammation and immunity in ovarian cancer. *EJC Suppl, 15*, 56-66. doi:10.1016/j.ejcsup.2019.12.002

Sanford, D. E., Belt, B. A., Panni, R. Z., Mayer, A., Deshpande, A. D., Carpenter, D., . . . Linehan, D. C. (2013). Inflammatory monocyte mobilization decreases patient survival in pancreatic cancer: a role for targeting the CCL2/CCR2 axis. *Clin Cancer Res, 19*(13), 3404-3415. doi:10.1158/1078-0432.CCR-13-0525

Schenk, M., Fabri, M., Krutzik, S. R., Lee, D. J., Vu, D. M., Sieling, P. A., . . . Modlin, R. L. (2014). Interleukin-1beta triggers the differentiation of macrophages with enhanced capacity to present mycobacterial antigen to T cells. *Immunology, 141*(2), 174-180. doi:10.1111/imm.12167

Schneider, S., Kadletz, L., Wiebringhaus, R., Kenner, L., Selzer, E., Fureder, T., . . . Heiduschka, G. (2018). PD-1 and PD-L1 expression in HNSCC primary cancer and related lymph node metastasis - impact on clinical outcome. *Histopathology, 73*(4), 573-584. doi:10.1111/his.13646

References

Schreiber, R. D., Old, L. J., & Smyth, M. J. (2011). Cancer immunoediting: integrating immunity's roles in cancer suppression and promotion. *Science, 331*(6024), 1565-1570. doi:10.1126/science.1203486

Schupp, J., Krebs, F. K., Zimmer, N., Trzeciak, E., Schuppan, D., & Tuettenberg, A. (2019). Targeting myeloid cells in the tumor sustaining microenvironment. *Cell Immunol, 343*, 103713. doi:10.1016/j.cellimm.2017.10.013

Seita, J., & Weissman, I. L. (2010). Hematopoietic stem cell: self-renewal versus differentiation. *Wiley Interdiscip Rev Syst Biol Med, 2*(6), 640-653. doi:10.1002/wsbm.86

Seliger, B., & Massa, C. (2021). Immune Therapy Resistance and Immune Escape of Tumors. *Cancers (Basel), 13*(3). doi:10.3390/cancers13030551

Serbina, N. V., & Pamer, E. G. (2006). Monocyte emigration from bone marrow during bacterial infection requires signals mediated by chemokine receptor CCR2. *Nat Immunol, 7*(3), 311-317. doi:10.1038/ni1309

Singhal, M., & Augustin, H. G. (2020). Beyond Angiogenesis: Exploiting Angiocrine Factors to Restrict Tumor Progression and Metastasis. *Cancer Res, 80*(4), 659-662. doi:10.1158/0008-5472.CAN-19-3351

Skobe, M., Hamberg, L. M., Hawighorst, T., Schirner, M., Wolf, G. L., Alitalo, K., & Detmar, M. (2001). Concurrent induction of lymphangiogenesis, angiogenesis, and macrophage recruitment by vascular endothelial growth factor-C in melanoma. *Am J Pathol, 159*(3), 893-903. doi:10.1016/S0002-9440(10)61765-8

Skobe, M., Hawighorst, T., Jackson, D. G., Prevo, R., Janes, L., Velasco, P., . . . Detmar, M. (2001). Induction of tumor lymphangiogenesis by VEGF-C promotes breast cancer metastasis. *Nat Med, 7*(2), 192-198. doi:10.1038/84643

Socinski, M. A., Jotte, R. M., Cappuzzo, F., Orlandi, F., Stroyakovskiy, D., Nogami, N., . . . Group, I. M. S. (2018). Atezolizumab for First-Line Treatment of Metastatic Nonsquamous NSCLC. *N Engl J Med, 378*(24), 2288-2301. doi:10.1056/NEJMoa1716948

Sokol, C. L., & Luster, A. D. (2015). The chemokine system in innate immunity. *Cold Spring Harb Perspect Biol, 7*(5). doi:10.1101/cshperspect.a016303

Srivastava, K., Hu, J., Korn, C., Savant, S., Teichert, M., Kapel, S. S., . . . Augustin, H. G. (2014). Postsurgical adjuvant tumor therapy by combining anti-angiopoietin-2 and metronomic chemotherapy limits metastatic growth. *Cancer Cell, 26*(6), 880-895. doi:10.1016/j.ccell.2014.11.005

Stacker, S. A., Caesar, C., Baldwin, M. E., Thornton, G. E., Williams, R. A., Prevo, R., . . . Achen, M. G. (2001). VEGF-D promotes the metastatic spread of tumor cells via the lymphatics. *Nat Med, 7*(2), 186-191. doi:10.1038/84635

Stanczuk, L., Martinez-Corral, I., Ulvmar, M. H., Zhang, Y., Lavina, B., Fruttiger, M., . . . Makinen, T. (2015). cKit Lineage Hemogenic Endothelium-Derived Cells Contribute to Mesenteric Lymphatic Vessels. *Cell Rep, 10*(10), 1708-1721. doi:10.1016/j.celrep.2015.02.026

Stoger, J. L., Goossens, P., & de Winther, M. P. (2010). Macrophage heterogeneity: relevance and functional implications in atherosclerosis. *Curr Vasc Pharmacol, 8*(2), 233-248. doi:10.2174/157016110790886983

Subramanian, A., Tamayo, P., Mootha, V. K., Mukherjee, S., Ebert, B. L., Gillette, M. A., . . . Mesirov, J. P. (2005). Gene set enrichment analysis: a knowledge-based approach for interpreting genome-wide expression profiles. *Proc Natl Acad Sci U S A, 102*(43), 15545-15550. doi:10.1073/pnas.0506580102

Sun, B., Li, F., Lai, S., Zhang, X., Wang, H., Li, Y., . . . Zheng, Y. (2021). Inhibition of CXCR2 alleviates the development of abdominal aortic aneurysm in Apo E-/- mice. *Acta Cir Bras, 36*(1), e360105. doi:10.1590/ACB360105

Sun, D., Luo, T., Dong, P., Zhang, N., Chen, J., Zhang, S., . . . Zhang, S. (2020). CD86(+)/CD206(+) tumor-associated macrophages predict prognosis of patients with intrahepatic cholangiocarcinoma. *PeerJ, 8*, e8458. doi:10.7717/peerj.8458

Sundlisaeter, E., Edelmann, R. J., Hol, J., Sponheim, J., Kuchler, A. M., Weiss, M., . . . Haraldsen, G. (2012). The alarmin IL-33 is a notch target in quiescent endothelial cells. *Am J Pathol, 181*(3), 1099-1111. doi:10.1016/j.ajpath.2012.06.003

Takasugi, N., Tomita, T., Hayashi, I., Tsuruoka, M., Niimura, M., Takahashi, Y., . . . Iwatsubo, T. (2003). The role of presenilin cofactors in the gamma-secretase complex. *Nature, 422*(6930), 438-441. doi:10.1038/nature01506

Taki, M., Abiko, K., Baba, T., Hamanishi, J., Yamaguchi, K., Murakami, R., . . . Matsumura, N. (2018). Snail promotes ovarian cancer progression by recruiting myeloid-derived suppressor cells via CXCR2 ligand upregulation. *Nat Commun, 9*(1), 1685. doi:10.1038/s41467-018-03966-7

Teleanu, R. I., Chircov, C., Grumezescu, A. M., & Teleanu, D. M. (2019). Tumor Angiogenesis and Anti-Angiogenic Strategies for Cancer Treatment. *J Clin Med, 9*(1). doi:10.3390/jcm9010084

Valastyan, S., & Weinberg, R. A. (2011). Tumor metastasis: molecular insights and evolving paradigms. *Cell, 147*(2), 275-292. doi:10.1016/j.cell.2011.09.024

van Baal, J., van Noorden, C. J. F., Nieuwland, R., Van de Vijver, K. K., Sturk, A., van Driel, W. J., . . . Lok, C. A. R. (2018). Development of Peritoneal Carcinomatosis in Epithelial Ovarian Cancer: A Review. *J Histochem Cytochem, 66*(2), 67-83. doi:10.1369/0022155417742897

Vanderbeck, A. N., & Maillard, I. (2019). Notch in the niche: new insights into the role of Notch signaling in the bone marrow. *Haematologica, 104*(11), 2117-2119. doi:10.3324/haematol.2019.230854

Veglia, F., & Gabrilovich, D. I. (2017). Dendritic cells in cancer: the role revisited. *Curr Opin Immunol, 45*, 43-51. doi:10.1016/j.coi.2017.01.002

Verginelli, F., Adesso, L., Limon, I., Alisi, A., Gueguen, M., Panera, N., . . . Locatelli, F. (2015). Activation of an endothelial Notch1-Jagged1 circuit induces VCAM1 expression, an effect amplified by interleukin-1beta. *Oncotarget, 6*(41), 43216-43229. doi:10.18632/oncotarget.6456

Vihervuori, H., Autere, T. A., Repo, H., Kurki, S., Kallio, L., Lintunen, M. M., . . . Kronqvist, P. (2019). Tumor-infiltrating lymphocytes and CD8(+) T cells predict survival of triple-negative breast cancer. *J Cancer Res Clin Oncol, 145*(12), 3105-3114. doi:10.1007/s00432-019-03036-5

Wang, Q., He, Z., Huang, M., Liu, T., Wang, Y., Xu, H., . . . Fan, Y. (2018). Vascular niche IL-6 induces alternative macrophage activation in glioblastoma through HIF-2alpha. *Nat Commun, 9*(1), 559. doi:10.1038/s41467-018-03050-0

Wang, W., Zou, W., & Liu, J. R. (2018). Tumor-infiltrating T cells in epithelial ovarian cancer: predictors of prognosis and biological basis of immunotherapy. *Gynecol Oncol, 151*(1), 1-3. doi:10.1016/j.ygyno.2018.09.005

Webb, P. M., & Jordan, S. J. (2017). Epidemiology of epithelial ovarian cancer. *Best Pract Res Clin Obstet Gynaecol, 41*, 3-14. doi:10.1016/j.bpobgyn.2016.08.006

Weidle, U. H., Birzele, F., Kollmorgen, G., & Rueger, R. (2016). Mechanisms and Targets Involved in Dissemination of Ovarian Cancer. *Cancer Genomics Proteomics, 13*(6), 407-423. doi:10.21873/cgp.20004

Wetzel, A., Chavakis, T., Preissner, K. T., Sticherling, M., Haustein, U. F., Anderegg, U., & Saalbach, A. (2004). Human Thy-1 (CD90) on activated endothelial cells is a counterreceptor for the leukocyte integrin Mac-1 (CD11b/CD18). *J Immunol, 172*(6), 3850-3859. doi:10.4049/jimmunol.172.6.3850

Wieland, E., Rodriguez-Vita, J., Liebler, S. S., Mogler, C., Moll, I., Herberich, S. E., . . . Fischer, A. (2017). Endothelial Notch1 Activity Facilitates Metastasis. *Cancer Cell, 31*(3), 355-367. doi:10.1016/j.ccell.2017.01.007

Wu, L., Saxena, S., Awaji, M., & Singh, R. K. (2019). Tumor-Associated Neutrophils in Cancer: Going Pro. *Cancers (Basel), 11*(4). doi:10.3390/cancers11040564

Wu, S. Y., Fu, T., Jiang, Y. Z., & Shao, Z. M. (2020). Natural killer cells in cancer biology and therapy. *Mol Cancer, 19*(1), 120. doi:10.1186/s12943-020-01238-x

Wynn, T. A. (2013). Myeloid-cell differentiation redefined in cancer. *Nat Immunol, 14*(3), 197-199. doi:10.1038/ni.2539

References

Xue, J., Schmidt, S. V., Sander, J., Draffehn, A., Krebs, W., Quester, I., . . . Schultze, J. L. (2014). Transcriptome-based network analysis reveals a spectrum model of human macrophage activation. *Immunity, 40*(2), 274-288. doi:10.1016/j.immuni.2014.01.006

Yang, H., Zhang, Q., Xu, M., Wang, L., Chen, X., Feng, Y., . . . Jia, X. (2020). CCL2-CCR2 axis recruits tumor associated macrophages to induce immune evasion through PD-1 signaling in esophageal carcinogenesis. *Mol Cancer, 19*(1), 41. doi:10.1186/s12943-020-01165-x

Yang, J. G., Sun, Y. F., He, K. F., Ren, J. G., Liu, Z. J., Liu, B., . . . Zhao, Y. F. (2017). Lymphotoxins Promote the Progression of Human Lymphatic Malformation by Enhancing Lymphatic Endothelial Cell Proliferation. *Am J Pathol, 187*(11), 2602-2615. doi:10.1016/j.ajpath.2017.07.019

Yang, Y., Garcia-Verdugo, J. M., Soriano-Navarro, M., Srinivasan, R. S., Scallan, J. P., Singh, M. K., . . . Oliver, G. (2012). Lymphatic endothelial progenitors bud from the cardinal vein and intersomitic vessels in mammalian embryos. *Blood, 120*(11), 2340-2348. doi:10.1182/blood-2012-05-428607

Yildirim, N., Akman, L., Acar, K., Demir, S., Ozkan, S., Alan, N., . . . Ozsaran, A. (2017). Do tumor-infiltrating lymphocytes really indicate favorable prognosis in epithelial ovarian cancer? *Eur J Obstet Gynecol Reprod Biol, 215*, 55-61. doi:10.1016/j.ejogrb.2017.06.005

Yonucu, S., Yiotalmaz, D., Phipps, C., Unlu, M. B., & Kohandel, M. (2017). Quantifying the effects of antiangiogenic and chemotherapy drug combinations on drug delivery and treatment efficacy. *PLoS Comput Biol, 13*(9), e1005724. doi:10.1371/journal.pcbi.1005724

Yousefi M., Dehghani S., Nosrati R., Ghanei M., Salmaninejad A., Rajaie S., Hasanzadeh M., Pasdar A. (2020). Current insights into the metastasis of epithelial ovarian cancer hopes and hurdles. *Cellular Oncology, 43*, 515–538.

Zhang, H., Ye, Y. L., Li, M. X., Ye, S. B., Huang, W. R., Cai, T. T., . . . Li, J. (2017). CXCL2/MIF-CXCR2 signaling promotes the recruitment of myeloid-derived suppressor cells and is correlated with prognosis in bladder cancer. *Oncogene, 36*(15), 2095-2104. doi:10.1038/onc.2016.367

Zhang, P., Yue, K., Liu, X., Yan, X., Yang, Z., Duan, J., . . . Han, H. (2020). Endothelial Notch activation promotes neutrophil transmigration via downregulating endomucin to aggravate hepatic ischemia/reperfusion injury. *Sci China Life Sci, 63*(3), 375-387. doi:10.1007/s11427-019-1596-4

Zhang, S., Liu, W., Hu, B., Wang, P., Lv, X., Chen, S., & Shao, Z. (2020). Prognostic Significance of Tumor-Infiltrating Natural Killer Cells in Solid Tumors: A Systematic Review and Meta-Analysis. *Front Immunol, 11*, 1242. doi:10.3389/fimmu.2020.01242

Zhang, Y., Kang, S., Shen, J., He, J., Jiang, L., Wang, W., . . . Liang, W. (2015). Prognostic significance of programmed cell death 1 (PD-1) or PD-1 ligand 1 (PD-L1) Expression in epithelial-originated cancer: a meta-analysis. *Medicine (Baltimore), 94*(6), e515. doi:10.1097/MD.0000000000000515

7 Publications

E. Alsina-Sanchis, R. Mülfarth, I. Moll, C. Mogler, J. Rodriguez-Vita*, Andreas Fischer*. *Intraperitoneal Oil Application Causes Local Inflammation with Depletion of Resident Peritoneal Macrophages*. Mol Cancer Res. 2021 Feb;19(2):288-300.doi: 10.1158/1541-7786.MCR-20-0650. Epub 2020 Nov 2.

E. Alsina-Sanchis, R. Mülfarth, A. Fischer. *Control of Tumor Progression by Angiocrine Factors*. Cancers. 2021 May 26;13(11):2610. doi: 10.3390/cancers13112610.

8 Acknowledgment